Exploring the Sensing Capability of Wireless Signals

Changlai Du

Dissertation submitted to the Faculty of the
Virginia Polytechnic Institute and State University
in partial fulfillment of the requirements for the degree of

Doctor of Philosophy
in
Computer Science and Application

Wenjing Lou, Chair
Ing-Ray Chen
Y. Thomas Hou
Anil Vullikanti
Yingying Chen

May 1, 2018
Falls Church, Virginia

Keywords: wireless security, wireless localization, motion sensing

Exploring the Sensing Capability of Wireless Signals

Changlai Du

ABSTRACT

Wireless communications are ubiquitous nowadays, especially in the new era of Internet of Things (IoT). Most of IoT devices access the Internet via some kind of wireless connections. The major role of wireless signals is a type of communication medium. Besides that, taking advantage of the growing physical layer capabilities of wireless techniques, recent research has demonstrated the possibility of reusing wireless signals for both communication and sensing. The capability of wireless sensing and the ubiquitous availability of wireless signals make it possible to meet the rising demand of pervasive environment perception. Physical layer features including signal attributes and channel state information (CSI) can be used for the purpose of physical world sensing. This dissertation focuses on exploring the sensing capability of wireless signals. The research approach is to first take measurements from physical layer of wireless connections, and then develop various techniques to extract or infer information about the environment from the measurements, like the locations of signal sources, the motion of human body, etc.

The research work in this dissertation makes three contributions. We start from wireless signal attributes analysis. Specifically, the cyclostationarity properties of wireless signals are studied. Taking WiFi signals as an example, we propose signal cyclostationarity models induced by WiFi Orthogonal Frequency Division Multiplexing (OFDM) structure including pilots, cyclic prefix, and preambles. The induced cyclic frequencies is then applied to the signal-selective direction estimation problem.

Second, based on the analysis of wireless signal attributes, we design and implement a prototype of a single device system, named MobTrack, which can locate indoor interfering radios. The goal of designing MobTrack is to provide a lightweight, handhold system that can locate interfering radios with sub-meter accuracy with as few antennas as possible. With a small antenna array, the cost, complexity as well as size of this device are reduced. MobTrack is the first single device indoor interference localization system without the requirement of multiple pre-deployed access points (AP).

Third, channel state information is studied in applications of human motion sensing. We design WiTalk, the first system which is able to do fine-grained motion sensing like leap reading on smartphones using the CSI dynamics generated by human movements. WiTalk proposes a new fine-grained human motion sensing technique with the distinct context-free feature. To achieve this goal using CSI, WiTalk generates CSI spectrograms using signal processing techniques and extracts features by calculating the contours of the CSI spectrograms. The proposed technique is verified in the application scenario of lip reading, where the fine-grained motion is the mouth movements.

Exploring the Sensing Capability of Wireless Signals

Changlai Du

GENERAL AUDIENCE ABSTRACT

Wireless communications are ubiquitous nowadays, especially in the new era of Internet of Things (IoT). Most of IoT devices access the Internet via some kind of wireless connections. The major role of wireless signals is a type of communication medium. Besides that, taking advantage of the growing physical layer capabilities of wireless techniques, recent research has demonstrated the possibility of reusing wireless signals for both communication and sensing. The capability of wireless sensing and the ubiquitous availability of wireless signals make it possible to meet the rising demand of pervasive environment perception. Physical layer features including signal attributes and channel state information (CSI) can be used for the purpose of physical world sensing. This dissertation focuses on exploring the sensing capability of wireless signals. The research approach is to first take measurements from physical layer of wireless connections, and then develop various techniques to extract or infer information about the environment from the measurements, like the locations of signal sources, the motion of human body, etc. Based on the analysis to cyclostationary properties of wireless signals, we propose a new method for indoor interference source localization. We also design a fine-grained human motion detection system using channel state information, which can be applied to application scenarios like lip reading.

Dedicated to my wife Wenbo and my daughter Tang.

Acknowledgments

It takes me six years to finish this dissertation. It would never have been possible for me to achieve it without the support and encouragement from my teachers, colleagues, family and friends. I know it is not only an individual but also a collaborative work. Therefore, I would like to acknowledge the help of many people during the past six years.

First and foremost, I would like to express my sincere gratitude to my advisor Dr. Wenjing Lou, for her continuous and intellectual guidance, support and patience. She guides me in my research with her insightful understanding of the research field, while encourages me to pursue my own research interests. I can't thank her more for her help with developing my research skills, for her discussion about my ideas and for the inspiration during my research process. I could not have imagined having a better advisor and mentor for my Ph.D. study.

I am also thankful to Dr. Y. Thomas Hou, Dr. Ing-Ray Chen, Dr. Yingying Chen and Dr. Anil Vullikanti for serving on my dissertation committee. Their insightful comments and suggestions have helped me to make this work better.

Of course, I would also like to thank my co-authors: Dr. Huacheng Zeng, Ruide Zhang, Dr. Ning Zhang, Dr. Yuichi Kawamoto and Dr. Xiaoqun Yuan. Thank you for your active participation and excellent collaboration in our research.

I wish to thank my labmates in the Complex Networks and Security Research (CNSR) lab: Dr. Qiben Yan, Dr. Yao Zheng, Dr. Bing Wang, Ethan Gabriel, Dr. Wenhai Sun, Yang Xiao, Tingting Jiang, Dr. Liguang Xie, Dr. Xu Yuan, Dr. Xiaoqi Qin, Dr. Tao Jiang, Dr. Wei Song, Dr. Jin Li, Dr. Xiaofeng Chen, Yaxing Chen, Dr. Feng Li, Dr. Guorui Li, Dr. Wenbo Shi, Dr. Li Yang, Dr. Liang Liu. Thank you for your insightful discussions in my research and help in my life.

Last but not least, my deepest thanks go to my family for their continuous love, support and trust during the journey of my life. Most importantly, I'm indebted to my wife Wenbo and my daughter Tang, the two most beautiful girls in the world. You are always my source of inspiration and motivation.

Funding Acknowledgments

Research work presented in this dissertation is supported in part by National Science Foundation (NSF) under grants CNS-1156318, CNS-1446478, CNS-1405747, CNS-1443889, and CNS-1343222.

Contents

List of Figures

List of Tables

Chapter 1

Introduction

Wireless signals exist ubiquitously in our daily life, especially in the new era of Internet of Things (IoT). The major role of wireless signals is a type of communication medium. Recent research has extended the role of ubiquitously available wireless signals to be a sensing platform of the physical world. This dissertation focuses on the problem of exploring the sensing capability of wireless signals. In this section, the research position and the current research status of wireless sensing is briefly introduce. The research goals, research methods as well as research contributions will be also be covered.

1.1 Sensing Using Wireless Signals

Sensing of objects and the environment using wireless signals is not a new concept. Radar has been extensively studied and employed to gather information about distant objects such as the range, angle or velocity [16] using radio waves. When electromagnetic wave encounters an object, some part of the electromagnetic energy is absorbed and the rest energy will be reflected back because of the sudden changes in conductivity in the medium. The reflected electromagnetic is then received by Radar antennas and analyzed to locate the objects. However, Radar techniques usually rely on dedicated hardware or ultra-wide bandwidth to achieve high range resolution, which impedes their daily life application.

On the other hand, wireless communication techniques have been tremendously developed and deployed in the new era of IoT. IoT is the network of "things", where each "thing" is uniquely identified through its embedded computing system and is able to communicate with others within the network. A "thing" in IoT can be any devices, mechanical or digital machines, objects, animals or people implanted with embedded computing systems. Kevin Ashton first mentioned the Internet of Things in a presentation he made to Procter & Gamble in 1999 [10]. Since then, IoT has been a hot topic both in the industry and in academia. It is estimated that Internet connected devices outnumber humans in sometime between

2008 and 2009 (Figure 1.1) by Cisco [37], which is believed to be the "birth" of the Internet of Things. Gartner's estimation is more conservative by suggesting that over 20 billion connected IoT devices will be in use by 2020 [1]. Most of IoT devices will be connect to the Internet using some kind of wireless connections because the cost of wireless radios has dropped tremendously. For example, in 2017, Sigfox pronounced a $0.20 IoT wireless module that is so cheap that even disposable items can become part of the internet of things [7].

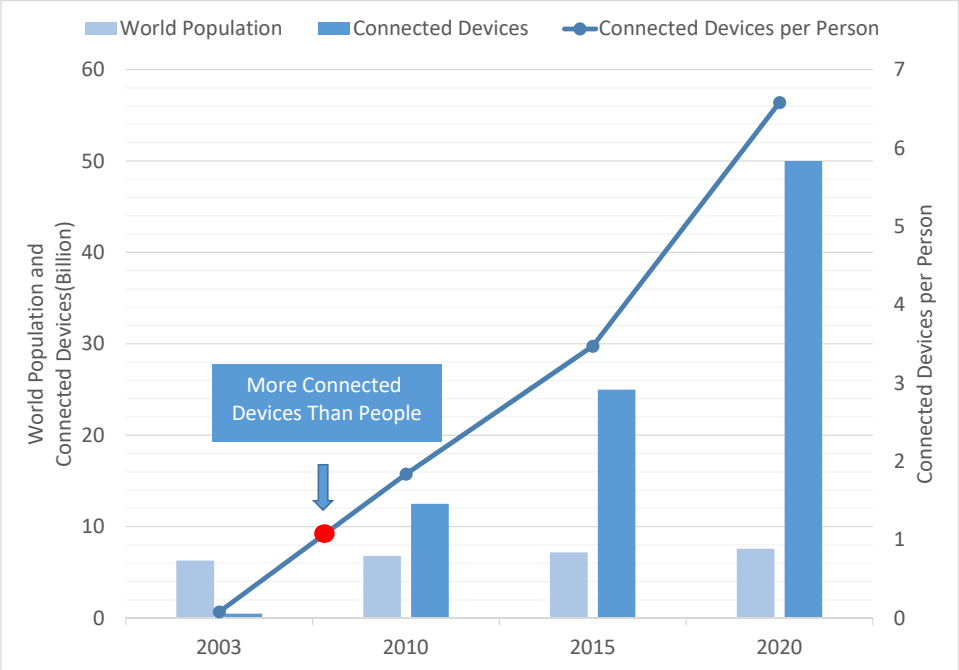

Figure 1.1: Cisco estimates that there will be over 50 billion connected devices by 2020. An important inflection point occurred in 2008, when the number of things connected to the Internet surpassed the human population, which is believed the "birth" of IoT.

The ubiquitous availability of wireless connections and wireless signals leaves a wide gap for the research community to explore. The technology of using wireless communication systems as the ubiquitous sensors has been named *wireless sensing* or *sensorless sensing* [121, 145]. To take after Kristen Woyach in [121], "*the radio itself, provided that it can measure the strength of the incoming signal, is the only sensor we use; with this sensorless sensing approach, any wireless network becomes a sensor network*".

It should be noted that the concepts of *wireless sensing* and *wireless sensor network(WSN)* [12] are very different. In WSN, a sensor node consists of sensing, data processing and communicating components, where the communication module uses some kind of wireless techniques. The "wireless" in its name only refers to the used communication technique, while its sensing capability relies on the sensors equipped on the nodes. In *wireless sensing*, the sensing capability comes from the wireless communication system itself. We are using

the "side channel" of wireless communications for the purpose of sensing.

Wireless sensing has various application possibilities, among which indoor localization and human motion sensing are the two most active research areas. In the next sub-sections, I will briefly introduce the state-of-art of research results along these two directions.

1.1.1 Indoor Localization

Wireless sensing based indoor localization spawns numerous location-based applications in a wide range of living, production, commence, and public services. In outdoor environments, global navigation satellite systems are used as the location service, among which Global Positioning System (GPS) is the most widely used. But in indoor environments, GPS signals are usually not accessible, which makes indoor localization more challenging than outdoor. Localization precision requirement is also higher than GPS system to room-level or even sub-meter level. Because of the ubiquitous deployment of wireless networks and devices, wireless sensing has been extensively studied for indoor localization during the past two decades The basic idea of wireless indoor localization is to map physical measurements derived from wireless signals into geometric parameters such as distances or directions from reference points.

The previous research literature can be briefly categorized according to the physical measurements. Power(RSSI, CSI), time and angle are the physical measurements for indoor localization with different accessibility and accuracy.

Received Signal Strength (RSS) based approach is one of the mostly widely used approaches for indoor localization because of its simplicity and direct availability [25, 47, 60, 63, 129, 131]. The value of Received Signal Strength Indication (RSSI) can be read from most wireless network interface cards (NIC). RSSI based solutions can be archived into two categories. One is the range based algorithms, which estimate the distances from multiple measurement points to the target using wireless signal propagation models and locate the target geometrically [134]. The other category is fingerprinting based [17, 92, 101, 130]. The problem of fingerprinting is that they need extensive accurate environment calibration workload before system deployment.

Channel State Information (CSI) provides more fine-grained channel measurements for every subcarrier for Orthogonal Frequency Division Multiplexing (OFDM) technology based wireless systems. It is potential to achieve accurate and pervasive indoor localization using CSI, which has attracted much recent research interests [100, 101, 118, 122, 123]. For example, [122] and [118] construct CSI fingerprinting to improve the performance of RSSI based fingerprinting methods. However, like RSSI, CSI fingerprinting localization methods suffers the same problem of environment calibration.

Time of Flight (ToF) or **Time of Arrival (ToA)** measures the signal propagation time to calculate the distance between the transceivers. ToA based ranging solutions require

dedicated hardware with high sampling rate. Instead of measuring signal propagation time directly, researchers usually turn to measuring frequency differences [11, 42] or using slower signals like acoustic signals [68, 81, 128, 143]. However, in order to distinguish line-of-sight (LoS) signal and non-line-of-sight (NLoS) signals, ToA based ranging solutions must apply extremely high sampling rate because the propagation distance difference between LoS component and the second arriving multipath component is only about tens of nanoseconds [108, 112].

Angle of Arrival (AoA) based estimation algorithms [95, 98] rely on antenna arrays to estimate the angle at which the transmitted signal impinges on the receiver [62, 125]. Signal samples collected from the antennas are processed using eigenvalue decomposition based methods to estimate signal AoAs. One challenge for AoA based approaches is to deal with the multipath phenomenon in indoor environments. Multipath components from the same source can be highly correlated, which makes eigenstructure based AoA estimation algorithms inaccuracy or even infeasible to estimate the AoAs. Recent techniques can overcome the multipath challenge by using a high density of Access Points (AP). For instance, [29] utilizes over 100 APs, ArrayTrack [125] leverages several WiFi APs with 7 to 8 antennas and PinPoint [52] assumes 5 APs on a floor.

1.1.2 Human Motion Sensing

Motion sensing based human localization, human tracking, gesture and activity recognition have been studied intensively in the research community. Existing work on motion sensing can be briefly divided in three categories: vision-based, wearable sensor-based and RF-based.

Vision-based approaches are the most popular for video gaming and virtual reality platforms. Such systems include Microsoft Xbox Kinect [2], Leap Motion [3], and Sony PlayStation Camera [5]. They use color and infrared cameras to do body-depth perception, motion tracking and gesture recognition. The main problem of vision-based motion sensing is that its performance is highly influenced by the condition of lighting. These systems also require LoS condition for proper operation.

Wearable device based methods like RF-IDraw [115] traces trajectory of fingers and hands by attaching Radio Frequency Identification Device (RFID) to the fingers. [126] uses smartwatch to identify 37 gestures. TypingRing [83] asks the users to wear a ring for text inputting with the capability of detecting and sending key events in real-time. AllSee [54] is a gesture-recognition system that can operate on a range of computing devices including those with no batteries. The problem of wearable device based methods is that they are invasive. The users have to wear extra devices all the time.

RF-based motion sensing can be briefly divided in two categories. The first category methods rely on specialized hardware. WiTrack [11] tracks 3D human body motion using an FMCW(Frequency Modulated Carrier Wave) radar at the granularity of 10cm. WiSee [89]

works by looking at the minute Doppler shifts and multi-path distortions for gesture recognition. Google Project Soli [6] uses on-chip 60GHz radar to detect fine-grained motion. However, the short effective range limit its application in long distance scenarios.

Recent work focuses more on Commercial Off-The-Shelf (COTS) instead of specialized hardware. By analyzing CSI dynamics from WiFi NICs, it's possible to estimate human motions. CSI-based method like CARM [117] builds a CSI-speed model and a CSI-activity model, which depicts the relationship between CSI value dynamics and human body parts movement speeds, and the relationship between the body movement speeds and specific human activities. WiKey [13] uses CSI waveform shape as the features and can recognize keystrokes in a continuously typed sentence. WiKey works well only in controlled environments and specific devices positioning. WiFinger [110] also uses CSI waveform shape as the features and can discern 8 finger gestures. WiFinger also requires static transceivers and finger motions must be near the LoS line of the transceivers. WindTalker [67] allows an attacker to infer the sensitive keystrokes on a mobile device using CSI. However, WindTalker requires that the mobile device being placed in a stable environment. Wi-Wri [22] uses WiFi signals to recognize written letters. WiDraw [104] leverages WiFi signals from commodity mobile devices to enable hands-free drawing in the air. WiHear [113] uses specialized directional antennas to obtain usable CSI variations for the purpose of lip reading.

RF-based motion sensing does not require users to wear any physical sensors. Because of the physical properties of RF signals, these approaches can sense user motion under both LoS and NLoS scenarios. The prevalence of RF wireless network infrastructures also enables large scale deployment.

1.2 Research Contributions

This dissertation explores the sensing capability of wireless signals. In the indoor localization research area, the problem of interference source localization is studied. We conquer two major challenges to do indoor interference localization: to identify the interfering signal type and to isolate the LoS component. In the human motion sending research area, we extended the research boundary of CSI based human motion sensing to fine-grained context-free quadrant.

The meaning of sensing capability can be explained using this DIKW model as shown in Figure 1.2. Sensing is the process of collecting data from physical world to cyber space. The collected data can be raw data open to interpretation, or have some higher level meaning to human, depending on how we define the sensor. Data need to be analyzed to extract some useful information. Combining multiple pieces of information, we may get some knowledge. And from knowledge, it's possible to learn some wisdom. The meaning of sensing capability should cover all the four levels and the four processing steps. The sensing capability depends not only on what data we can collect, but also on how we interpret the data and what to

learn from the data.

In this dissertation, we use the DIKW model to determine the roadmap of each piece of work. For the interference localization problem, we use a top-down method. We start from problem because the problem definition is clear. We then identify three types of methods to uniquely define a location point, namely distances, directions and environment fingerprints. We then go to the data layer, and identify what kind of data we can collect: the RSSI, CSI, ToF and the phase array raw signals and how we can map the collected data to the localization methods. Comparing their pros and cons, we make the selection of our roadmap.

For the fine-grained motion sensing problem. We use a bottom-up method. We firstly identify CSI as one of the promising research topics. We then analyze CSI to determine what kind of information we can get from CSI streams. We find out that spectrogram is promising for context-free human motion detection. At last we select the research topic of fine-grained motion sensing because it's out of the boundary of the current research status.

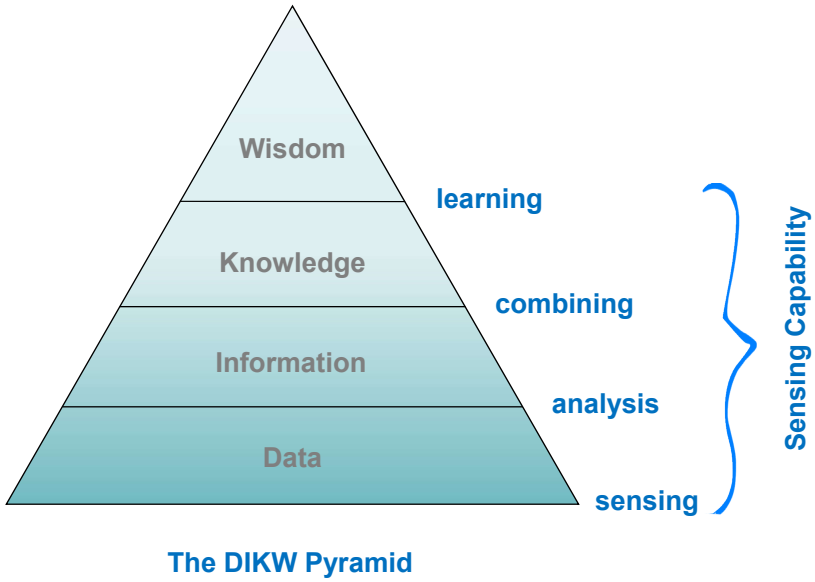

Figure 1.2: The DIKW model. Sensing is the process of collecting data from physical world to cyber space. Data need to be analyzed to extract some useful information. Combining multiple pieces of information, we may get some knowledge. From knowledge, it's possible to learn some wisdom. Wireless sensing should cover all the four processing steps.

The first piece of work is wireless signal attributes analysis. Specifically, the cyclostationarity properties of WiFi signals are studied, which are induced by OFDM features like pilots, cyclic prefix (CP), and preambles. Signal models of these features is first proposed. Then the spectral correlation functions are derived. The induced cyclic frequencies is studied of its applicability to the signal-selective direction estimation (SSDE) problem. Theoretical

analysis is verified using simulation results. The analysis results (e.g., OFDM feature induced cyclostationarity) are also useful for other applications, such as signal detection and identification in Cognitive Radio (CR) networks.

The second piece of work is to solve the problem of indoor interference localization. We design and implement a prototype of a single device system that can locate indoor interfering radios. The goal of designing MobTrack is to provide a lightweight, handhold system that can locate interfering radios with sub-meter accuracy with as few antennas as possible. With a small antenna array, the cost, complexity as well as size of this device will be also reduced. MobTrack is the first single device indoor interference localization system without the requirement of multiple pre-deployed access points.

Channel state information is then studied in human motion sensing applications. We design and implement the prototype of WiTalk, the first context-free fine-grained motion sensing system using WiFi physical layer channel information. Similar to previous CSI-based motion sensing solutions, WiTalk infers human motion by analyzing the CSI dynamics. WiTalk is the first feasible system in the context-free fine-grained quadrant of motion sensing solution plane using WiFi CSI dynamics. We show the existence of this quadrant I solution by identifying the CSI spectrograms as the intrinsic stable properties that correlate to fine-grained human motion. We identify and extract effective features from CSI spectrograms by calculating the contours of CSI spectrograms. These new discerning features solve the problem of low time-frequency resolution using discrete wavelet transform(DWT). We verify the feasibility of WiTalk by applying it to the lip reading scenario. Experiment results show that WiTalk achieves comparable results to previous fine-grained context-related solutions.

1.3 Organization

The dissertation is organized as follows.

Chapter 2 introduces the background knowledge related to this dissertation. We briefly overview the knowledge background of wireless signals and technologies related to this dissertation. The purpose of this overview is to set a whole map for understanding the position of the research work of this dissertation. Different types of wireless signals are firstly introduced as well as their specific properties both for the purpose of communication and sensing. The introduction is mainly focus on RF signals. Measurement methods of RF signal attributes as well as applications of using these attributes will be listed. At last, the superposition properties of RF signals are introduced, including interference superposition and multipath superposition.

Chapter 3 presents the work on cyclostationary analysis of WiFi signals for direction estimation. We present our solution for the first step of solving the indoor interference localization problem by analyzing the cyclostationary properties of wireless signals. We take WiFi signals as an example and illustrate how to model wireless signals and perform cyclostationary anal-

ysis and how to use these properties to help solving the signal selective direction estimation problem.

In Chapter 4, the complete solution to the indoor interference localization problem is presented. We first introduce the related work and research method. The four system work flow steps are then detailed one by one. We then present the implementation details as well as the performance evaluation.

In Chapter 5, we introduce the research work on WiFi based fine-grained motion sensing. We first briefly talk about the concept of CSI and the preliminary of CSI-based motion sensing. The six system work flow steps are then presented in detail, among which we concentrate on interference elimination and feature extraction. We implement and evaluate the system design using the lip reading application.

Chapter 6 summarizes the research achievements, concludes this dissertation and list several possible future research directions.

Chapter 2

Sensing Using Wireless Signals: Fundamentals and Applications

In this chapter, we briefly overview the knowledge background of wireless signals and technologies related to this dissertation. The purpose of this overview is to set a whole map for understanding the position of the research work of this dissertation. Different types of wireless signals is firstly introduced as well as their specific properties both for the purpose of communication and sensing. The introduction will focus on RF signals. Measurement methods of RF signal attributes as well as applications of using these attributes will be listed. The superposition properties of RF signals are introduced, including interference superposition and multipath superposition. At last, we briefly introduce the concept of physical layer security, which is an application of wireless sensing.

2.1 Wireless Signals and Communications

In a broad sense, wireless signals can be any signals that are transferred without wire connection. The most commonly used wireless technologies are radio waves. Other types of wireless signals include visible light and acoustic based techniques. Recent developed counterfactual communication uses quantum mechanics to transfer information without any particles travelling between two recipients. In a sense, this counterfactual communication is also wireless, though there is no traditional "signals".

Radio

A radio frequency (RF) signal refers to a wireless electromagnetic signal used as a form of communication. The radio frequencies of radio waves are in range from 3kHz to 300GHz. Frequency refers to the rate of oscillation of the radio waves. RF signals can cover a large distance and is able to penetrate opaque objects like wall and human body. This property

allows radio signals to be used in through-the-wall sending applications. RF wave is electromagnetic radiation and can propagate at the speed of light and does not need a medium like air to travel. The high propagation speed makes it hard to accurately measure its travelling time in a distance at an indoor scale.

Many RF communication systems have been broadly deployed in industry and in our daily life. Exiting RF technologies which has been used to provide wireless sensing services include WiFi [50], Bluetooth [21, 78, 79], Zigbee 1 [18, 57, 65], and Radio Frequency Identification Device (RFID) [39,64,120]. As we previously mentioned, RSSI, CSI, ToF and AoA techniques can be used to provide wireless sensing services using these RF communication signals.

Visible Light

Visible light (VL) as well as its nearby bands like infrared (IR) and ultraviolet (UV) consists of a wide frequency bands on the electromagnetic spectrum. Optical wireless communication (OWC) [15, 30, 35, 59] uses light propagating in free space to transmit wirelessly data. "Free space" means the light beams travel through the open air or outer space instead of transmission lines such as optical fiber.

Compared to RF, optical wireless has several technology-specific characteristics. First, RF networks suffer from spectrum congestion. Some of the RF bands are licensed to specific organizations. OWC provides the unlicensed, free of charge optical band. At the same time it has potentially much larger available bandwidth. So OWC is considered be to a promising network technology. Second, optical wireless has its own technical limitations compared to RF, such as the absence of line of sight (LoS) and infeasibility of uplink transmission.

Current OWC technologies include visible light communication (VLC) [86, 93], light fidelity (LiFi) [33, 46, 71], optical camera communication (OCC) [44, 127, 144] and free space optical (FSO) communication [20, 55, 75].

Using optical signals as remote sensing technology for very-high-resolution 3D mapping is also proposed such as LiDAR [140].

Sound and Ultrasound

Unlike electromagnetic, sound [58] is a mechanical pressure wave resulting from the back and forth vibration of the particles of the medium. The frequency band of sound waves is between 20Hz and 20kHz, while ultrasound [105] is sound waves with frequencies higher than 20kHz. Ultrasound devices can be used to detect objects and measure distances [87, 107].

Sonic and ultrasonic short range communication systems have been studied and proposed in the literature [66]. Recently, near ultrasound based localization and raging systems have been well studied. These systems leverage the ubiquitous microphone sensors in smartphones and voice assistant systems to capture acoustic signals emitted by microphones and estimate the user locations [45,70,82,141]. Traditionally, acoustic-based localization transmits modulated acoustic signals, containing time stamps or other time related information for the purpose of ToF estimation by the microphone sensors. Another solution is to use the phase and

frequency shift of the Doppler effects in the received acoustic signal, which is caused by a moving object to estimate the relative position and velocity.

Quantum communication

Before this *counterfactual quantum communication*, all our communication is essentially physical, which is to say, all the information is transmitted using actual objects. For example, in previously mentioned RF and optical communications, the information is carried by photons and transmitted at the speed of light. However, in the most recently developed quantum communication domain, information can be transmitted using the transfer of q quantum state instead of an actual quantum or classical particle [23, 96].

In quantum physics, a quantum is described as a possibility wave function. When the quantum is observed, the wave function will collapse. In 1993, Avshalom Elitzur and Vaidman designed a thought experiment as shown in Figure 2.1 [36]. In this experiment, photons are divided into two paths using a beam splitter and reunite at the second beam splitter. The paths can interfere at detector $D1$ constructively and $D2$ destructively. So the photons will be detected on $D1$ but not on $D2$. If an obstacle like a bomb is placed in one of the paths, the wave function collapses and the photons will use other path only, which will be detected on both $D1$ and $D2$. In 2013, Hatim Salih designed a protocol for direct counterfactual quantum communication [96] by repeating the split-reunite structure. If Bob controls the "bombs" in the series of paths, he can use them to send information to Alice's detectors even he does not send any particles to Alice. In 2013, Jianwei Pan and his team implemented this experiment by transmitting a 100×100 bitmap of Chinese knot across a tabletop, and the results are published in 2017 [23].

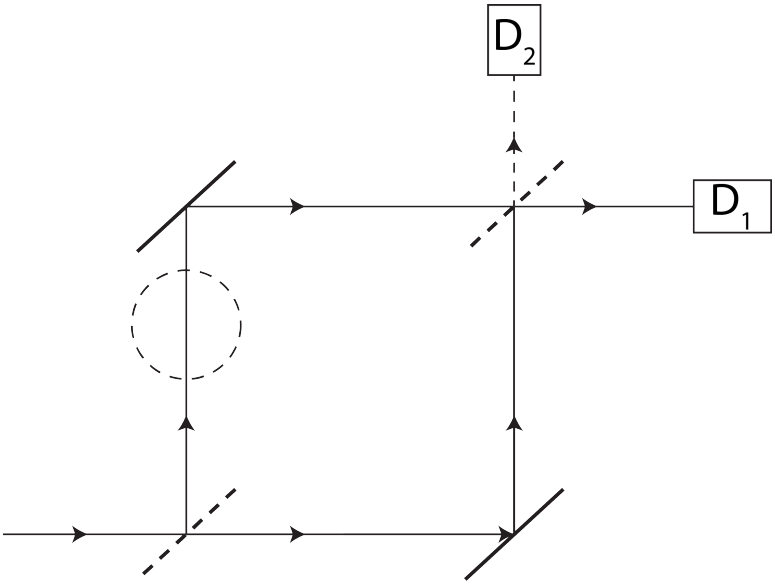

Figure 2.1: Bomb-testing problem diagram. This diagram includes a photon emitter, the bomb to be tested, two photon detectors. Mirrors in the lower left and upper right corners are semi-transparent.

Though there is no classical *signals* transmitted, the quantum wave function does demonstrate its ability of sensing at least the presence/absence of an obstacle. Whether it's possible to be used as a more general sensing method needs future study.

2.2 Measurement of RF Signals Attributes

In this dissertation, we mainly focus on the sensing capability of RF signals, because RF communication are the main technologies used in our daily life. To reuse the RF communication systems as a sending method, we first identify what measurements we can do to RF signals and how these measurements can help us in the sensing applications.

An RF signal is an electromagnetic wave that communications systems use to transport information through air from one point to another. The basic elements of a RF signal is depicted in Figure 2.2, including its amplitude, phase and frequency.

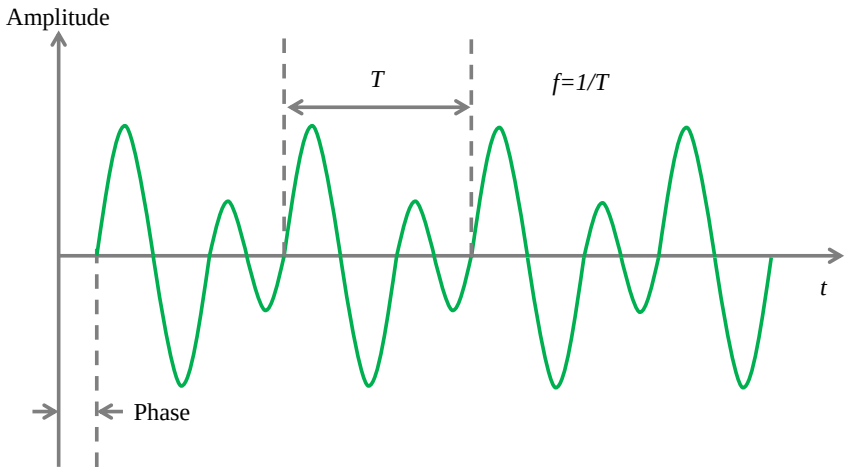

Figure 2.2: The basic elements of RF signals: the amplitude, phase and frequency.

Amplitude

The amplitude of a radio wave is the difference between its maximum and its minimum value during one cycle. Radio waves have amplitudes with units used for the intensity of electronic field, the *Volt (V)*. The amplitude of a radio indicates its strength. In practice, the power rather than the amplitude of signal is measured, because it's difficult to perform voltage measurements with Alternating Current (AC), especially for high frequency RF signals. Power measurement is simpler and more accurate, and the measurement of power can be converted to amplitude.

Power

The power of a RF signal is the transfer rate of energy per unit time. In terms of electromagnetic signals, power represents the amount of energy necessary to push the signal over a particular distance. As the power increases, so does the range. Power is measured with the unit of *Watt*s or in dBm units (decibels referenced to 1 mW) to represent the amplitude of radio waves. The dBm is the amount of power in watts referenced to 1 mW. Zero (0) dBm equals 1 mW. The dBm values are positive above 1 mW and negative below 1 mW.

In practical systems, RSSI is the measurement of power. The higher the RSSI values, the stronger the signal. Different from dBm, RSSI is a relative index while dBm is the absolute number representing power levels in mW. For most widely used wireless techniques ranging from UWB, ZigBee, and WiFi to cellular networks, RSSI is handily accessible.

The main drawback of RSSI measurement is that it's not stable in complex indoor environments. RSSI not only varies over distance but also suffers from shadow fading and multipath fading, as shown in Figure 2.3. RSSI also fluctuates over time even at a static link because of the multipath effect.

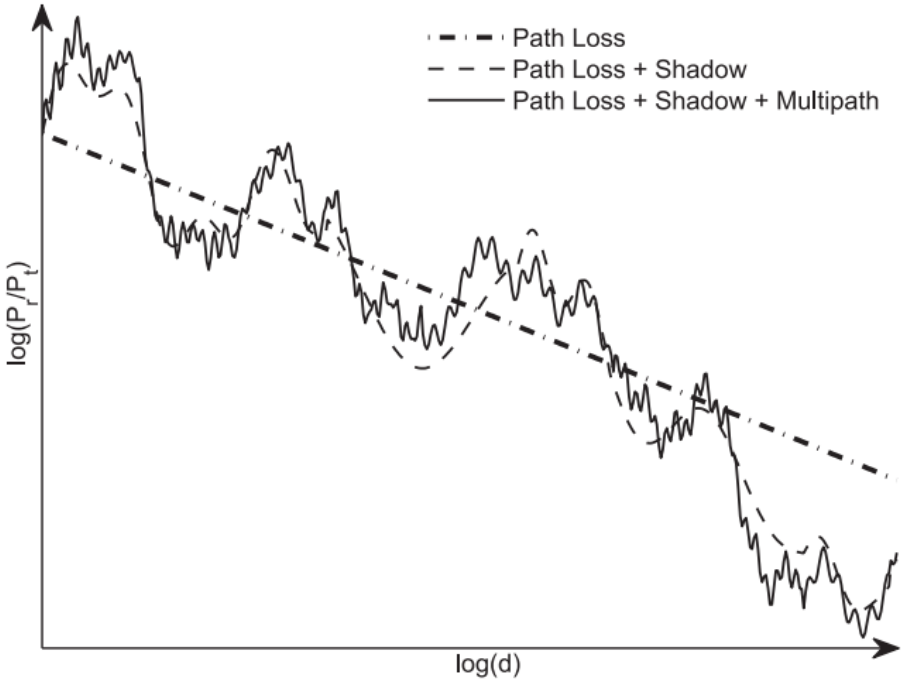

Figure 2.3: RSSI variations due to path loss, shadow fading and multipath fading [129].

Phase

The phase of a radio wave corresponds to how far the signal is offset from a reference point (such as a particular time or another signal). By convention, each cycle of the signal spans 360 degrees. For example, a signal might have a phase shift of 90 degrees, which means that the offset amount is one-quarter (90/360 = 1/4) of the signal [41].

The phase measurement is important in RF wireless applications. The phase measurement techniques include: direct oscilloscope methods, Lissajous figure methods, and zero-crossing methods [84].

Time-of-Arrival

The measurement of RF signal transmission time is name the measurement of Time Of Arrival (ToA) and Time Difference Of Arrival (TDoA). ToA is the time used for a signal to flight from the transmitter to the receiver. The measurement of ToA is based on knowing the exact time the signal leaves the transmitter and the exact time it arrives at the receiver. However, it's hard to exactly synchronize the transmitters. TDoA is more versatile than ToA by measuring "time difference of arrival" (TDOA) of a signal from the emitter at three or more synchronized receiver sites. The main drawback of ToA measurement is that it requires a high Analog-Digital Converter (ADC) sampling rate to get high accuracy.

Frequency Modulated Continuous Waveform (FMCW) is typically used for accurate ToA measurement. In FMCW, an electromagnetic signal is continuously transmitted with time-varying frequencies. As shown in Figure 2.4, the signal with an continuously changing frequency is named a chirp. The difference in frequency between the transmitted signal and the reflected signal can be calculated by mixing the two signals, producing a new signal whose frequency is in base band and can be measured to determine the time of flight because the frequency difference is proportional to the transit time. The time can then be mapped to distance or velocity. FMCW radar is an indirect method of ToA measurement.

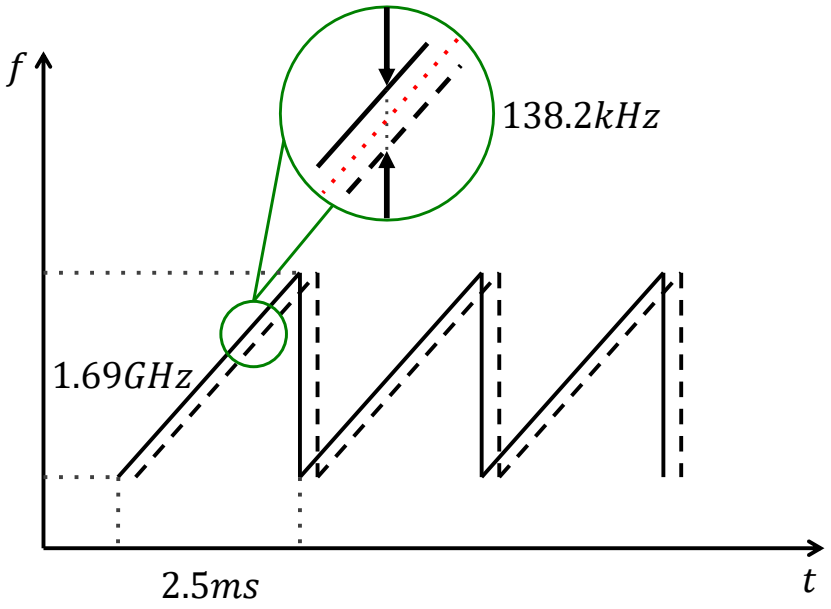

Figure 2.4: The FMCW system estimates the ToF by measuring the frequency difference.

Angle-of-Arrival

The measurement of Angle of Arrival (AoA) is to determine the electromagnetic wave directions of arrival on a sensor. It is important to many wireless sensing systems. Angle information is an orthogonal dimension to distance. For geometric mapping, angle can be combined with distance to estimate the location of a target from a single reference point. The measurement of angle can be distinguished in two categories. The first category is to measure the maximum signal strength during the antenna rotation and then use algorithms like maximum likelihood to determine the AoA. The second category is the high resolution method using an antenna array [27], which is high cost specific hardware. However, with the development software defined radio and MIMO technology, it's not that hard to construct an antenna array with more than a dozen of antennas.

Instantaneous frequency

The frequency of a radio wave is the number of times per second that the signal repeats itself. The unit for frequency is Hertz (Hz), which is actually the number of cycles occurring each second. The frequency of radio waves impacts heir propagation. Lower-frequency signals have longer wavelengths. The lower the frequency, the smaller the propagation loss and the longer the coverage distance. But as the lower frequency bands are limited, low-frequency radio waves are mainly used for broadcast, TV and paging systems. On the other hand, the higher the frequency is, the greater the propagation loss and the closer the coverage distance.

In practice, RF signals have a set of frequencies, which is named frequency spectrum. Frequency spectrum is measured using spectrum analyzers. Spectrum analyzers use fast Fourier transform (FFT) to analyze the frequency components of the RF signals.

Time-Frequency Spectrogram

A spectrogram is a visual representation of the spectrum of frequencies as the signals vary with time. Using spectrogram, we not only can see the signal energy at specific frequencies, but also we can see how the frequency spectrum changes over time. Spectrogram are two dimensional graphs: the time and the frequency. The energy level of the signals are represented by colors.

The spectrogram can be generated using short-time Fourier transform (STFT) [90]. An example of a liner chirp and its corresponding spectrogram is shown in Figure 2.5.

2.3 Superposition of RF Signals

When two RF signals encounter, they will combine to generate a resultant wave whose amplitude is the algebraic sum of the individual waves. Two types if superposition can be identified, namely interference and multipath propagation. Interference signals are from different signal sources, while multipath components are signals from the same source.

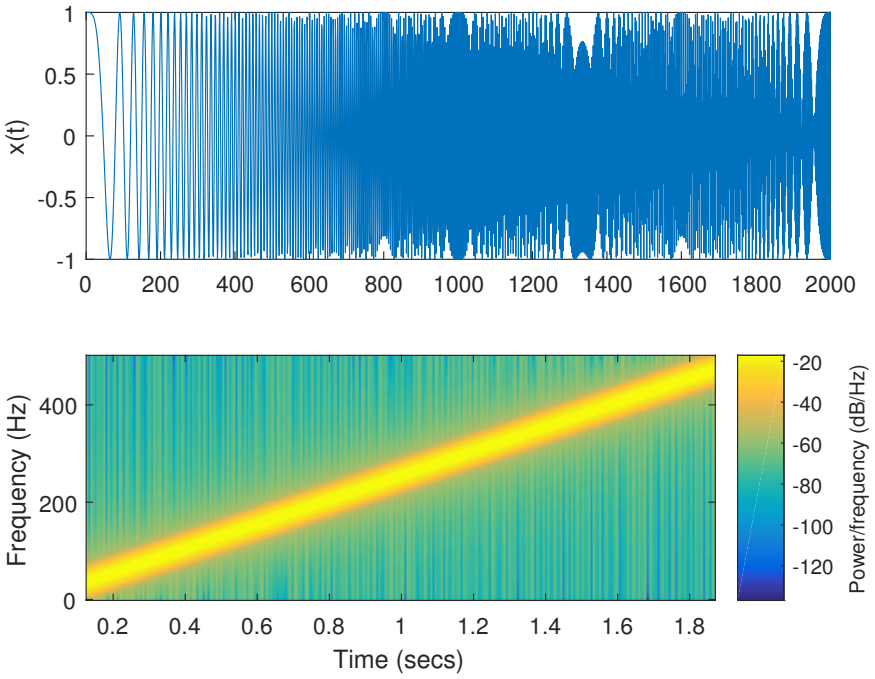

Figure 2.5: A liner chirp and its corresponding spectrogram.

2.3.1 Interference

Interference occurs when two different signals are present at the receiving station at the same time. The two signals have the same frequency band. When interference happens, the RF communication will be degraded because the receiver will fail to decode the signals. Interference can be express as $x = s + i + n$, where x is the received interfered signal, s is the sent signal, i is the interfering signal and n is background noise.

To reduce the possibility of signal interference between different systems, the Federal Communications Commission (FCC) regulates the use of most frequency bands and modulation types. However, radio interference can still occur, especially with systems operating in license-free bands. For example, the ISM band is heavily used by many systems include WiFi, cordless phones, microwave ovens, and Bluetooth devices. When these types of RF devices are in use, the performance of a wireless network can significantly decrease because of retransmissions and competition on the network for use of the medium. This requires careful planning and consideration of other radio devices that might interfere with the wireless network.

To combat RF interference, it is important to eliminate the sources of interference. Orgnizations may set policies for using wireless devices in their network, but it is hard or even impossible to completely restrict the use of wireless devices becuase the large number of

them. Another way to avoid interferene is to use a frequency band that does not confict. However, as the radio frequency regulated by FCC, it is usually hard to find unused frequency band. In this situation, it is an urgent need for network operators to identify and locate the interference sources as quick as possible.

2.3.2 Multipath

Multipath propagation occurs when portions of an RF signal take different paths when propagating from a source to a destination node, such as an access point, as shown in Figure 2.6. A portion of the signal go directly to the destination, which is the line of sight (LoS) component; and another part might bounce from the ceiling, and then to the destination, which is a static reflected component. The part bonce from the moving human body and then to the destination is the dynamic reflected component. Multipath components encounter delay and travel longer paths to the receiver [38].

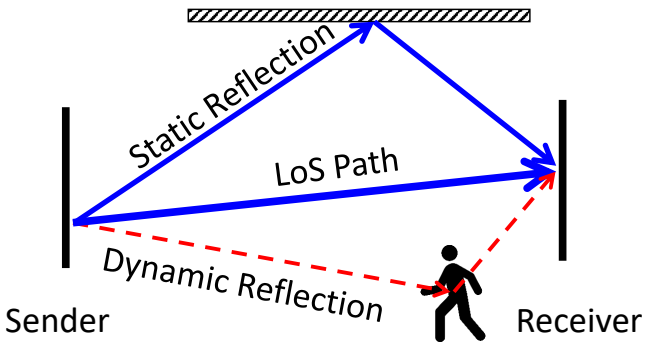

Figure 2.6: Multipath components of the signal include the line of sight component, static reflected components, and dynamic reflected components.

Multipath propagation may cause interference. If two components are in phase, then they are constructive factors, otherwise, they are desctructive factors as shown in Figure 2.7.

In case where the LoS path is much stronger than reflected paths, multipath interference effects may be negligible. However, the LoS path may not always be available and multipath signals may cause significant corruption of the communication. What is worse, the multipath channel characteristics may change over time because of the change of channel geometry. In indoor environments, the propagation path contains all kinds of reflectors like walls, ceilings, the floor, desks , file cabinets, *etc.* The net channel characteristics result from the sum of all the individual reflection channels. For example, when a user move a little bit, the electrical lengths of all the paths reflected from the user change simultaneously. This will both change the delays and the phases of the signals. Small differences in the delay and phases can make

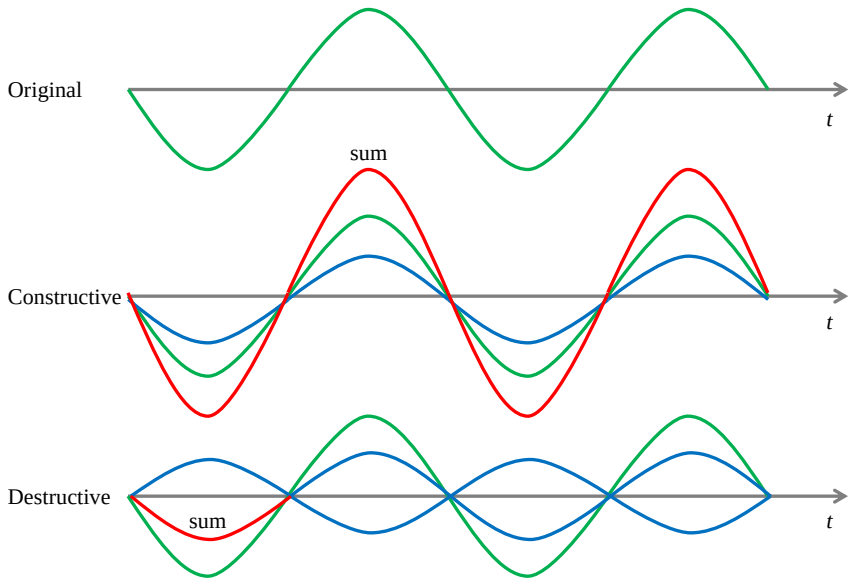

Figure 2.7: Multipath components. Multipath superposition may be constructive or destructive.

big differences in the received signal because of the superposition effects. For example, for 2.4GHz WiFi, the signal wavelength is about 6cm, and the path delay of half a wavelength will totally null the received signal if we assume the signal strength of the two paths are the same.

OFDM is specially designed to eliminate multipath effects in the wireless communications. Multipath delays cause inter-symbol interferences (ISI). OFDM divides the total signal bandwidth in to number of small subcarriers and transmits information on each of the subcarriers. By inserting guard time that is longer than the delay of the channel, OFDM is able to mitigate ISI.

2.4 Physical Layer Security

The application of wireless sensing in security domain is physical layer security (PLS). PLS exploits the unpredictable features of wireless channels such as channel fading. Using the DIKW model, the data collected is the channel/signal status, and then the data are analyzed to extract useful information like physical layer keys for security applications. Like motion sensing, physical layer security does not rely on the communication system but utilize the sensing capability of the wireless signals. Thus we identify PLS as an application of wireless sensing.

Conventional wireless systems are protected using classical cryptosystems which are mainly based on computational security. However, there are challenges in applying these approaches

in IoT, especially the low-end IoT devices. Those devices are usually embedded devices, which are low-cost and low-energy with limited computing ability. They can't afford the additional size, power consumption, and code space needed to perform the expensive mathematical calculations of cryptographic methodologies [111]. In addition, IoT devices that work in a device-to-device communication mode may not have access to a secured public key infrastructure (PKI) for the distribution of public keys.

While the main security streams have focused on the upper layers, another research thread has been active in recent years, which leverage physical layer to enhance security as well as to decrease hardware complexity requirement and energy cost. Physical layer security enhancement is twofold as shown in Figure 2.8 [136]. Information-theoretic security [88] which is also known as physical layer security (PLS), exploits the unpredictable features of wireless channels such as channel fading. PLS transmission techniques achieve security through artificial noise [43], jamming [72], or beamforming [80], etc. However, these PLS transmission schemes are not practical yet because they require complex coding and the perfect channel state information (CSI) of the receiver and imperfect CSI of the eavesdroppers [146]. Physical layer key generation, which is promising and an active branch of PLS, is implementable because the legitimate users are able to agree on the same key from the noisy channel estimation [135], which can be used as an alternative to PKI in many circumstances.

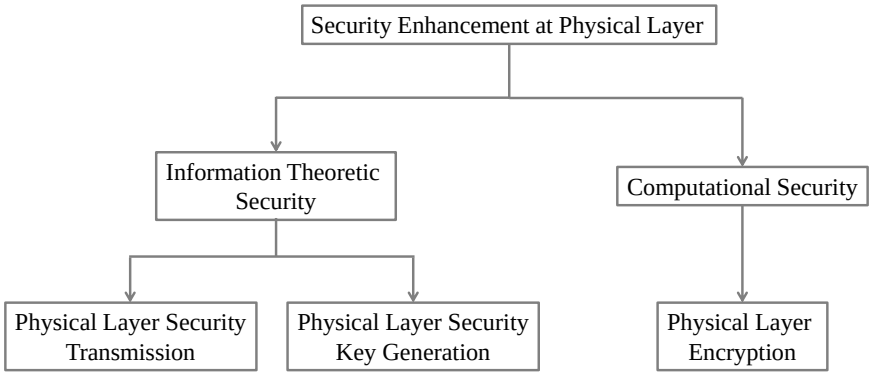

Figure 2.8: Taxonomy of physical layer security enhancement techniques.

Physical layer encryption (PLE) is a hybrid approach, which integrates information theoretical security and computational security schemes. Physical layer key generation is used over the noisy channel to generate common keys using pilot signals. The key generation protocol that consists of channel probing, quantization, information reconciliation, privacy amplification. The key is then fed to the PLE, which performs encryption operations at the modulation stages of the physical layer, and protects the IoT wireless transmission. The integration of information-theoretic security schemes and computational security schemes has some advantages over conventional upper layer encryption-based security primitives. It simplifies the process of common key distribution and removes the requirement of access to

PKI. It also protects physical layer package headers from side-channel analysis attacks [91].

Physical layer key generation depends on the randomness of wireless channels, and is built on three physical principles of the channels: channel reciprocity, temporal variation and spatial decorrelation. In physical layer key generation protocols, the wireless devices measure the highly correlated wireless channel characteristics such as channel impulse response(CIR), received signal strengths(RSS), channel state information(CSI), and use the measured values as the randomness sources to generate a shared secret key. Physical layer key generation has the potential to achieve information-theoretic security because it does not rely on the hardness of a computational problem. Thus, it does not require expensive computation.

Channel reciprocity means the channel responses of the forward and backward links are the same, which is the basis for key generation. When two users measure the same channel parameters at the same frequency in a time-division duplex (TDD) mode, the measurements at Alice and Bob are impacted by the non-simultaneous sampling and noise. However, a high correlation between channel measurements of Alice and Bob can still be maintained and eligible for key generation in a slow fading channel, as demonstrated in many practical experiments [51, 77, 139].

Temporal variation indicates that there is randomness residing in the dynamic channel, which ensures the extracted keys are random. A random key will make the cryptographic applications robust against attacks such as brute force. In the urban area, the interference may be chaotic, because of the densely deployed access points [53]. The interference will impact the channel measurements accuracy but will not affect randomness nature of the wireless link between users. In addition, the statistical features of the channel may be deterministic [28], but key generation is exploiting the instantaneous channel variation, which is random in nature.

Spatial decorrelation implies that when located a half-wavelength away from the legitimate users, the eavesdropper experiences an uncorrelated channel compared to that between Alice or Bob, guaranteeing the security of the key generation. When the system works at 2.4 GHz, a half-wavelength is about 6cm, which is quite short. These principles have been theoretically modeled and analyzed in [137, 138].

Chapter 3

Cyclostationary Analysis of WiFi Signals for Direction Estimation

In this chapter, we present our solution for the first step of solving the indoor interference localization problem by analyzing the cyclostationary properties of wireless signals. We take WiFi signals as an example and illustrate how to model wireless signals and perform cyclostationary analysis and how to use these properties to help solving the signal selective direction estimation problem.

3.1 Motivation and Objects

Wireless communication has become ubiquitous all over the world. In indoor environments, IEEE 802.11 (WiFi) is the predominant wireless communication solution. However, due to the "open air" property of wireless media and the crowded unlicensed industrial, scientific, and medical (ISM) band, WiFi communication may be easily interfered with by itself or other ISM systems (e.g., Bluetooth). When WiFi communication is interrupted by interference, quick and accurate detection and localization of the interfering source is of great importance to resolve the problem, especially in business scenarios like enterprises and hospitals. If the interfering source can be localized, it is possible to restore WiFi communication (e.g., by turning off the interfering source). Signal-Selective Direction Estimation (SSDE) is a popular method for interfering source localization. The basic idea of SSDE is to compute the coordinates of the interfering source based on the Angle of Arrival (AoA) of the line-of-sight signal from the interfering source at a set of anchoring WiFi nodes [40, 95, 98]. A prerequisite, which is also a major challenge, of the SSDE problem is that at an anchoring WiFi node, one should distinguish the signal of the targeted interference source from the signals of other (interfering or desired) signal sources.

Cyclostationary based direction estimation algorithms (see [40]) have been proposed to ad-

dress this challenge, by exploiting the signal selection properties of cyclic frequencies. A signal can be modeled as cyclostationary if its cyclic autocorrelation function (CAF) is nonzero for some nonzero cyclic frequencies. The Spectral correlation density function (SCD) is the Fourier transform of a CAF, which can be estimated efficiently from discrete samples of the signals. A cyclic frequency is a frequency at which the CAF is not zero, which can be determined by examining the peaks on the signal CAF or SCD surfaces. Once a cyclic frequency of the target signal is identified, the Cyclic MUSIC algorithm [97] can be used to estimate the signal AoA. The Cyclic MUSIC algorithm takes a cyclic frequency of the target signal as an input, and then performs the MUSIC algorithm in [98] to estimate only the desired signal directions of arrival. Therefore, estimation of signal cyclic frequencies is the first step to exploit the Cyclic MUSIC algorithm for direction estimation. A thorough analysis and evaluation of WiFi cyclostationary properties needs to be performed to estimate signal cyclic frequencies.

OFDM is widely used as the modulation technique for major communication applications such as WiFi (IEEE 802.11a/g/n) to improve spectrum efficiency. For the purpose of signaling, channel estimation, and synchronization, OFDM frame structure introduces some features including pilots, cyclic prefix (CP), and preambles. These features generate peaks on the SCD surface at specific cyclic frequencies, which can be utilized to distinguish WiFi signals from other signals.

In this chapter, we analyze WiFi cyclostationarity induced by these OFDM features. We first present the signal models of these features and then derive their spectral correlation functions. After that, we investigate the applicability of the induced cyclic frequencies to the SSDE problem. Simulation was conducted and the results are in agreement with our theoretical analysis. The work of this chapter are the first to analyze the cyclostationary properties of OFDM-based WiFi signals comprehensively for this purpose. The analysis results (e.g., OFDM feature induced cyclostationarity) are also useful for other applications, such as signal detection and identification in the Cognitive Radio (CR) networks.

The rest of this chapter is organized as follows. Related work is presented in section 3.2. Section 3.3 offers essential background of the cyclostationary analysis. Section 3.4 presents the cyclostationary analysis induced by OFDM features of WiFi. In section 3.5 we evaluate the influence of these features on the direction estimation of WiFi signals. Section 3.5 concludes this chapter.

3.2 Related Work

Cyclostationary analysis is widely studied for the purpose of signal detection and identification. In [103], the authors proposed an OFDM system identification scheme for CR networks based on pilot-induced cyclostationarity. In [106], an embedded cyclostationary signature method for OFDM-based waveform identification was proposed. They generated a cyclo-

stationary signature using OFDM subcarrier set mapping, thus a spectral correlation was created in each OFDM symbol by simultaneously transmitting data symbols on more than one subcarrier. In [24, 73, 99], the authors discussed pilot-induced and preamble-induced cyclostationarity as well as their applications for signal detection in CR networks.

Cyclostationary property based interfering radio localization was proposed in [49, 52]. In these papers, the authors exploited cyclostationary analysis to extract feature vectors to detect signal types, the occupied spectrum, and the AoAs of arriving signals at the detecting radio. However, the authors did not provide the details of how cyclic frequencies(in these papers named pattern frequencies) were generated. They only gave a conclusion that the pattern frequencies of WiFi is any one between $[f_c - \frac{BW}{2}, f_c + \frac{BW}{2}]$ in [49]. Our work is inspired by these two papers, with a focus on the how cyclostationary properties are induced by WiFi OFDM structures.

3.3 Cyclostationarity Preliminary

In this section, we introduce the concept of signal *cyclostationary* properties and the Cyclic MUSIC algorithm.

3.3.1 Cyclostationary Properties

A signal $x(t)$ in time domain is shown in Figure 3.1 (a). If $x(t)$ contains some finite-strength additive sine-wave components with frequency f_n,

$$x(t) = a_0 + \sum_{n=1}^{N} a_n \cos(2\pi f_n t)$$

if the corresponding Fourier coefficients is not zero. The frequency spectrum of $x(t)$ will peak at these f_n values, as shown in Figure 3.1 (b).

As shown in Figure 3.1 (c). Real life signals contain more frequency components, noise and high order "hidden" periodicity [40]. Unlike first order periodicity, signals with high order periodicity do not give spectral lines in spectrum. A signal can be modeled as cyclostationary if its cyclic autocorrelation function (CAF) is nonzero for a nonzero cyclic frequency. The *Cyclic Autocorrelation Function* (CAF) is defined by

$$\mathbf{R}_x^{\alpha}(\tau) \triangleq < x(t+\tau/2)x^*(t-\tau/2)e^{-j2\pi\alpha t} >, \tag{3.1}$$

where the $< \cdot >$ is the time averaging operation defined by

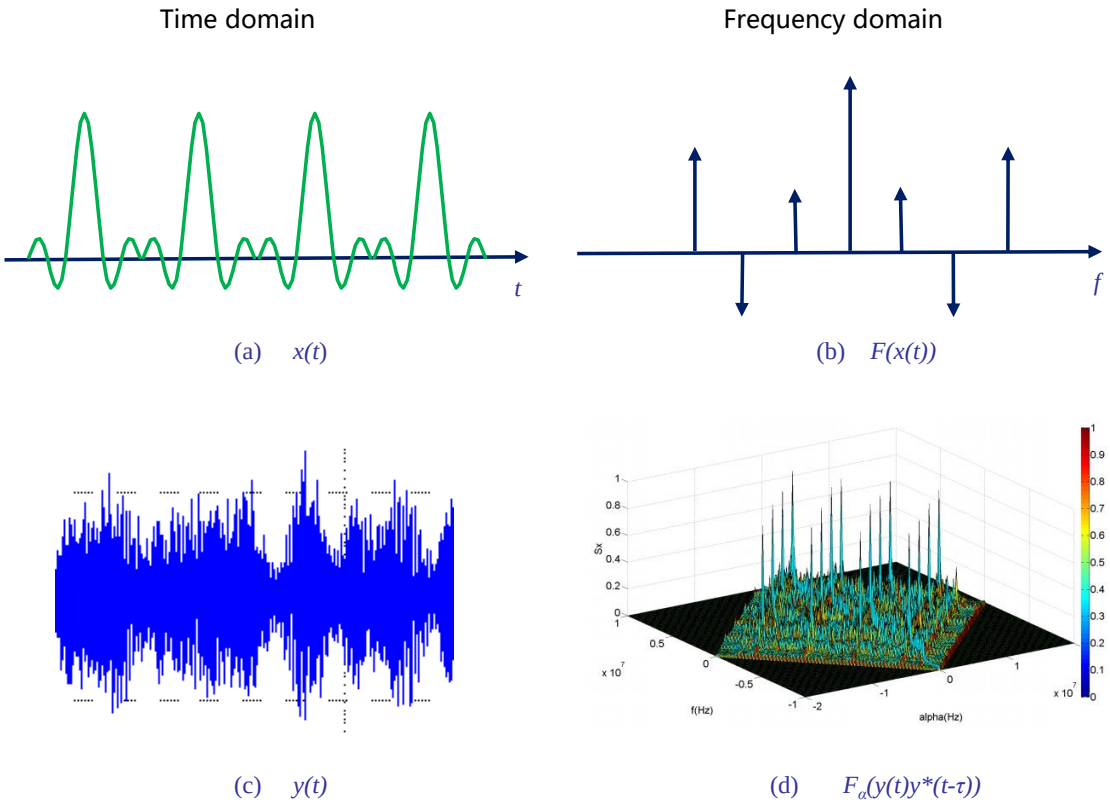

Figure 3.1: A signal can be modeled as cyclostationary if its cyclic autocorrelation function (CAF) is nonzero for a nonzero cyclic frequency.

$$< \cdot >^{\triangleq} \lim_{T\to\infty} \frac{1}{T} \int_{-T/2}^{T/2} (\cdot) dt.$$

If for some cyclic frequency α and delay τ, $\mathbf{R}_x^\alpha(\tau) \neq 0$, then this signal x is a cyclostationary signal, as shown in Figure 3.1 (d). When $\alpha = 0$, $\mathbf{R}_x^\alpha(\tau)$ reduces to a conventional autocorrelation function.

Equation (3.1) can be further interpreted as

$$\mathbf{R}_{uv}(\tau) =< u(t+\tau/2)v^*(t-\tau/2) >, \tag{3.2}$$

where $u(t) = x(t)e^{-j\pi\alpha t}$ and $v(t) = x(t)e^{j\pi\alpha t}$.

We can see from Equation (3.2) that a signal exhibiting the cyclostationary property correlates with a frequency-shifted version of itself, which means that the signal exhibits the

spectral coherence property.

The Fourier transform of CAF is *spectral correlation density function* (SCD), which is defined by

$$\begin{aligned} \mathbf{S}_x^\alpha(f) &= \int_{-\infty}^{\infty} \mathbf{R}_x^\alpha(\tau) e^{-j2\pi f\tau} d\tau \\ &= \lim_{B\to 0} \frac{1}{B} < [h_B^f(t) \otimes u(t)][h_B^f(t) \otimes v(t)]^* >, \end{aligned} \tag{3.3}$$

where $\otimes$ denotes convolution, $u(t)$ and $v(t)$ are given in Equation (3.2), and $h_B^f(t)$ is the impulse response of a one-sided bandpass filter with center frequency f (see [40] for details).

In the discrete domain, the continuous signal $x(t)$ is sampled as a series $x[n]$ and the values of SCD must be estimated from the samples. The algorithm we choose here is Fast Fourier Transform (FFT) accumulation (FAM) [94].

3.3.2 Signal Direction Estimation

MUltiple SIgnal Classification (MUSIC) is an algorithm to determine the parameters of multiple wavefronts arriving at an antenna array. MUSIC algorithm can be used to asymptotically unbiased estimates the number of signals, directions of arrival, strengths and cross correlations among the directional waveforms and strength of noise or interference.

Array Signal Measurement Model

For simplicity, we assume a Uniform Linear Array (ULA) for the antenna elements, which consists of M antennas with an interval of d between adjacent antennas. The array signal model is illustrated in Figure 3.2. Assume I signals exist in the referred space and for the ith signal, there are K_i multipath components perceptible by the antenna array. Further, we assume that the signal sources are far field sources, which means the impinging signals are plane waves.

The signal received by the mth antenna can be expressed as

$$x_m(t) = \sum_{i=1}^{I} \sum_{k=1}^{K_i} s_{ik}(t - \frac{(m-1)dsin\theta_{ik}}{c}) + n_m(t) \tag{3.4}$$

where $s_{ik}(t)$ and θ_{ik} are the wavefront of kth component of ith signal impinging on the ULA and its AoA respectively. $n_m(t)$ is additive measurement noise with zero mean value and no cyclostationary property.

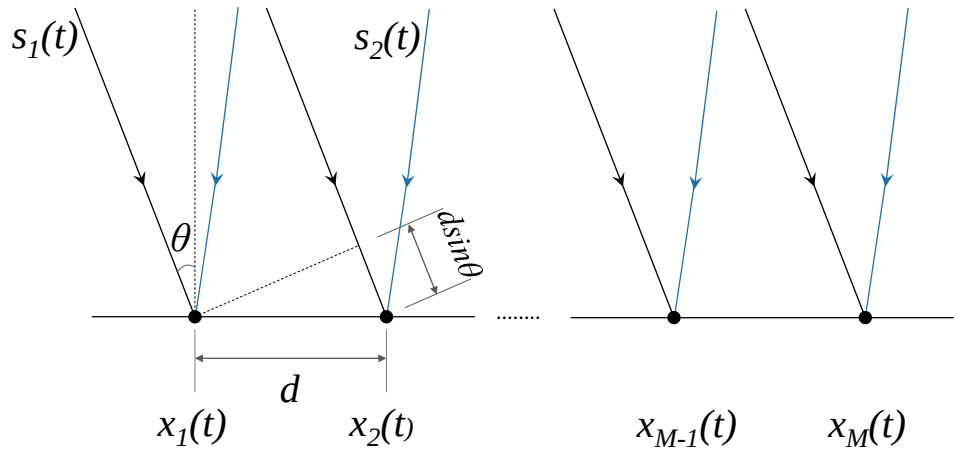

Figure 3.2: Phase Array Data Model. Multipath components from multiple sources impinge on the antenna array. Antenna array is a Uniform Liner Array with interval distance $d = \lambda/2$. Propagation phase delay between array elements can be used to infer the incoming angle θ.

We further assume $d = \lambda/2$, then we make the narrowband assumption and the effect of propagation delay is simply a phase shift.

We then simplify the non-interested signals, and omit the subscript of signal of interest (SoI) without loss of generality

$$x_m(t) = \sum_{k=1}^{K} s_k(t) e^{-j\pi(m-1)sin\theta_k} + i_m(t) + n_m(t) \tag{3.5}$$

where $i_m(t)$ is the sum of all signals other than the SoI measured by mth antenna and K is the number of multipath components of SoI.

Denoting

$$\mathbf{a}(\theta_k) = [1, e^{-j\pi \sin\theta_k}, ..., e^{-j\pi(M-1)\sin\theta_k}]^T \tag{3.6}$$

The antenna array signal measurement model can be expressed in a matrix form as

$$\mathbf{x}(t) = \mathbf{A}(\boldsymbol{\theta})\mathbf{s}(t) + \mathbf{i}(t) + \mathbf{n}(t) \tag{3.7}$$

where

- $\boldsymbol{x}(t) = [x_1(t), ..., x_M(t)]^T$ is the measurement vector;
- $\mathbf{s}(t) = [s_1(t), ..., s_K(t)]^T$ is the wavefront vector ;

- $\mathbf{i}(t) = [i_1(t), ..., i_M(t)]^T$ is uninterested signals vector;
- $\mathbf{n}(t) = [n_1(t), ..., n_M(t)]^T$ is the measurement noise vector;
- $\boldsymbol{A}(\boldsymbol{\theta}) = [\mathbf{a}(\theta_1), ..., \mathbf{a}(\theta_K)]$.

Note that $\mathbf{x}(t), \mathbf{i}(t), \mathbf{n}(t), \mathbf{a}(\theta_k) \in \mathcal{C}^M$, $\mathbf{s}(t) \in \mathcal{C}^K$ and $\mathbf{A}(\boldsymbol{\theta}) \in \mathcal{C}^{M*K}$ and $()^T$ denotes transpose.

As defined in Equation 3.6, $\mathbf{a}(\theta)$ is the *steering vector* of the array, which is a function of the AoA of the incoming signals.

Conventional MUSIC algorithms

Conventional MUSIC algorithms [98] are based on decomposition of the autocorrelation matrix of the input signal $\mathbf{x}(t) = \mathbf{A}(\boldsymbol{\theta})\mathbf{s}(t) + \mathbf{n}(t)$

$$\mathbf{R}_{xx} \triangleq E\{xx^*\} = \mathbf{A}\mathbf{R}_{ss}\mathbf{A}^* + \sigma^2\mathbf{I} \tag{3.8}$$

where $\mathbf{A}$ is composed of the steering vectors of the antenna array, and σ^2 is the variance of noise $\mathbf{n}(t)$. $\mathbf{R}_{ss} = E\{\mathbf{ss}*\}$ is the source autocorrelation matrix. If the signals $s(t)$ are modeled as stationary processes, and uncorrelated with the noise, then $\mathbf{R}_{ss}$ is a Hermitian matrix and $\mathbf{A}\mathbf{R}_{ss}\mathbf{A}^*$ is positive semidefinite whose rank is the number of the incoming signals I. MUSIC requires that number of antenna $M > I$.

The autocorrelation matrix $\mathbf{R}_{xx}$ is then eigen-decomposed to get M eigenvalues. The smallest $M - I$ eigenvalues are all equal to noise variance σ^2. Using this property, the number of incoming signals can be estimated.

Corresponding to the eigenvalues, the M eigenvectors span two subspaces: signal subspace $\mathbf{E}_s$ and noise subspace $\mathbf{E}_N$. The eigenvectors whose eigenvalues are σ^2 span the noise subspace. For each $\mathbf{e}_i \in \mathbf{E}_N$, we have

$$\mathbf{R}_{xx}(t)\mathbf{e}_i = \mathbf{A}\mathbf{R}_{ss}\mathbf{A}^*\mathbf{e}_i + \sigma^2\mathbf{e}_i$$

so

$$\begin{aligned} \mathbf{A}\mathbf{R}_{ss}\mathbf{A}^*\mathbf{e}_i &= 0 \\ \mathbf{A}^*\mathbf{e}_i &= 0 \end{aligned} \tag{3.9}$$

Equation 3.9 means that for every *steering vector* $\mathbf{a}(\theta_k) \in \mathbf{A}$, $\mathbf{a}(\theta_k) \perp \mathbf{e}_i$. The set of $\mathbf{a}(\theta)$ is named the *array manifold* as shown in Figure 3.3 [95]. For our azimuth-only AoA estimation problem, the array manifold is a one-parameter "line" in the M-dimensional space spanned by the eigenvectors of $\mathbf{R}_{xx}(t)$.

As $\mathbf{a}(\theta_k) \perp \mathbf{e}_i$, the intersections of array manifold $\mathbf{a}(\theta)$ and signal subspace $\mathbf{E}_s$ are the solutions of estimating θ_k. The spacial spectrum function is selected to use the inverts of

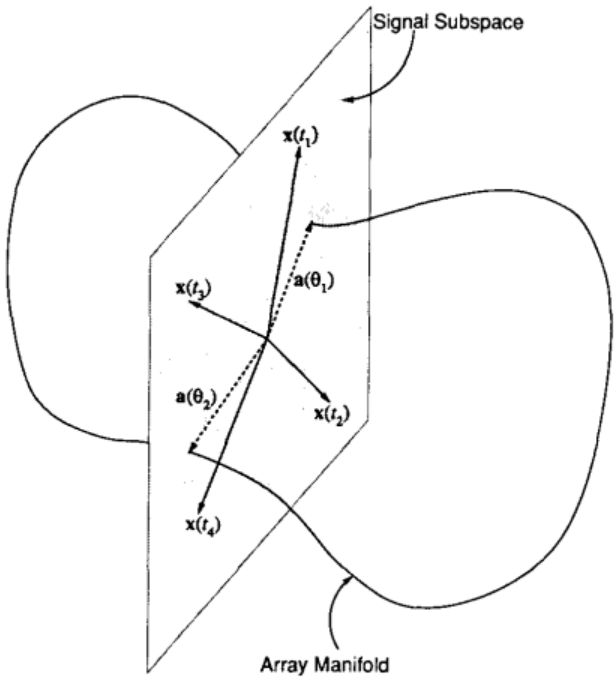

Figure 3.3: Illustration of the concept of *array manifold* and *signal subspace*. This three-sensor two-source example illustrate the geometry of MUSIC [95].

the distance between a point moving along the array manifolds and $\mathbf{E}_s$, who will peak at the signal AoAs

$$P(\theta) = \frac{1}{\mathbf{a}^*(\theta)\mathbf{E}_N\mathbf{E}_N^*\mathbf{a}(\theta)} \tag{3.10}$$

Cyclic MUSIC

Cyclic MUSIC [97] algorithms automatically classify signals based on their known spectral correlation properties and estimate only the desired signals' directions of arrival. Cyclic MUSIC algorithms perform singular value decomposition on the signals' *cyclic autocorrelation matrix* defined in Equation (3.1). Improved Cyclic MUSIC algorithms [26, 132] perform singular value decomposition (SVD) on composition of the cyclic autocorrelation matrix.

The incoming signals can be written as

$$x(t) = \sum_{i=1}^{I} s_i(t) + n(t),$$

where $s_i(t)$ is the ith incoming signal, $n(t)$ is the noise, and I is the number of incoming signals.

In discrete domain, continuous signal $x(t)$ is sampled and becomes a series $x[n]$. The values of SCD should be estimated from the samples. There are several SCD estimation algorithms in the literature. Considering the computation efficiency and result accuracy, we choose a time-smoothing algorithm here named Fast Fourier Transform (FFT) accumulation (FAM) [94] to calculate the bi-frequency SCD values.

The block diagram of FAM is shown in Figure 3.4 [94]. Let f_s be the sample rate. $T_s = 1/f_s$ is the sample duration. In a time period of Δt, $N = \Delta t/T_s$ data are sampled and input into the algorithm. The bandpass filter is implemented using a tampering Hamming Window whose length is T. $N' = T/T_s$ is the number of samples in the window, which is the size of the first FFT. In the frequency domain, $\Delta f = 1/T$ defines the frequency resolution. The window slides all over N samples, with a hopping step of L samples. $P = N/L$ is the number of windows, which is the size of the second FFT. $\Delta\alpha = 1/\Delta t$ defines the cyclic frequency resolution.

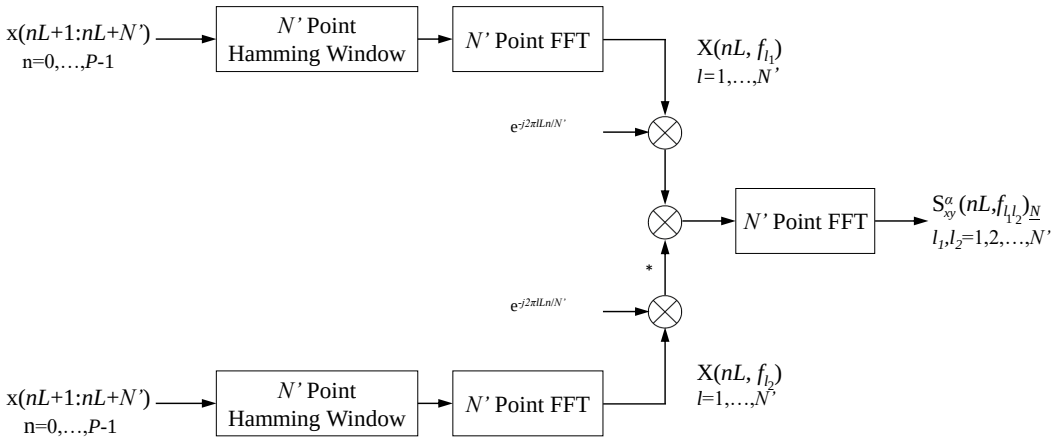

Figure 3.4: FAM Block Diagram. There are two FFT stages. Frequency resolution is $\Delta f = 1/T$; Cyclic frequency resolution is $\Delta\alpha = 1/\Delta t$.

Then we have

$$\mathbf{S}_x^\alpha(f) = \sum_{i=1}^{I} \mathbf{S}_{s_i}^\alpha(f) + \mathbf{S}_n^\alpha(f). \tag{3.11}$$

For signal i which has a particular cyclic frequency α_i, the SCD in Equation (3.11) can be simplified to

$$\mathbf{S}_x^{\alpha_i}(f) = \mathbf{S}_{s_i}^{\alpha_i}(f). \tag{3.12}$$

This equation follows from the fact that at cyclic frequency α_i, all other signals and noise are uncorrelated with s_i. This is the *signal selection property* of cyclic frequencies, which we exploit to solve the SSDE problem.

3.4 WiFi Cyclostationary Analysis

WiFi standards (IEEE 802.11a/g/n) implement OFDM as the physical layer modulation method. OFDM is a modulation scheme that uses multiple carriers to transmit data. For the purpose of signaling, channel estimation, and synchronization, OFDM frame structure introduces some features including pilots, Cyclic Prefix (CP), and preambles. In this section, we analyze the cyclostationary properties induced by these features.

3.4.1 OFDM Frame Structure

The basic frame structure of an 802.11a burst is shown in Figure 3.5. A frame contains a preamble field followed by a SIGNAL field and multiple data fields.

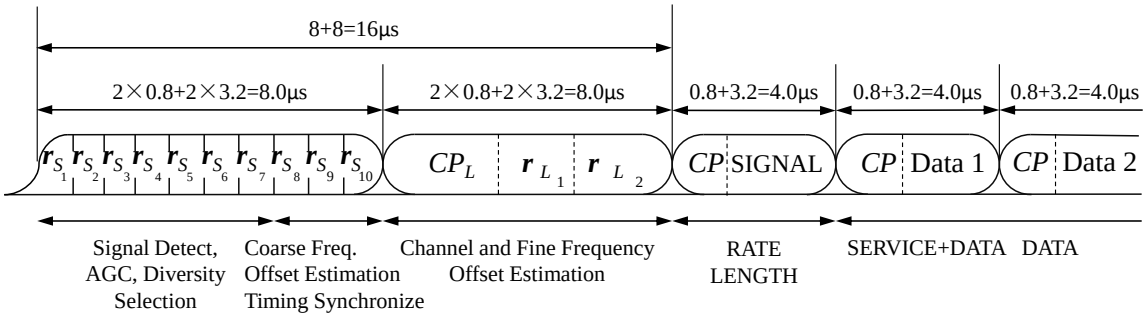

Figure 3.5: IEEE 802.11 a/g OFDM frame structure [50]. The OFDM structure contains features that generate cyclostationary properties: pilots, CP, and preambles.

The preamble contains a short training sequence and a long training sequence. The tenfold repetition of the short training sequence $r_{S_1}, ..., r_{S_{10}}$ is used by the receiver to detect the frame, while the two long training sequence symbols are used by the receiver to perform channel response estimation.

The SIGNAL symbol contains the RATE and LENGTH fields. The RATE field transmits the data rate, which conveys information about the type of subcarrier modulation, and the coding rate used in the rest of the packet.

The cyclic prefix acts as a buffer region or guard interval to protect the OFDM signals from intersymbol interference (ISI). CP is inserted into the OFDM symbol by copying a portion of the higher index IFFT output samples and appending it to the front of the OFDM symbol.

3.4.2 Pilot-Induced Cyclostationarity

Pilots are a key component in the structure of OFDM signals, making it possible to perform channel estimation and frequency compensation. Figure 3.6 illustrates the subcarrier layout of a 16 subcarrier OFDM structure [99]. Ten data subcarriers and two pilot subcarriers are adopted in this structure. Three guard subcarriers and a DC Null are also depicted. All the subcarriers are indexed by the offset to DC Null. Data values are random complex numbers while the pilots are fixed complex numbers. As the pilots are fixed and of higher power, they exhibit some peaks on their SCD surface over data and noise, where a cyclostationary pattern is formed.

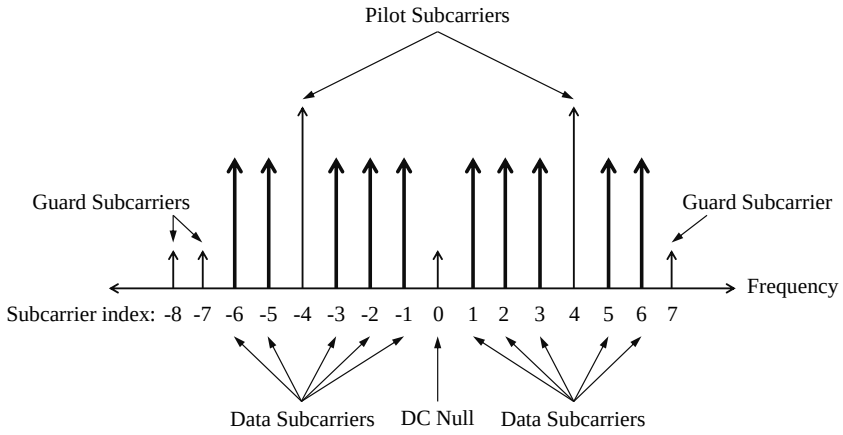

Figure 3.6: OFDM Subcarriers. Ten data subcarriers and two pilot subcarriers are included. Three guard subcarriers and a DC Null are also depicted. All the subcarriers are indexed.

The discrete-time baseband transmitted OFDM signal with pilots (but without CP[1]) can be modeled as

$$x(m) = \sqrt{\frac{E_s}{N}}[x_d(m) + x_t(m)] \tag{3.13}$$

where

$$x_d(m) = \sum_{k} \sum_{\substack{n=0 \\ n \notin \mathcal{I}}}^{N-1} a_k(n) e^{j2\pi \frac{n}{N}(m-kN)} \cdot q(m-kN)$$

[1]The cyclostationary feature of CP in OFDM signals will be analyzed later.

and

$$x_t(m) = \sum_k \sum_{n \in \mathcal{I}}^{N-1} b_k(n) e^{j2\pi \frac{n}{N}(m-kN)} \cdot q(m-kN).$$

E_s is the signal power and $a_k(n)$ is the transmitted data at the nth subcarrier of the kth OFDM symbol. $\mathcal{I}$ denotes the set of pilot subcarrier indices and $b_k(n)$ is the pilot symbols. $q(m)$ is the pulse shaping filter. For WiFi, the pilot's index subset $\mathcal{I}$ stays the same with all OFDM symbols and is determined by the implementation.

From Equation (3.3), it is easily derived that the SCD surface peaks when the frequency-shifted versions of the OFDM subcarrier layouts align at a pilot subcarrier. Take Figure 3.6 as an example, when $\alpha = 0$, SCD peaks at $f = \pm 4B$, where B is subcarrier frequency spacing. For simplicity, we omit B afterward, and use the index numbers to indicate the frequencies. Further, when $\alpha = \pm 8$, SCD peaks at $f = 0$.

In general, suppose that OFDM signals have $2K$ pilots evenly and symmetrically distributed and the index distance between two adjacent pilots is $2p$, then SCD peaks at

$$\begin{array}{ll} \alpha = \pm 4kp, & f = \pm p, \pm 3p, ..., \pm(2K-1-2k)p, \\ \alpha = \pm(4k+2)p, & f = 0, \pm 2p, ..., \pm(2K-2-2k)p, \end{array} \tag{3.14}$$

where $0 < k < K$.

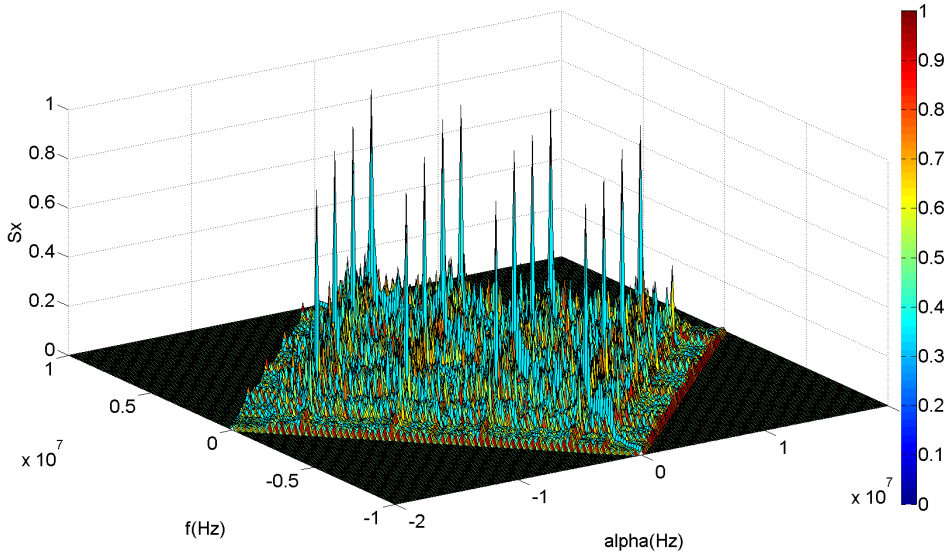

Figure 3.7: WiFi SCD Surface by simulation. SCD surface is bi-frequency, with one dimension the frequency and the other the cyclic frequency. The peaks are induced by pilots on the OFDM subcarriers. Sampling frequency is 20MHz with 64 points FFT. The pilots index are $\{-21, -7, 7, 21\}$ and pilot gain is set to 3db.

Figure 3.7 and Figure 3.8 illustrate the simulation results of the SCD of OFDM with no CP. The number of subcarriers is $N = 64$, with 48 data subcarriers, 4 pilot subcarriers and 12 null subcarriers. The sampling frequency is 20 MHz (with subcarrier spacing of 325 kHz). The indices of subcarriers are set to $\{-21, -7, 7, 21\}$. We can see from Fig. 3.8 that when $f = 0$, the peaks of the SCD surface appears at the cyclic frequencies $\alpha = \pm 4.375$ MHz, ± 13.125 MHz. We note that in order to illustrate the SCD peaks, the power of pilot subcarriers is given a 6 dB gain.

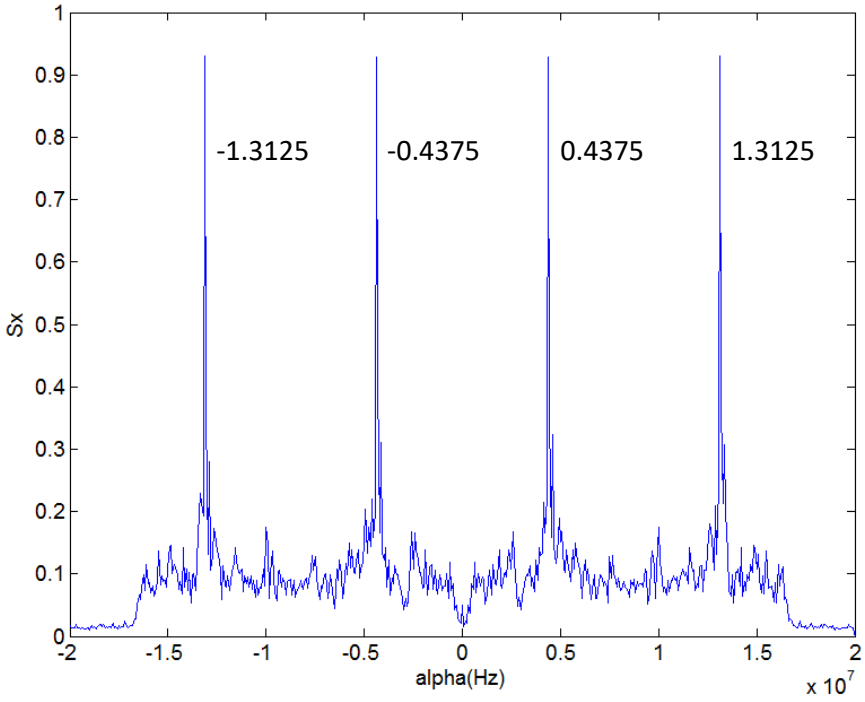

Figure 3.8: Cyclic frequencies when $f = 0$. The cyclic frequencies are $\alpha = \pm 4.375$ MHz, ± 13.125 MHz.

3.4.3 CP-Induced Cyclostationarity

In OFDM modulation, the data and pilot on the frequency subcarriers are converted to time-domain signals via IFFT operations. A CP is then inserted into the OFDM symbol by copying a portion of the higher index IFFT output samples and appending it to the front of the OFDM symbol. The purpose of the CP is to combat Inter-Symbol Interference (ISI) between neighboring OFDM symbols caused by transmission in a multipath channel.

IEEE 802.11 a/g OFDM frame structure is shown in Figure 3.5, which has 64-point IFFT operations and a CP of 16 points. For a 20 MHz sampling frequency, a standard OFDM symbol with CP is $4\mu s$ in time duration.

The discrete-time baseband OFDM signal with CP can be modeled as

$$x(m) = \sqrt{\frac{E_s}{N}} \sum_{k} \sum_{n=0}^{N-1} a_k(n) e^{j2\pi \frac{n}{N}(m-D-k(N+D))} \cdot q(m - k(N+D)), \tag{3.15}$$

where D is the number of points of CP and $a_k(n)$ is an independent and identically distributed (i.i.d) message symbol sequence. Notice that in this model we only consider CP-induced cyclostationarity, as pilot-induced cyclostationarity has been studied in the previous subsection.

The spectral correlation can be derived as:

$$S_x^{\alpha}(f) = \begin{cases} \frac{E_s}{N} \sum_{n=0}^{N-1} Q(f - \frac{n}{N} + \alpha/2) \\ \cdot Q^*(f - \frac{n}{N} - \alpha/2) & \alpha = \frac{d}{N+D} \\ 0 & \alpha \neq \frac{d}{N+D} \end{cases} \tag{3.16}$$

where $Q(f) = \frac{\sin(\frac{\pi f}{N})}{\pi f}$ is the Fourier transform of the square shaping pulse $q(m)$.

From Equation (3.16) we can see that CP-induced peaks at the bi-frequency SCD surface appear at $\frac{d}{N+D}$, where $d \in \mathbb{Z}$.

Figure 3.9 illustrates the simulation results of the SCD for OFDM with $N = 64$, $D = N/4$, and sampling frequency $F = 20$ MHz. We note that to illustrate CP-induced cyclostationarity more clearly, the cyclic frequency resolution of the FAM algorithm is set to $F/256$ in the simulation, so that the SCD peaks only at $\pm\frac{5l}{4}$ MHz, with $l \in \{1..13\}$.

3.4.4 Preamble-Induced Cyclostationarity

A WiFi physical protocol layer data unit (PPDU) begins with a preamble. As depicted in Figure 3.5, the preamble consists of two parts: the short and long preamble training sequences. The preamble in an OFDM signal is designed to provide the means to estimate the channel, estimate frequency offset, and identify the beginning of the OFDM signal through a preamble correlation process.

Different OFDM implementations have distinct preamble patterns, which enables the receiver to detect the presence of a compliant signal. Although it seems to be a promising method of signal identification by cyclostationary analysis, the random WiFi package transmission pattern makes it impossible.

It is worth pointing out that the strategy of inserting specific subcarrier patterns into preambles to induce cyclostationarity does not work for our purpose. This is because in the SSDE problem it is assumed that we have no control of the signal structure of the interfering sources.

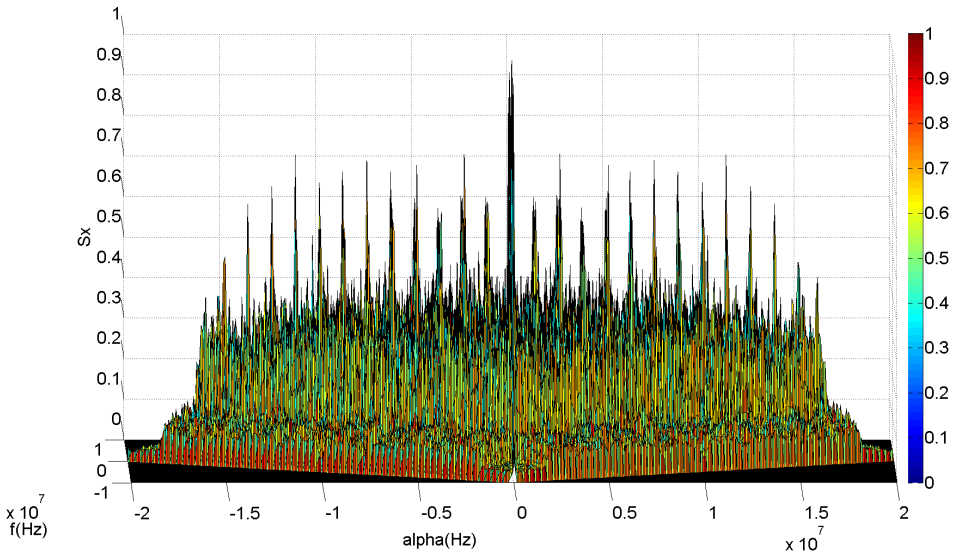

Figure 3.9: CP-induced Cyclostationarity. SCD surface peaks at the cyclic frequencies $\pm\frac{5l}{4}$ MHz, with $l \in \{1..13\}$.

3.5 Performance Evaluation

In this section, we evaluate how these (pilot-induced and CP-induced) cyclic frequencies perform when using them in Cyclic MUSIC algorithms to estimate the signal direction of arrival. We evaluate their performance by conducting simulation in Matlab, the simulation parameters are listed in Table 3.1.

Table 3.1: Simulation Parameters

FFT size	64
Sampling frequencey	20 MHz
Subcarrier spacing	0.325 MHz
# of data subcarriers	48
# of pilot subcarriers	4
Pilot subcarrier index	-21, -7, 7, 21
# of OFDM frames	10
WiFi signal AoAs	-60, -45, -30, -15
Bluetooth Signal AoAs	15, 30, 45, 60
# of array sensors	16
Sensor space	0.5 wavelength
Pilot gain	2.5 dB

We assume that there are two signal sources: one WiFi and one Bluetooth. The channel from each signal source to the anchoring node for detection consists of 4 multipath components.

An antenna array with 16 sensors (i.e., 16 antenna elements) in a Uniform Linear Array (ULA) are used to collect signals from the signal sources.

Two AoA estimation algorithms are employed for the purpose of comparison: Spatial smoothing MUSIC algorithm (SS-MUSIC) in [125] and Cyclic MUSIC with spatial smoothing in [97]. Although SS-MUSIC is not able to distinguish different types of signals, SS-MUSIC efficiently eliminates the correlation between multipath components of the same signal source.

MUSIC-based AoA estimation algorithms differentiate signals and noises according to their corresponding singular values (or eigenvalues). Intuitively, Cyclic MUSIC algorithm will decrease the singular values of undesired signals at proper cyclic frequencies, which make them easier to differentiate. Simulation results in Figure 3.10 illustrate this effect, where singular values after the 5th point are decreased.

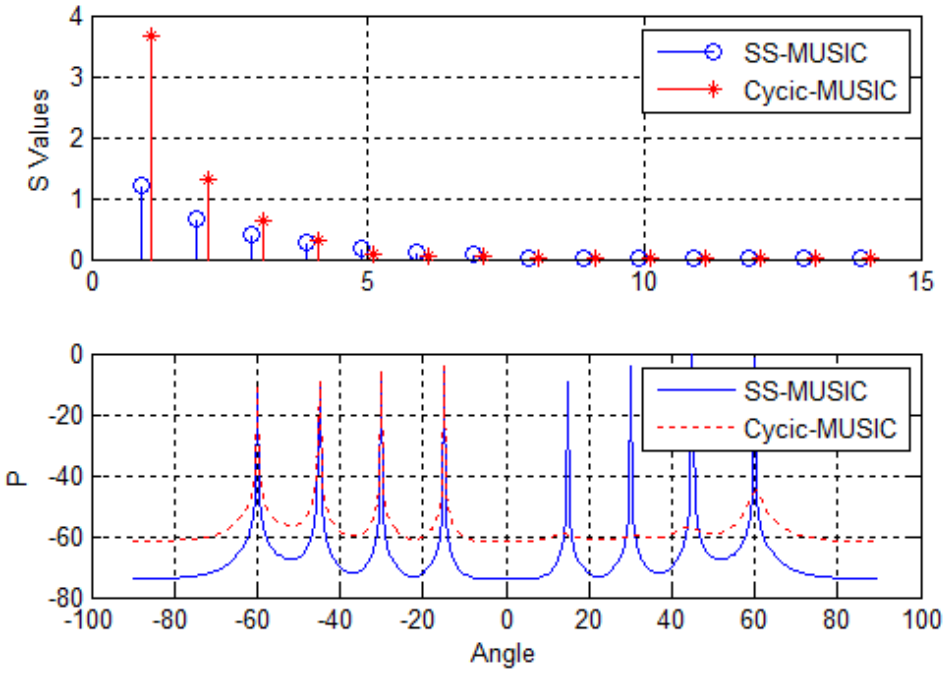

Figure 3.10: Cyclic MUSIC and Spatial Smoothing MUSIC. Cyclic MUSIC decreases the ratio of the largest undesired singular value and the smallest desired singular value.

Based on this consideration, we employ the ratio of the largest undesired singular value and the smallest desired singular value as a metric to evaluate the performance of different cyclic frequencies in the SSDE problem.

Figure 3.11 depicts the simulation results. The ratio values are the average of 50 runs. From the figure we can see that the ratio values calculated by pilot-induced cyclic frequencies are smaller than those by CP-induced cyclic frequencies, which indicates that at pilot-induced cyclic frequencies, it is easier to distinguish desired signals from undesired signals. Suppose that the threshold value is set to 0.3, as depicted in Figure 3.11. We can see that pilot-

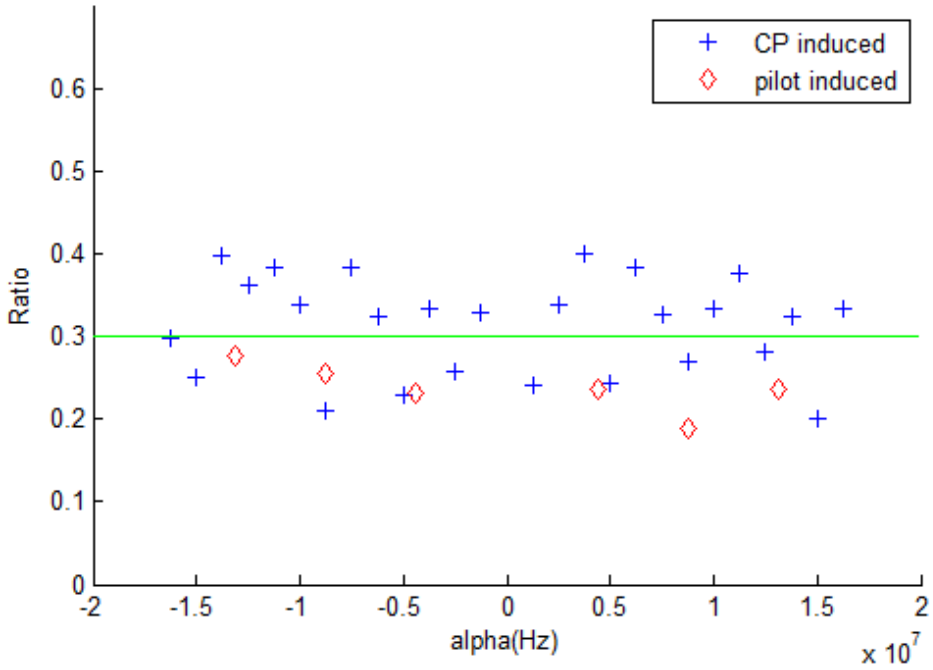

Figure 3.11: Ratios of singular values. The ratio values calculated by pilot-induced cyclic frequencies are smaller than those by CP-induced cyclic frequencies.

induced cyclic frequencies can differentiate noise successfully while some of the CP-included cyclic frequencies cannot. We thus conclude that pilot-induced cyclic frequencies are better than CP-induced cyclic frequencies to solve the SSDE problem.

3.6 Summary of Contributions

In this chapter, we analyzed the cyclostationary property of IEEE 802.11 (WiFi) signals induced by the features of underlying OFDM frame structure, including pilots, CP, and preambles. We studied the influence of these features on the signal's spectral correlation function. We also evaluated the applicability of the induced cyclic frequencies to solve the SSDE problem. Simulation results confirmed that pilot-induced cyclic frequencies are a better approach for the SSDE problem when compared to CP-induced cyclic frequencies. Following the current results, future work will be undertaken to estimate the localization of interference radios by exploiting the estimated cyclic frequencies and signal directions.

Chapter 4

MobTrack: Locating Indoor Interfering Radios With A Single Device

In this chapter, the complete solution to the indoor interference localization problem is presented. This chapter is based on the previous chapter and use its analytical results as the fundamental tools in the system design. We first introduce the related work and research method. The four system work flow steps are then detailed one by one. We then presents the implementation details as well as the performance evaluation.

4.1 Motivation and Objects

As the coming of more wireless devices working on the unlicensed ISM band are produced, this portion of the radio spectrum is becoming more and more crowded, which inevitably leads to interference between these devices. When interference happens, the wireless communication performance may be severely degraded. For example, we all have the experience that though we are close to the WiFi Access Point, our device still experience poor communication performance. Besides WiFi, many other types of devices like Bluetooth speakers, baby monitors, cordless phones and microwave ovens also work on the same frequency band, which causes interference to our WiFi communications from time to time. The interference problem becomes even more crucial especially in some circumstances like hospitals or business environments, where sudden poor wireless performance may lead to serious outcomes.

WiFi has become the predominant wireless communication solution in indoor environments nowadays. In this chapter, we consider the scenario of WiFi being interfered by one or multiple unknown radios. When interference happens, a quick and accurate method to find and terminate the interfering radio will be helpful. However, in indoor environments, it is

not easy to locate the interfering signal.

There are many previous research work on the topic of wireless localization in the literature. However, none of them are applicable for the problem of locating indoor interfering radios. Traditional solutions to the wireless localization problem follows three research lines by measuring the values of Received Signal Strength Indication (RSSI), Time of Arrival (ToA) or Angle of Arrival (AoA). RSSI based solutions [17, 134] collect RSSI values and then use signal propagation models to compute the distances. However, under the circumstance of interference, both interfering and working signals impinge on antennas at the same time and the power is the sum of all incoming signals, which makes it infeasible to differentiate interfering radios from working signals. ToA based ranging solutions [11, 68] require high time resolution measurement and usually rely on dedicated hardware or leverage slower waveforms like acoustic signals. AoA based algorithms [95, 98] rely on antenna arrays to do angle estimation. However, traditional AoA based algorithms cannot address all the challenges encountered by our problem.

Locating indoor interfering radios using AoA based methods has many specific challenges. First, as the nature of the interfering radios are unknown to us, nor can we expect cooperation from the interfering radios, a way to differentiate the interfering radios from working signals is needed. On the other hand, because of the multipath phenomenon, too many signal components will impinge on the antenna array simultaneously, which significantly increase the demand for antenna numbers. The second challenge is to isolate the LoS components from Non-LoS (NLoS) components. Among all the multipath components, only the LoS component contributes to calculation of signal source position using AoA, so the LoS component must be isolated from all Non LoS components.

Recent research has made great advances to address these challenges. In Pinpoint [52], an modified Access Point (AP) infrastructure is leveraged to compute LoS AoA. Their algorithms are based on cyclostationary signal analysis to identify the source of interference. To meet the challenge of multipath propagation, they isolate the LoS component by finding the relative delays between LoS and NLoS components and the relative delays between different antennas at APs. However, as the difference of propagation distance between LoS component and the second arriving multipath component is only about several meters, which corresponds to tens of nanoseconds [108], it is hard to differentiate them without expensive dedicated hardware with high sampling rate. Pinpoint uses a modified frontend that was able to send and receive arbitrary waveforms in the entire 100MHz ISM band [49]. Another work ArrayTrack [125] proposes algorithms to eliminate the effects of multipath by paring peaks in AoA spectrum. Their multipath suppression algorithm could make 71% percent of success to find the LoS by moving the mobile device for five centimeters. However, in our scenario, we have no control to the interfering radio and can not move the source arbitrarily, which makes the solution in ArrayTrack not feasible to our problem. These systems achieve sub-meter location accuracy, but the problem is that their performance relies heavily on the number of cooperating APs. However, though the density of WiFi APs has increased largely, it is not necessary and infeasible to deploy 4 to 5 APs on the same channel in a single area

because of the distributed channel assignment algorithms by the IEEE standards [76].

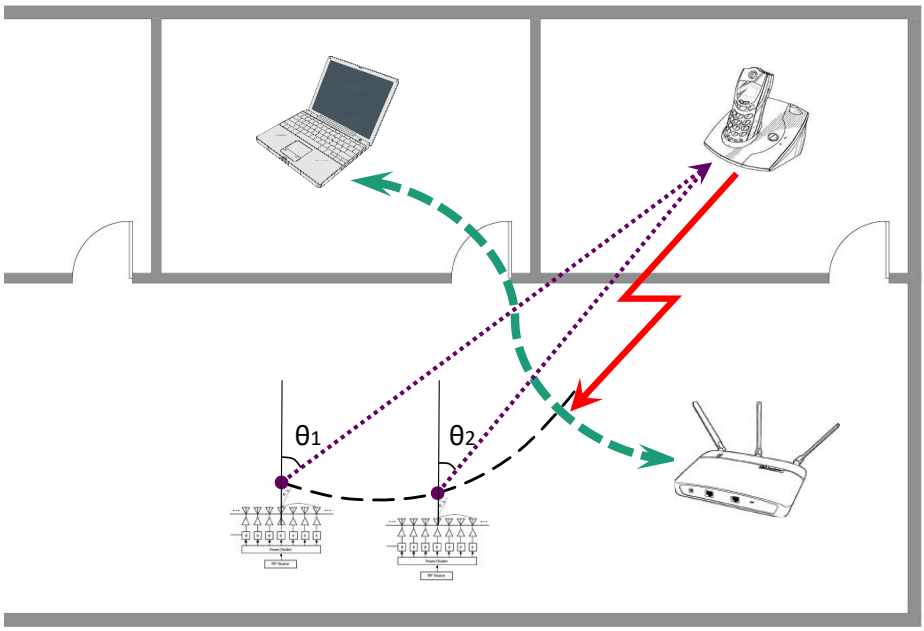

Figure 4.1: System Model. WiFi communication between AP and client are working signals. The interfering radio source is a cordless phone which is the target we are trying to locate. MobTrack locates the interfering radio by compute the LoS AoA of the cordless phone at multiple positions on its moving trace.

In this chapter, we present MobTrack, a single device system that locates indoor interfering radios. The goal of designing MobTrack is to provide a lightweight, handheld system that can locate interfering radios with sub-meter accuracy with as less antennas as possible. MobTrack eliminates the dependence on the AP infrastructure. With small antenna array, the cost, complexity as well as size of this device will be also reduced.

MobTrack system model is shown in Figure. 4.1. A MobTrack device consists of an antenna array, signal processing firmware and our novel algorithms to compute the LoS AoA and estimate the source location. The device is started when an interference is detected. By moving it around, our multipath suppression algorithm can isolate the LoS component from all other impinging components. At the same time, the angles of the LoS component on the movement trace are collected to do triangulation.

Based on cyclostationary signal analysis on existing protocols, we design novel algorithms to classify the signal types and find the cyclic frequencies. Different from PinPoint which creates a dummy signal as the test signature, we analyze cyclostationary signatures of different

signal types theoretically and store their cyclostationary signature in bi-frequency domain locally. Thus we don't need to store the dummy signals for every cyclic frequencies. Another difference is that we adopt Cyclic-MUSIC algorithm [97] to calculate AoAs. In contrast, Pinpoint leverages a optimization method, whose target is a residual function of both signal components delays and the angle of arrival. Our algorithms doesn't work on time domain for the purpose of efficiency and designing goal of a lightweight system without dedicated wireless frontends.

To address the problem of multipath propagation, we design a novel algorithm that effectively find the LoS components based on the stability difference of LoS and NLoS components. The key insight of our multipath suppression algorithm is that with the movement of MobTrack device, the values of LoS AoA tend to be continuous, while reflected paths AoA values are more segmented. Using this property, MobTrack finds LoS AoA by selecting the longest continuous AoA line on the angle-movement plane explained in Section 4.3.3.

The main contributions of this work are summarized as follows:

- To the best of our knowledge, MobTrack is the first single device indoor interference localization system without the requirement of multiple pre-deployed Access Points.
- We propose a novel algorithm to eliminate the multipath effect in the indoor environment. Our multipath suppression algorithm could robustly and efficiently isolate the LoS component from other reflected components.
- We propose a novel signal type identification algorithm for MobTrack to calculate the AoAs of only interfering radios, which significantly reduces the requirement to antenna numbers and device complexity.

A prototype system of MobTrack is implemented on Ettus USRP platform with 6 antennas as the wireless frontend. The location performances are evaluated on a test bed at 16 points over one floor of our department building. Experimental results show that within a movement of 1 meter, MobTrack achieves a median 55cm location accuracy using data collected from 5 points with an LoS isolation correction of 95%.

The rest of the chapter is organized as follows. The system design details are presented in Section 4.3. Implementation is stated in Section 4.4. Section 4.5 elaborates the simulation and experimental results. We discuss related work in Section 4.2 and conclude the chapter in Section 4.6.

4.2 Related Work

The previous research literature can be briefly categorized according to the physical measurements. Power(RSSI, CSI), time and angle are the physical measurements for indoor

localization with different accessibility and accuracy.

RSSI based solutions can be archived into two categories. One is the range based algorithms, which estimate the distances from multiple measurement points to the target using wireless signal propagation models and locate the target geometrically [134]. However, it can not distinguish different signals. The other category is fingerprinting based [17] [130] [92] [101] but they need extensive accurate environment calibration workload before system deployment.

ToA based ranging solutions require dedicated hardware with high sampling rate. Instead of measuring signal propagation time directly, researchers usually turn to measuring frequency differences [11] or using slower signals like acoustic signals [68]. However, in order to distinguish LoS signal and NLoS signals, ToA based ranging solutions must apply extremely high sampling rate because the propagation distance difference between LoS component and the second arriving multipath component is only about tens of nanoseconds [108].

AoA based estimation algorithms [95, 98] relies on antenna arrays. Signal samples collected from the antennas are processed using eigenvalue decomposition based methods to estimate signal AoAs. The challenge for AoA is the multipath phenomenon in our scenario. Multipath components from the same source can be highly correlated, which makes eigenstructure based AoA estimation algorithms inaccuracy or even infeasible to estimate the AoAs. Nevertheless, MobTrack follows the AoA based research line and solve the multipath challenge.

Recent techniques require no costly equipments and they can overcome the multipath challenge, but they assume a high density of APs. For instance, EZ [29] utilizes over 100 APs, ArrayTrack [125] leverages several WiFi APs with 7 to 8 antennas and PinPoint [52] assumes 5 APs on a floor. Because of the popularity of WiFi, the density requirement seems to be acceptable. Nevertheless, there exists some practical limitations. First of all, 4 to 5 strong APs with known locations are necessary with multilateraion, which are not realistic in most circumstances such enterprise or hospital network. Second, FCC permits 802.11 b/g/n standard to employ 14 channels in the 2.4GHz frequency band, so it is difficult to find 4 to 5 strong APs on the same channel even if they do exist. And this problem requires WiFi scanning technique, which is an energy hungry operation and can reduce the battery life of mobile devices by over 2-3 time [14] even if the scanning operation is invoked once every 10 seconds for continuous location tracking. Third, when the APs are operating scanning, regular data communication cannot happen, which impacts the user experience, especially for real-time service like VoIP. In comparison, MobTrack only utilize a single device and thereby will not have the limitations above.

Research Roadmap

We analyze the related work and present the selection of our research roadmap as shown in Figure 4.2. The most intuitiveway to calculate distance is to measure the time-of-flight. However, the time-of-flight is very hard to measure because of the high speed of wireless signals. In indoor environments, it is typically several nanoseconds. We need high speed Analog-Digital Converter (ADC) to get high resolution. So this path is not feasible. Raw

signal data from antenna arrays can be used to calculate the signal directions. The raw signals are ready to use. But we need special hardware, the antenna array. With the help of software defined radio (SDR), this solution looks very promising. Fingerprinting methods are based on the measurement of received signal strength RSSI or channel state information CSI. The RSSI is ready to use. However its very cumbersome to build and maintain the fingerprint database. So we also pass this roadmap. In summary, we choose the direction based solution.

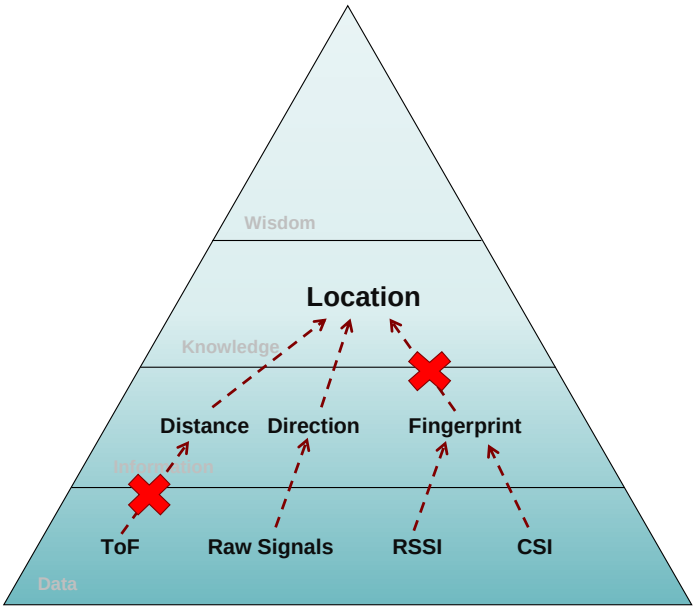

Figure 4.2: The research roadmap. We select AoA based method with the help of promising software defined radio (SDR) technique.

4.3 System Design

We describe the system design of MobTrack following the data flow in system architecture as shown in Figure 4.3. We assume that the interfered communication is a WiFi link between an AP and a client. The interference to this communication from a nearby device is the signal we want to locate. MobTrack is a movable device equipped with an antenna array. We choose the number of antennas to be 6, which will be explained in Section 4.4. This device is carried by an operator moving around in the interfered area to locate the interfering radio and get an increasing accuracy continuously by moving towards it.

As we have stated in the introduction, there are two major challenges to do indoor interference localization using a single device: to identify the interfering signal type and to isolate

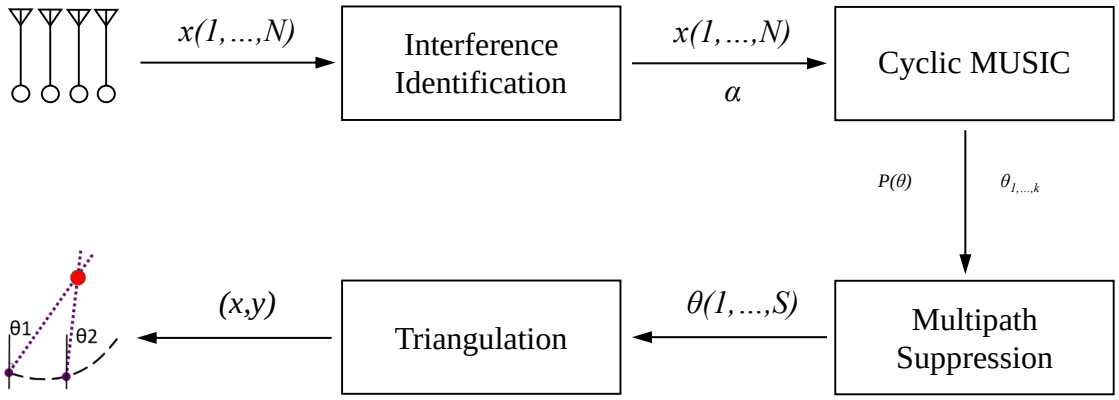

Figure 4.3: MobTrack Architecture. Raw samples are phase aligned and then input into the interference detection process, where cyclic frequencies α are extracted. Spacial smoothed cyclic-music algorithm is applied to estimate the AoAs of the multipath components of only the interfering radio. Multipath suppression algorithm is then applied to isolate the LoS component and identify its AoA. LoS AoAs at different points are used to locate the source by triangulation.

the LoS component. Our system design meets these challenges as well as achieve our goal of a lightweight system. By identifying signal type and using Cyclic-MUSIC algorithm, we can significantly reduce the demand for the number of antennas. The system is designed to be a single device, so that we are able to move it to get angles from different points and suppress multipath effect at the same time. The challenges are addressed step by step. We follow the data flow and make a brief introduction to each step first before diving into the details.

1. **Identify the interfering radio type (Section 4.3.1):** MobTrack takes the phase-aligned signal samples as input. It has to eliminate the influence of noise and signals except the interfering radio first. The property it utilizes is the cyclostationarity property of the interfering radio. MobTrack correlates the received signal with pre-stored signal signatures to determine the interfering signal type. Then it picks a cyclic frequency α which is unique to this interfering radio and pass it along with the received samples to the next step.

2. **Calculate the AoAs of only interfering radio (Section 4.3.2):** Cyclic-Music algorithm takes advantage of the signal selection property of cyclic frequencies. If α selected is unique to the interfering radio, all impinging components from other signals are filtered. Only AoAs from the interfering radio are left. Furthermore, multipath components from the same signal source correlate with each other, which degrades the performance of MUSIC algorithm. To handle this problem, a spacial smoothing method is adopted. In this step, we address the fist challenge. The output of this step is the AoAs of impinging components from the interfering radio only.

3. **Isolate the LoS AoA among multiple NLoS AoAs (Section 4.3.3):** At this step, MobTrack can finally address the second challenge. It leverages a novel algorithm

called LongestCurveFitting to separate LoS signals from NLoS signals and thus find the LoS AoA of interfering radio. The output of this step is LoS AoAs at multiple points on the device moving trace.

4. **Triangulation to find the interfering radio (Section 4.3.4):** The above steps help MobTrack figure out the relative angle between itself and the targeted interfering radio. It can now tell us the direction of the interfering radio. By triangulation, we use least square method to est*mate its location. Thereby we can follow its lead to find the target and turn it off.

4.3.1 Interference Identification

WiFi signals are packet based. As we assume that we don't know the nature of the interfering radio, it may be constant or intermittent. Once the samples of a packet are received from the antenna array, we test whether it is interfered using our interference identification algorithm described below. If no interfering radio is detected, the samples are dropped off and MobTrack waits for the next packet. Otherwise, it is analyzed to find its signal type. In this section, we introduce signal cyclostationary properties first, and then we elaborate our interference identification algorithm. The purpose of identifying the interfering radio is to find its cyclic frequencies which are used as input in Cyclic-MUSIC algorithm in Section 4.3.2.

Cyclostationary Property

Different types of signals exhibit different *cyclic signatures*, on which we can rely to detect interference or even determine the interference source type. We first review the concept of signal *cyclostationary* properties and then elaborate on the algorithms to find the *cyclic frequency* α.

A signal can be modeled as cyclostationary if its cyclic autocorrelation function (CAF) is nonzero for a nonzero cyclic frequency. The definition of *Cyclic Autocorrelation Function* (CAF) can be found in Equation(3.1).

Instead of CAF, its Fourier transform is more often used in cyclostationary signal analysis because of computation efficiency [40], which is called the *spectral correlation density function* (SCD). SCD is defined by

$$\mathbf{S}_x^{\alpha}(f) = \int_{-\infty}^{\infty} \mathbf{R}_x^{\alpha}(\tau) e^{-j2\pi f\tau} d\tau \tag{4.1}$$

In discrete domain, continuous signal $x(t)$ is sampled to be a series $x[n]$. The values of SCD should be estimated from the samples using algorithms like Fast Fourier Transform (FFT) Accumulation (FAM) [94].

The simulated WiFi SCD surface is plotted in Figure 3.7. SCD surface is bi-frequency, with one dimension the frequency and the other the cyclic frequency. The peaks are induced by pilots on the OFDM subcarriers. Sampling frequency is 20MHz with 64 points FFT. The pilots index are -21,-7,7,21 and pilot gain is 3db. As shown in previous chapter, WiFi signals exhibit cyclostationary properties because of the OFDM structure like pilots and cyclic prefixes. Similarly, other protocols also exhibit similar cyclostationary properties. With different physical layer implementations, these protocols has their unique cyclic frequencies, on which we rely to differentiate them.

Interference Identification

We make a reasonable assumption here that the WiFi signal modulation parameters are known, including the number of subcarriers and the positions of the pilot subcarriers. These parameters define the value of cyclic frequencies.

MobTrack utilizes peak patterns on the SCD surface to differentiate signal types. By doing cyclostationary analysis on the signal universe (including WiFi, Bluetooth, ZigBee, DECT cordless phone, etc), we calculate their possible SCD peak patterns and store the "ideal" SCD surfaces locally. An "ideal" SCD surface take values of only 1 or 0. If there is a peak at a coordinate (α, f), its value is 1. Otherwise, it's 0.

Once the interfered samples are received and the corresponding SCD surface is calculated, We calculate the correlations of the SCD with each stored "ideal" SCD surface. We define a threshold C_{TH}. If a correlation is found over C_{TH}, then we say that the interfering radio of this type exists.

The interference identification algorithm is summarized in Algorithm 1.

Algorithm 1 Interference identification algorithm

1: Analyze signal universe, store "ideal" surfaces $\mathcal{S}_N$
2: Calculate the sample surface S_c
3: **for** each "ideal" surface $S_i \in \mathcal{S}_N$ **do**
4: Calculate the correlation C_{ic} of S_i and S_c
5: **if** $C_{ic} > C_{TH}$ **then**
6: Set S_i as the interfering radio type
7: **end if**
8: **end for**

This algorithm may return two or more signal types. In this situation, we assume more than one interference exists. We can find unique cyclic frequencies for them separately and all these interfering signals can be located. However, in this work, we focus on the scenario where there's only one interference.

What should be noted is that unlike previous work on signal classification using cyclostationary approaches [56] [49], we don't use machine learning methods. Instead of training the algorithm when interference happens, we analyze the signal universe and store their signatures.

4.3.2 AoA Spectrum Computation

Once the interfering radio is identified, we select a cyclic frequency that is unique to the interfering radio, and use Cyclic-MUSIC algorithm to calculate the AoA spectrum. Signal components impinging on the antenna array from different directions with different power. AoA spectrum is the incoming signal's power as a function of angle of arrival. We locate the peaks on the AoA spectrum and say that there is a signal component at this direction. However, the directions may or may not be the actual direction of the source because of multipath propagation. Nor the highest peak means that it is the direct path because the direct path signal may be blocked. The concept of phase array model, the MUSIC algorithm and Cyclic-MUSIC algorithm have been introduced in Section 3.3.2.

Spacial Smoothing to Eliminate Correlation

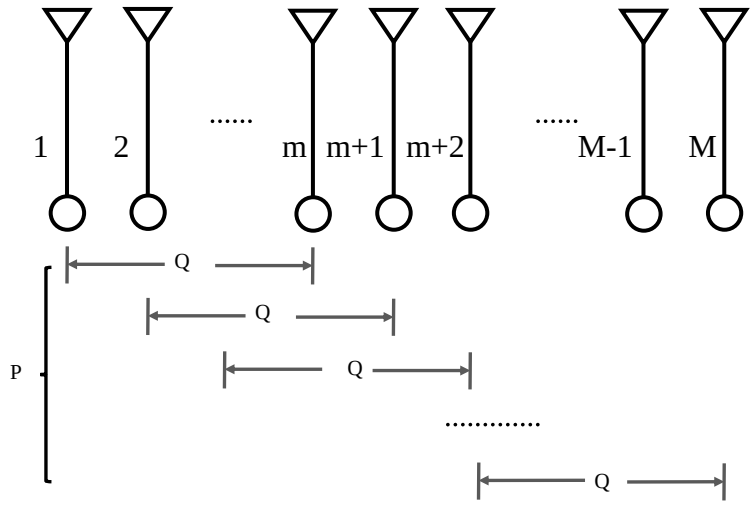

Figure 4.4: Subarray Spacial Smoothing Totally M antennas in P groups with Q antennas in each group. $M = P + Q - 1$.

By selecting cyclic frequency α, we have eliminated the influence of noise and other signals. But in our application scenarios, there is another challenge. Multipath components from the same interference source are apparently correlated. If the multipath components are

fully correlated, the rank of $\mathbf{R}_{xx}^{\alpha}$ will be 1. This will degrade the performance of eigen-decomposition based algorithms or even make them infeasible. In order to increase the rank of CAF so that we can estimate all the multipath components, we adopts the *spacial smoothing algorithm* [102] to eliminate the correlation between multipath components.

An illustration of spacial smoothing is shown in Figure 4.4. We group the antennas in the array into P groups with Q antennas in each group. For group p, the cyclic correlation matrix R_p is calculated as in Equation 3.9.

The *spatially smoothed cyclic correlation matrix* is defined by

$$\bar{\mathbf{R}} = \frac{1}{P}\sum_{p=1}^{P}\mathbf{R}_p \tag{4.2}$$

It is proved that as long as the number of antenna groups is more than the number of multipath components, namely $P > K$, the spatially smoothed cyclic correlation matrix $\bar{\mathbf{R}}$ ranks K [102]. Thus, we can use MUSIC algorithm to calculate the AoAs of multipath components of the SoI by eigen-decomposition of $\bar{\mathbf{R}}$. Figure 4.5 compares the eigenvalues before and after spacial smoothing. There are two independent signal sources with four multipath components respectively in this example. Spacial smoothing successfully increases the detectable eigenvalues from six to eight.

Cyclic MUSIC Algorithm

The difference between *cyclic MUSIC* algorithm and conventional MUSIC algorithm [97] is that instead of the autocorrelation matrix, the decomposition of the *cyclic autocorrelation matrix* is leveraged here. Assuming that all signals are not fully correlated, we can then choose a cyclic frequency α, at which the K of them exhibit spectral correlation. Because of the frequency selection property of cyclic frequency α, the cyclic autocorrelation matrix of $\mathbf{i}(t)$ and $\mathbf{n}(t)$ are all zeros, and the cyclic cross-correlation between $\mathbf{s}(t)$ and $\mathbf{i}(t)$ and $\mathbf{n}(t)$ are also zeros. So we get

$$\mathbf{R}_{xx}^{\alpha} = \mathbf{A}\mathbf{R}_{ss}^{\alpha}\mathbf{A}^{*} \tag{4.3}$$

whose rank is K and $K < M$.

The rest of the cyclic MUSIC algorithm is the same as conventional MUSIC algorithm. It is worth noting that different from autocorrelation matrix, the CAF matrix $\mathbf{R}_{xx}^{\alpha}$ is not a Hermitian matrix. So the eigendecomposition method is not applicable here and the singular value decomposition (SVD) method must be applied.

Because of the signal selection property we stated above, Cyclic-MUSIC does not require higher number of antennas than the number of multipath components. Taking the unique

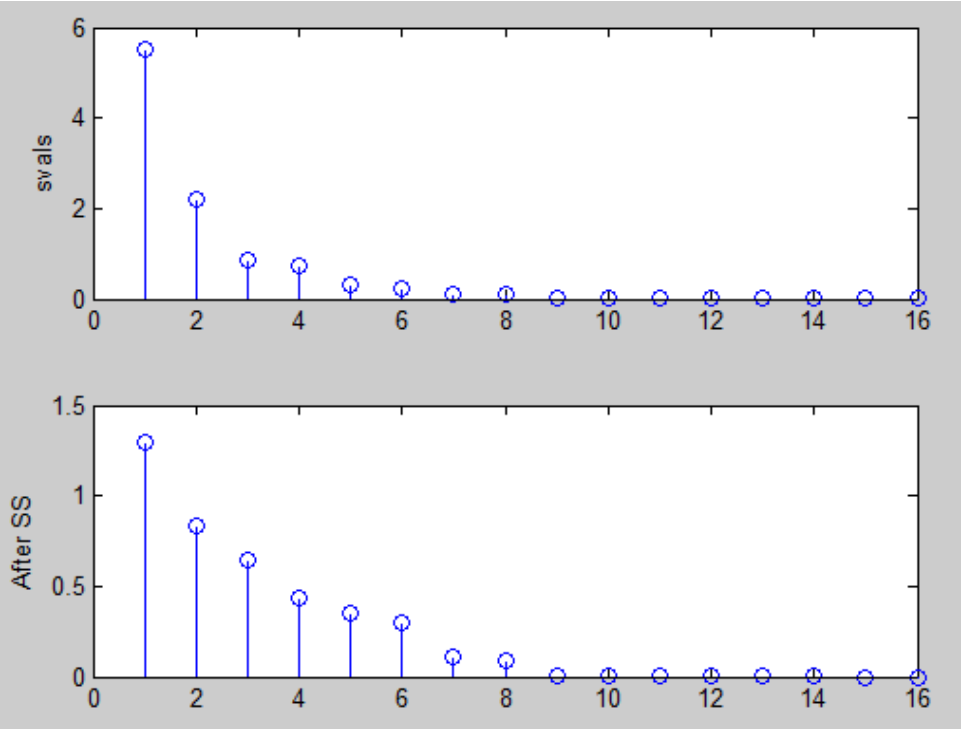

Figure 4.5: The eigenvalues before and after Spacial Smoothing. Spacial smoothing successfully increases the detectable eigenvalues from six to eight.

cyclic frequency of interfering radio as input, it successfully output the AoAs of only the interfering radio. Taking advantage of this property, we only need a number of antennas to separate the multipath components from only one signal source. In indoor environments, there are usually 5 multipath components that can be detected. As MobTrack is movable, the blocking effect of LoS is eliminated when moving around. So we equip MobTrack with 6 antennas as we can always find places where LoS component is in the strongest three.

4.3.3 Multipath Suppression

Now we get the directions of all the components of the interfering radio including both LoS and NLoS components. The next step is to isolate the LOS component in order to find the target interference. The algorithm we employ to achieve multipath suppression is motivated by the observation that LoS components and NLoS components have different stabilities with the movement of the device. As illustrated in Figure 4.6, the LoS component is continuous compared to discrete NLoS components when we move MobTrack and record the angle data. This is because if the location of MobTrack change successively, the angle between the target interference and MobTrack will change consecutively. But this is not true for multipath components, which bounce on walls or object surface which is inconsecutively themselves. Based on this observation, we develop an algorithm which can find the longest

continuous path in the angle-movement plane, which is the LoS component.

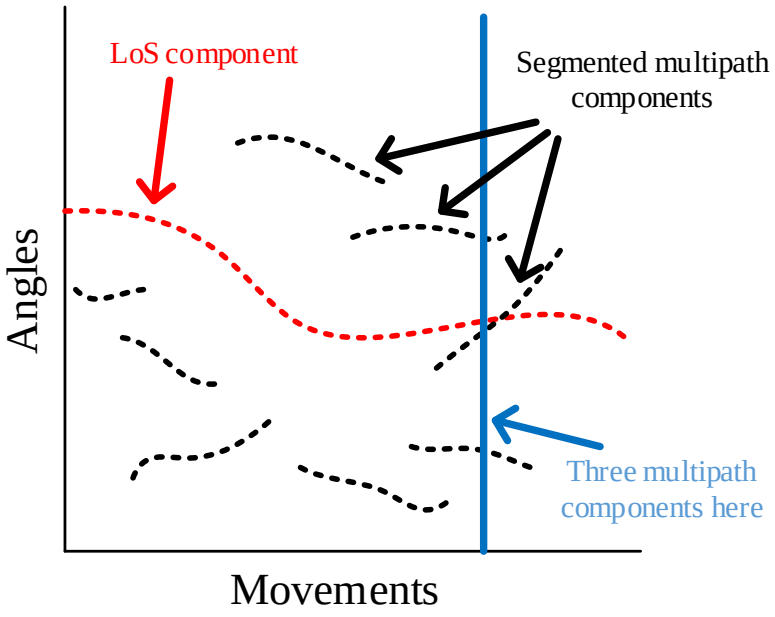

Figure 4.6: Multipath Suppression. We record the peaks and plot it as a dot in this figure. With the movement of MobTrack device, the LoS AoA changes continuously, but NLoS components will disappear intermittently. By finding the longest line, we can isolate the LoS component.

The multipath suppression algorithm is summarized in Algorithm 2. We name this algorithm LongestCurveFitting. It takes the AoA spectrum as the inputs, finds the peaks and records their coordinates. It then uses the Curve Fitting algorithm to test which curve line the peak dots belong to. If a curve line is segmented, it is removed from the candidate set. If there is only one curve line left in the candidate set, we terminate the function and set it as the LoS component.

An experimental result will be presented in Section 4.5. Using the above algorithm, we are able to find the LoS AoAs within a movement distance less than half a meter.

As long as we find the LoS AoAs from several points, we can estimate the source location using triangulation methods.

4.3.4 Triangulation

As MobTrack is a moveable or handheld device, we can simply find the interference by following the direction which MobTrack is pointing to. We run MobTrack continuously

Algorithm 2 LongestCurveFitting

```
Set the LoS candidate set 𝒮 to be Φ
while The LoS components is not found do
    Find the peaks on current AoA Spectrum
    For every peak do CurveFitting
    Find the current longest curve C
    if Length of C > L_TH then
        C is the line corresponding to LoS AoAs
    end if
end while
```

at different locations on the movement trace and then we adopt triangulation to estimate the location of interference with AoAs displayed. As shown in Figure 4.7, we observe that the directions which MobTrack points to will not intersect at a single point because of the estimation and measurement errors. Thus, we apply the well-known least square algorithm in linear algebra to calculate a single estimation point. When employing the least square method, the known variables are the 2D locations of the MobTrack and the θs in the figure while the unknown variables are the 2D location of the estimation point. The matrix A and vector b in Ax = b are formed by the 2D locations of the MobTrack and the θs. Because the directions which MobTrack points to can not form a single point, so Ax = b will have no solution. Then we project vector b onto the column space of matrix A to get the projection vector p. By solving Ax = p, we get the single estimation point we desire.

4.4 Implementation

We implement the MobTrack prototype on Ettus USRP software defined radio platform, as shown in Figure 4.8. The system consists of 6 USRP-N200 software defined radio platform. Four of the USRP devices are equipped with a daughterboard XCVR2450, and two of them are equipped with a daughterboard SBX, which provides the support of 2.4GHz WIFI channel. The distances between antennas are set to be 6.13cm, which is half the wavelength of 2.4G signal.

Figure 4.9 explains the connections between the devices of our prototype. Every two of the six USRPs are connected using a MIMO cable, which provide communication as well as synchronization between them. The master USRP in each group is connected to the host computer via a Gigabyte Ethernet switch. Another USRP N200 works as a phase reference tone provider. The transmit antenna of this USRP is cable connected to the six receivers using an SMA (SubMiniature version A) splitter. The cables have the same length, which provide the receivers a stable reference tone. The master USRP in each group as well as the reference transmitter are all connected to an external clock, which provides a

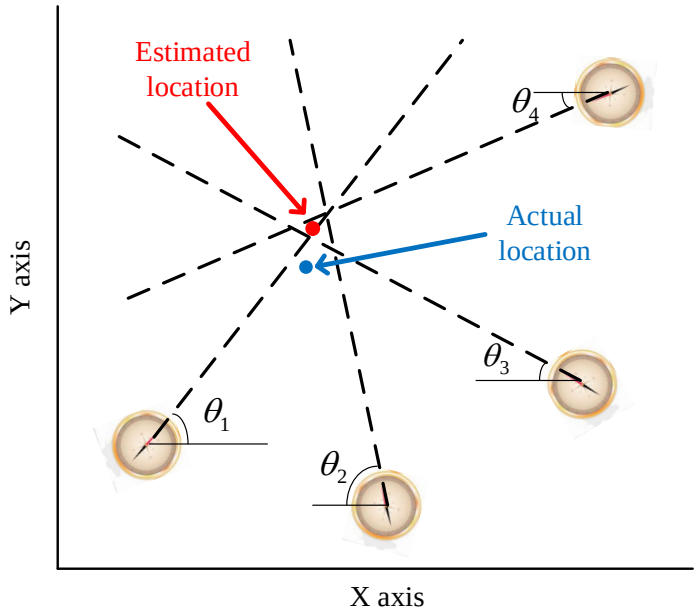

Figure 4.7: MobTrack Triangulation. We apply the well-known least square algorithm in linear algebra to calculate a single estimation point. When employing the least square method, the known variables are the 2D locations of the MobTrack and the θs in the figure while the unknown variables are the 2D location of the estimation point.

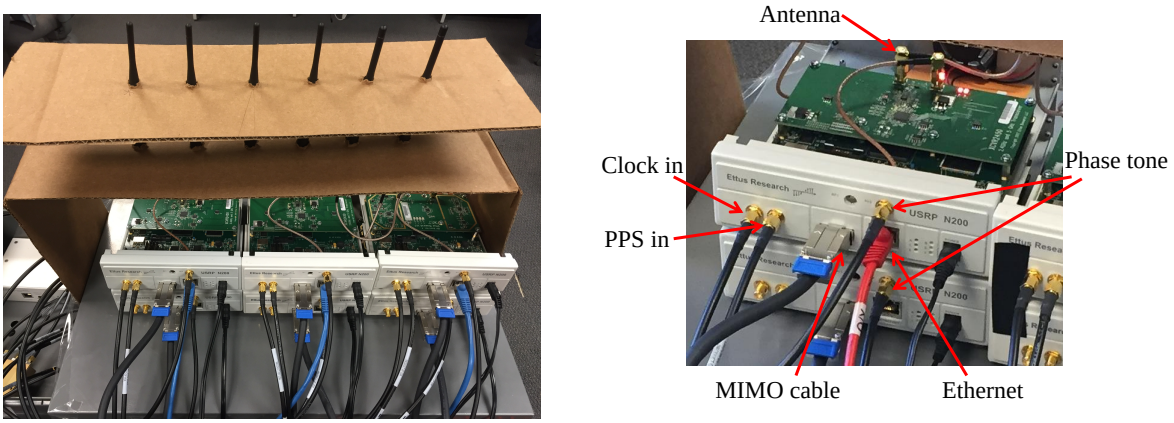

Figure 4.8: Prototype implementation. The MobTrack prototype is composed of six USRP radios mounted on a movable case, which form an antenna array. Another USRP works as the phase alignment reference, and one more works as the interferer(not shown in picture).

synchronized 10MHZ reference clock and the PPS signal for the purpose of frequency and time synchronization.

The phase reference tone and signals received over the air are sampled to GNURadio. Two band pass filters are used to split them into separate data streams. The data streams are

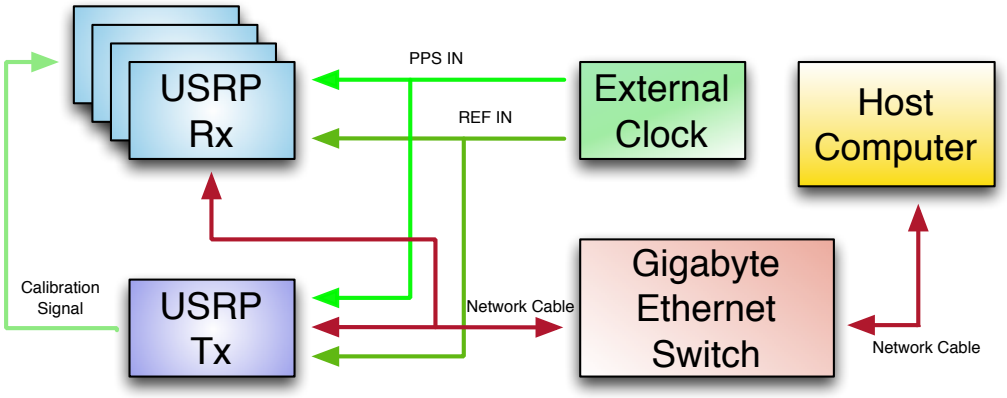

Figure 4.9: MobTrack prototype connections.Every two of the six USRPs are connected using a MIMO cable. The master USRP in each group are connected to the host computer via a Gigabyte Ethernet switch. All master USRPs are connected to an external clock for time and frequency synchronization. A phase reference tone is provided by another USRP.

then transmitted to a Matlab script via a named pipe. The phase differences are calculated from the phase reference tone and compensated to data streams over the air. And then start our interference identification process.

4.4.1 Time and Frequency Synchronization

Every two USRP N200s are a group and are synchronized with the USRP MIMO cable. The master USRP in each group as well as the reference transmitter are all connected to an external clock, which provides a synchronized 10MHZ reference clock and the PPS signal for the purpose of frequency and time synchronization.

We use a Ettus OCTOCLOCK-G 8-Channel clock distribution module with integrated GPS disciplined oscillator (GPSDO) [4] as the clock and PPS source. The *Ref In* ports of the master USRPs are connected to the 10 MHz reference from which the ADC/DAC clocks and local oscillator are derived. The *PPS In* ports can be used as a standard pulse per second port or as a general purpose digital trigger input line.

4.4.2 Phase Synchronization

Beamforming and direction finding applications place additional requirements on the antenna array and sampling system. In addition to time and sample clock alignment, the system must maintain a known phase relationship between each RF input. Due to phase ambiguities caused by phased- locked loops which are used for up and down-conversion, some calibration may be required to determine this phase relationship [9].

For phase synchronization, we use a reference tone generated from another USRP (phase tone USRP) to calibrate the multi-channel system. The tone is split using an SMA splitter and then distributed to the inputs of each master USRP device with match-length RF cables. The reference tone we use is a 10kHz sine wave as shown in Figure 4.10.

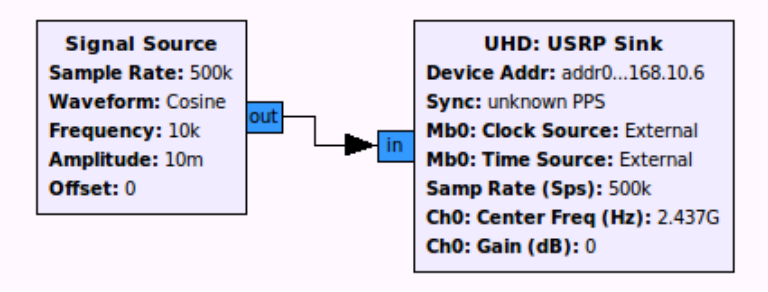

Figure 4.10: The GRC flowgraph for phase tone USRP. We use 10kHz sine wave as the phase tone signal.

The phase reference tone is transmitted to the host computer via the Ethernet. For each USRP receiver, we applied two band pass filters to separate the reference tone and the over-the-air signal as shown in Figure 4.11. This is figure is not a complete version for the purpose of simplicity. We only show the filter channels of one USRP. The other USRPs use the filters with the same parameters.

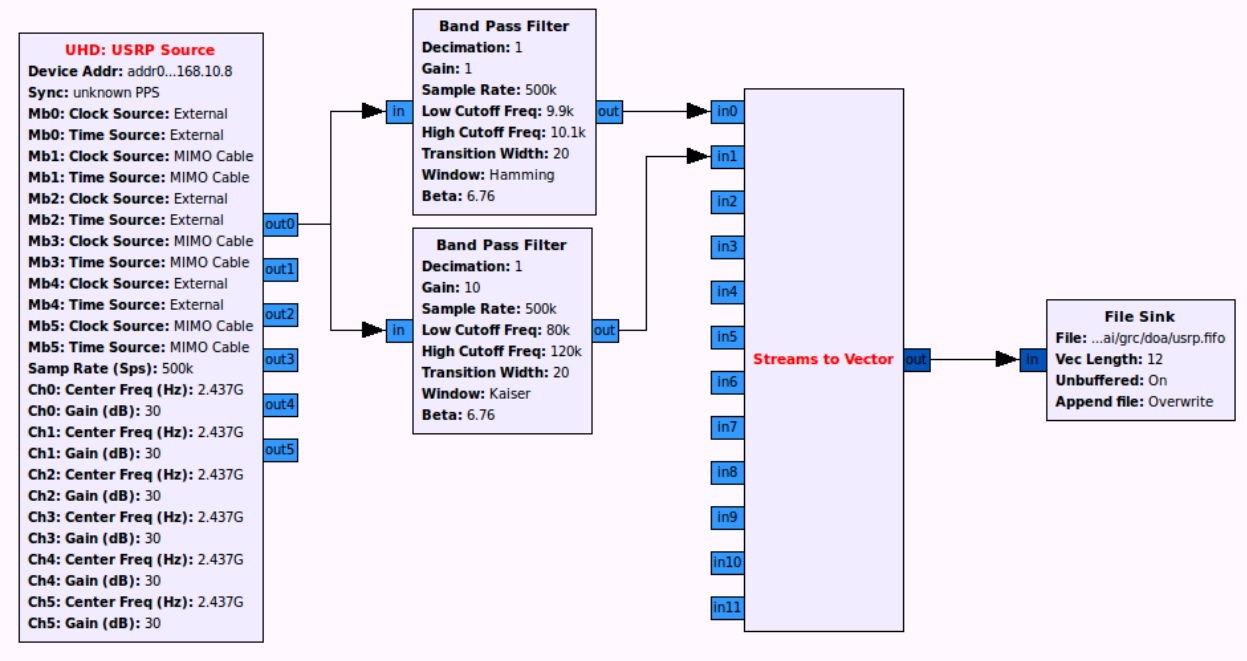

Figure 4.11: The GRC flowgraph for the antenna array. This is figure is not a complete version for the purpose of simplicity. We only show the filter channels of one USRP. The other USRPs use the filters with the same parameters.

The phase was then synchronized using a piece of phase compensation Matlab code:

$air(:, n) = air(:, n). * exp(-1i * angle(direct(:, n)));$

where *air* is the split over-the-air signals, *direct* is the split reference tone signals, and n is the index of USRP devices.

4.5 Performance Evaluation

To illustrate the performance of MobTrack in real indoor environments, we present experiment results in this section. We first describe the test bed setup methodology. The we present an experimental results of LoS signal stability. After that, we present the location accuracy MobTrack can achieve, comparing with the results of Pinpoint. We also explore the effects of number point we use to do triangulation on the movement trace on the performance of MobTrack.

4.5.1 Test Bed Setup

The location performances are evaluated on a test bed over one floor of our department building, as shown in Figure 4.12. The interfering radio is placed at the blue point in Room 314, which is in the same room as the WiFi AP. Our device follows the trace in the figure on the same floor. Most of the test points are in the hall and some of them are in the lab mentioned above. The distance of the whole trace are 20 meters. Along this trace, we take a measurement every 25 centimeters. The ground truth are measured before the experiment with an accuracy of 1cm.

4.5.2 LoS Signal Stability

To illustrate the difference of stabilities between LoS component and NLoS components, we set up an experiment in our office room. The transmitter works at frequency 2.437GHz (Channel 6) and locates in the same room as the MobTrack device. The distance between the transmitter and MobTrack is 172cm. We move MobTrack along the parallel direction of the antenna array and the transmitter. In a distance of 1 meter, we record the angles of arrive estimated by MobTrack, including both LoS and NLoS components. The results are shown in Figure 4.13. The distance between each location is 2.5cm. As we can see from this figure. The LOS component AoA changes from 0 degree to about -26 degree following a continuous curve. Our curve fitting algorithm finds this line as the longest successfully.

On the other hand, NLoS components change intermittently. We list the percentage of segmented curves in this Figure 4.13 using LongestCurveFitting algorithm. From Table 4.1, we can see that most of the distance of multipath components is about 15cm, which means that by moving MobTrack for 15cm, the multipath components almost always change their

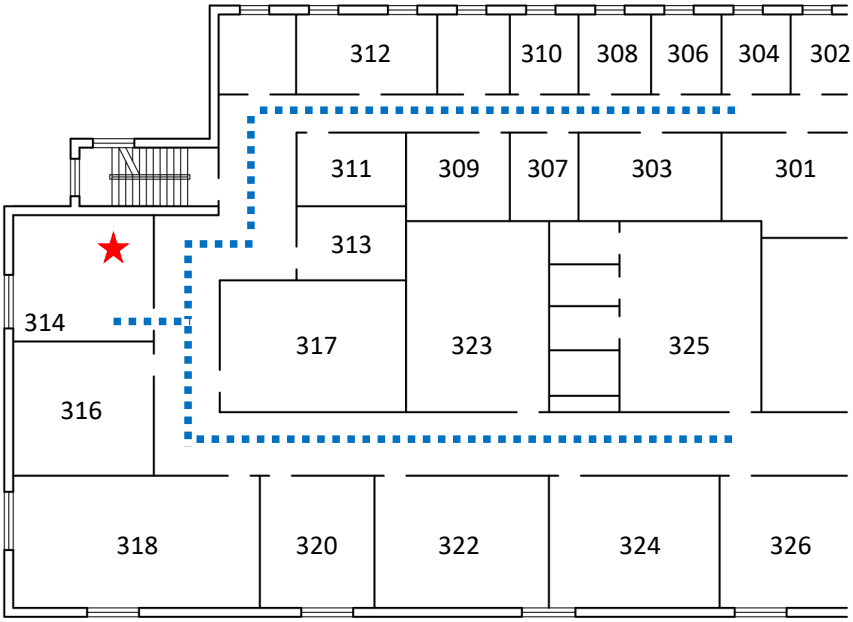

Figure 4.12: Test bed. This figure is a part of the floor our lab sits on. The dotted line in this figure is the trace of executed experiments. The blue point in the lab is the interfering radio we would like to locate. Following the trace, we conduct a test per 25 centimeters.

impinging direction. This experiment verifies that our multipath suppression algorithm is feasible.

Table 4.1: Percentage of segmented multipath curves

Distance	5cm	10cm	15cm
Percentage of Segmented	30%	75%	95%

4.5.3 Localization Accuracy with Different Calculation Points

This section presents the localization accuracy changes with different calculation points. In Figure 4.14, we estimate the location of interfering radio by the information provided by MobTrack at different locations. We employ respectively 2, 3, 4 and 5 different locations in the triangulation step in our estimation. We can see that the more locations we select to do the calculation, the more accurate results we can achieve. The distances between two locations range from 10cm to 1 meter. We prefer to use longer distance because the longer distance between the points, the better performance it will achieve. Estimating in 5 locations, MobTrack achieves a median localization error of 0.55 meter. Comparing with Pinpoint locating the interfering radio using 5 static APs with accuracy of 0.97 meter, our

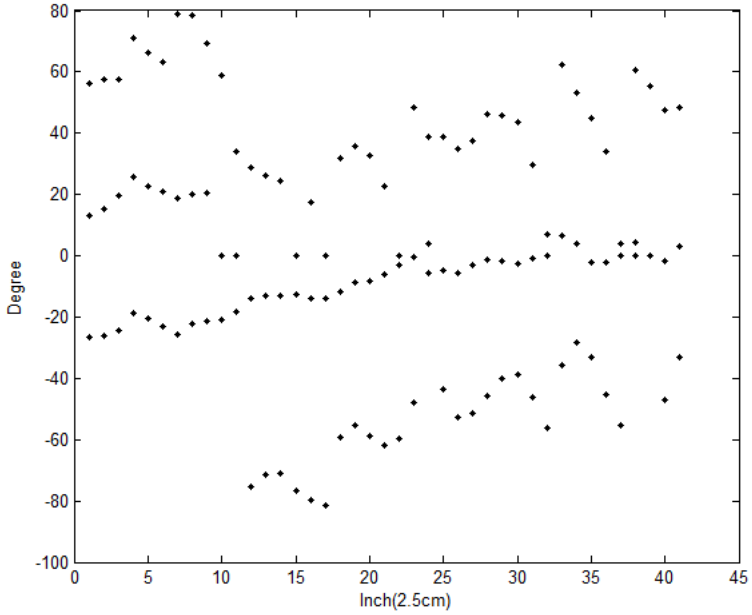

Figure 4.13: The stability of LoS and NLoS components. The distance between the transmitter and MobTrack is 172cm. The distance between each location is 2.5cm.

scheme performs better. The reason for this better performance is that, MobTrack starts estimating the location from the second point and leads moving towards the target. It will perform the estimation repeatedly. At the 5th point, MobTrack has moved 4 meters at most towards the interfering radio. Besides, MobTrack's antenna array contains 6 antennas, while Pinpoint has 4 antennas.

4.5.4 Localization Accuracy with Different Moving Distances

As shown in Figure 4.15, we also test if we can achieve a valuable estimation within a short distance. We calculate the location from 5 locations within different distances. And the results shows we can achieve an accurate estimation even if we only move around a meter. If we want to make an estimation in half a meter, the accuracy drops, but still it can tell the location with a median location error of 2 meters. This is vital for us, because MobTrack is a single device designed for users to carry with them, with the ability to find the interference in a meter, MobTrack is proved practical.

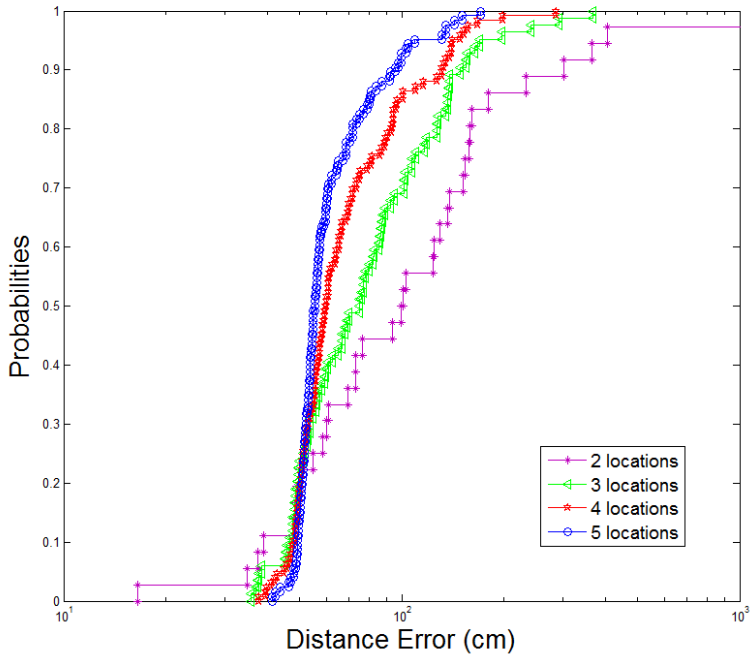

Figure 4.14: Localization Accuracy with Different Calculation Points. The median error is 0.55m estimating from 5 locations.

4.6 Summary of Contributions

MobTrack is a single device system that can locate indoor interfering radios with sub-meter accuracy. Comparing to previous solutions, it significantly reduces the requirement to AP infrastructure and the number of antennas. By moving the device around for a short distance within several meters, it depresses multipath effects and determines the LoS component. Simultaneously, the AoAs at these locations are recorded to estimate the location of the interfering radio by triangulation methods. In order to decrease the physical size of this device and make it suitable for handhold, the method of synthetic array can be explored where the number of antennas can be further reduced to two.

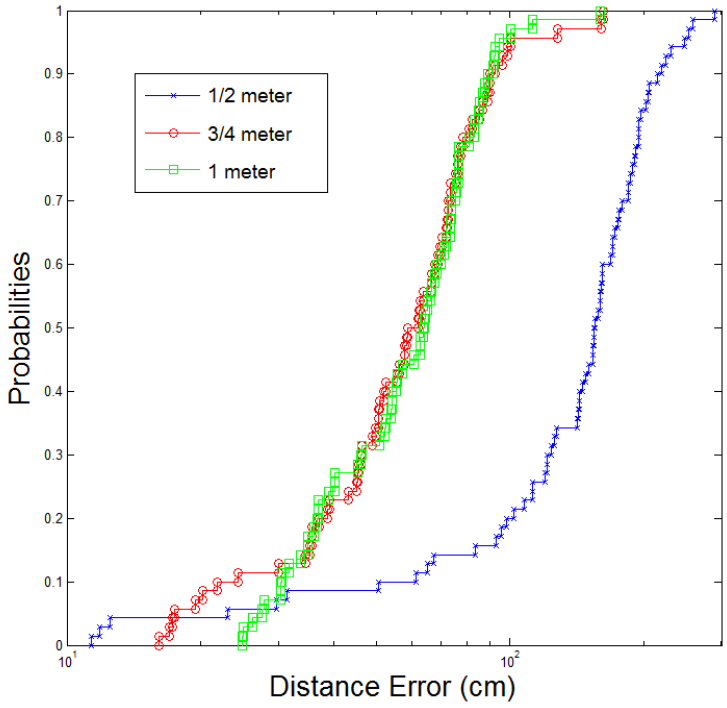

Figure 4.15: Localization Accuracy with Different Moving Distances. The longer distance between the calculation points, the more accurate MobTrack achieve.

Chapter 5

Context-Free Fine-Grained Motion Sensing using WiFi

In this chapter, we introduce the research work on WiFi based fine-grained motion sensing. This is the second research area that we explore under the topic of wireless sensing. Unlike interference localization, in wireless motion sensing, the wireless signal transmitter and receiver are both parts of the system. We take advantages of the signal reflection to sense the motion of human body. We first briefly talk about the concept of CSI and the preliminary of CSI-based motion sensing. The six steps of the system work flow are then presented in detail, among which we concentrate on interference elimination and feature extraction. We implement and evaluate the system design using the lip reading application.

5.1 Motivation and Objects

WiFi-based motion sensing has received a lot of research attention in recent years, leveraging the fact that human motion will change the channel states between transceivers. By monitoring these channel state changes, researchers are able to extract useful information to infer human motion. Channel State Information(CSI) is one of the most popular measurements for the purpose of motion sensing because it provides more fine-grained channel information than Received Signal Strength Index(RSSI). CSI is the time series of the channel frequency responses(CFR) which can be collected from physical layer of off-the-shelf WiFi devices thanks to the previously released CSI collecting tools [48, 124].

Previous work on human motion sensing has made grate effort focusing on several application scenarios like human localization [122, 129], activity detection and recognition [117, 119], human authentication [116, 133], health care [69, 114] and fine-grained motion sensing [13, 67, 110, 113, 142]. Using a quadrant classification method, we position these previous research works and the proposed work in this chapter in Figure 5.1. The four quadrants

are determined by whether the motion to be detected is coarse-grained or fine-grained, and by whether the detection is context-free or not. For example, E-eyes [119] can recognize human activities by comparing the testing CSI measurements to a set of CSI profiles. The CSI profiles constructed in time domain are not the same in different contexts such as at different locations. E-eyes needs to set up a profile group for a single human activity. We classify E-eyes into quadrant III as a coarse-grained context-related solution. On the other hand, CARM [117], WifiU [116] extract features from CSI spectrograms in time-frequency domain. CSI spectrogram is proved to be intrinsically correlated to the moving speed of different human body parts but not correlated to contexts. We classify them into quadrant II as coarse-grained context-free solutions. The work proposed by Liu *et al.* [69] makes use of channel information in both time and frequency domain to capture human breathing rate and heart rate. These scalar values of vital signs are estimated in frequency domain and are uncorrelated to contexts. Thus we also classify it into quadrant II.

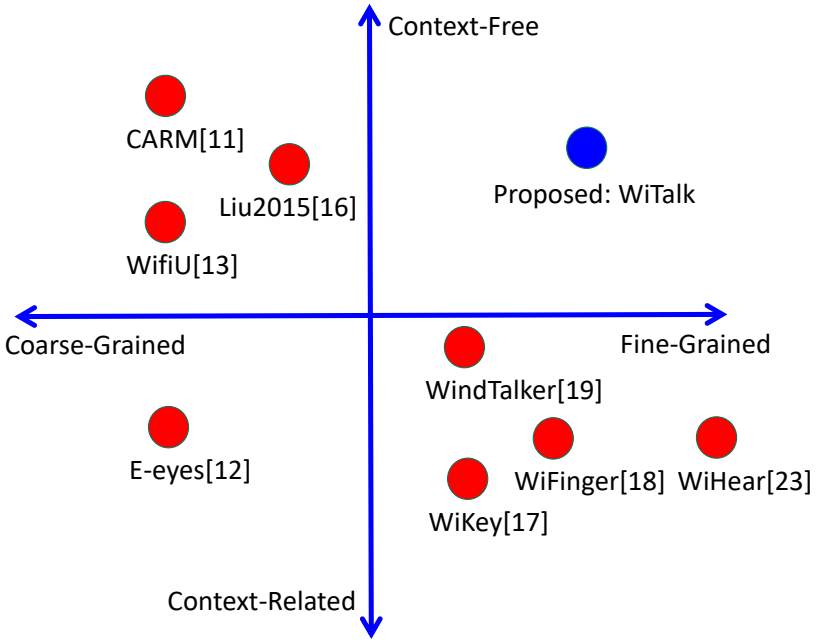

Figure 5.1: Research Position. The interpretation of the four quadrants classification method. We classify the works in the literature according to whether they are fine-grained or course-grained, and whether they are resilient to context change.

In the right half plane of Figure 5.1, existing fine-grained motion sensing solutions construct the CSI profiles in time domain. Time domain CSI profiles are subject to changes of contexts, including changes of locations, users or multipath environments. For example, WiKey [13] recognizes keystrokes based on *CSI-waveform* for each key. WindTalker [67] inferences mobile device keystrokes exploiting the strong correlation between the CSI fluctuation and the keystrokes. WiFinger [110] senses and identifies subtle movements of finger gestures by examining the unique patterns in CSI. WiHear [113] detects and analyzes fine-grained radio reflections from mouth movements by introducing Mouth Motion Profile. These solutions

are all context-related. They require the construction and testing of the CSI profiles in the same contexts. For a different user, different location, or a different multipath environment, the profiles need to be reconstructed. We classify them into quadrant IV as fine-grained context-related solutions.

The piece of work follows the bottom-up research method. Three type of information that can be analyzed from CSI streams are identified, the waveform, the frequency and the time-frequency spectrogram. Using these information and mainly the machine learning tools, previous work implemented the various applications as shown in Figure 5.2. WiTalk follows the solution roadmap from CSI to spectrogram to fine-grained motion detection.

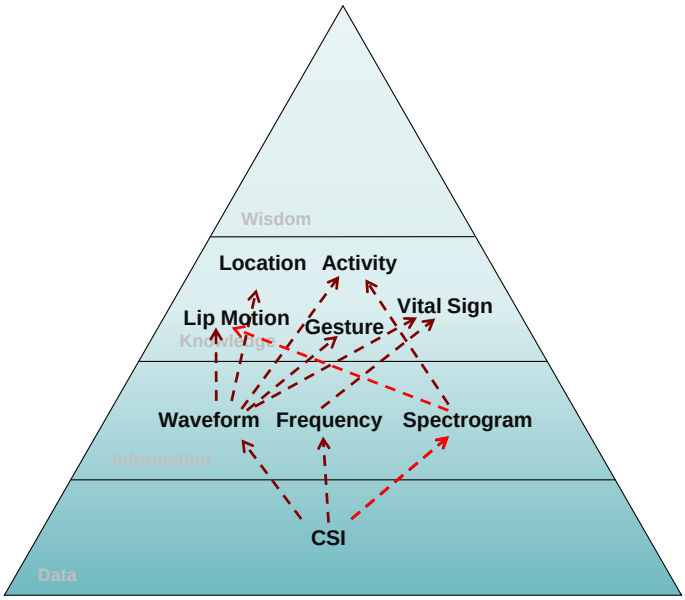

Figure 5.2: The research roadmap. WiTalk follows the solution roadmap from CSI to spectrogram to fine-grained motion detection.

To design a context-free fine-grained motion sensing solution in quadrant I, some specific *challenges* that differ from previous research settings must be addressed. First, WiFi signal reflections from fine-grained human motion are very tiny, much smaller than those from large-scale human movements. CSI dynamics caused by fine-grained human motion are easily buried in noise and interferences. To ensure the CSI dynamics to be detectable, previous solutions make some assumptions or use special tools. For example WiKey [13] assumes that the tested motion takes place near one end of the transceivers. WiFinger [110] assumes that the tested motion takes place near the line of sight(LOS) between the transceivers. WiHear [113] and WindTalker [67] use special purpose directional antennas to enhance signal-to-noise ratio(SNR) in CSi dynamics. Second, effective denoise methods must be adopted to reduce noises and interferences and obtain a clean CSI waveform that reflects the motion to be detected. Third, to design a context-free solution, intrinsic properties in CSI dynamics that

are only correlated to fine-grained motion to be detected must be identified. To effectively detect the fine-grained motion, feasible features must also be carefully identified and selected.

In this chapter, we present WiTalk, the first context-free fine-grained motion sensing system using WiFi physical layer channel information. Similar to previous CSI-based motion sensing solutions, WiTalk infers human motion by analyzing the CSI dynamics. To effectively denoise CSI streams, we use principal component analysis(PCA) filtering methods based on the observation that signal fluctuations on all subcarriers are correlated. To address the context-free challenge, we identify CSI spectrogram in time-frequency domain as the stable property in CSI dynamics and extract features from CSI spectrograms by calculating the contours of the spectrograms.

We verify the feasibility and performance of WiTalk in the application scenario of lip reading. To ensure that the CSI dynamics generated by mouth movements are detectable, we make similar assumptions as in previous solutions. Specifically, we assume that mouth movements take place near one end of the transceivers similar to [13], based on the observation that people tend to hold the phone close to the cheek while talking over the phone. Directional antennas can also be used to further amplify CSI dynamics and eliminate CSI noises. We leave this as future research work.

The main contributions of WiTalk are summarized as follows:

- To the best of our knowledge, WiTalk is the first feasible system in the context-free fine-grained quadrant of motion sensing solution plane using WiFi CSI dynamics. We show the existence of this quadrant I solution by identifying the CSI spectrograms as the intrinsic stable properties that correlate to fine-grained human motion.
- We identify and extract effective features from CSI spectrograms by calculating the contours of CSI spectrograms. These new discerning features solve the problem of low time-frequency resolution using discrete wavelet transform(DWT).
- We verify the feasibility of WiTalk by applying it to the lip reading scenario. Experiment results show that WiTalk achieves comparable results to previous fine-grained context-related solutions.

We implement WiTalk on a commercial laptop and demonstrate its feasibility through experiments. The performance is evaluated under various contexts with different transceivers distances, different locations and users. The results show that WiTalk can achieve over 92.3% recognition accuracy to discern a set of 12 syllables and 74.3% accuracy to discern a set of short sentences up to six words.

The rest of the chapter is organized as follows. We discuss related work in Section 5.2 and introduce the technical background in Section 5.3. The system design is detailed in Section 5.4. The performance of WiTalk is verified in Section 5.5 under the lip reading scenario. We conclude the chapter in Section 5.6.

5.2 Related work

Motion sensing. Motion sensing based human localization, human tracking, gesture and activity recognition have been studied a lot in the research community. Existing work on motion sensing can be divided in three categories: vision-based, sensor-based and RF-based.

The most popular approaches for video gaming and virtual reality platforms are vision-based. Such systems include Microsoft Xbox Kinect [2], Leap Motion [3], and Sony PlayStation Camera [5]. They use color and infrared cameras to do body-depth perception, motion tracking and gesture recognition. The main problem of vision-based motion sensing is that its performance is highly influenced by the condition of lighting. These systems also require line-of-sight (LOS) for proper operation.

Wearable device based methods like RF-IDraw [115] traces trajectory of fingers and hands by attaching RFID to the fingers. Xu et. [126] uses smartwatch to identify 37 gestures with an accuracy of 98%. TypingRing [83] asks the users to wear a ring for text inputting with the capability of detecting and sending key events in real-time with an average accuracy of 98.67%.

Earlier work on RF-based motion sensing rely on specialized hardware. WiTrack [11] tracks 3D human body motion using an FMCW(Frequency Modulated Carrier Wave) radar at the granularity of 10cm. WiSee [89] works by looking at the minute Doppler shifts and multi-path distortions for gesture recognition. Google Project Soli [6] uses on-chip 60GHz radar to detect fine-grained motion. However, the short effective range limit its application in long distance scenarios.

CSI-based method like CARM [117] builds a CSI-speed model and a CSI-activity model, which depicts the relationship between CSI value dynamics and human body parts movement speeds, and the relationship between the body movement speeds and specific human activities. CARM is coarse-grained as it discerns human activities like walking, falling and sitting down. Different from CARM, WiTalk is fine-grained and reads the motion of human mouth. CARM also requires a sampling rate as high as 2500 samples per second. It is very difficult to reach such high sampling rate in WiTalk scenario. WiKey [13] uses CSI waveform shape as the features and can recognize keystrokes in a continuously typed sentence with an accuracy of 93.5%. WiKey works well only in controlled environments and specific devices positioning. WiFinger [110] also uses CSI waveform shape as the features and can discern 8 finger gestures with 93% recognition accuracy. WiFinger also requires static transceivers and finger motion must be near the LOS line of the transceivers. Different from WiKey and WiFinger, WiTalk removes the limitation of static transceivers and works on mobile devices. WindTalker [67] allows an attacker to infer the sensitive keystrokes on a mobile device using CSI. However, WindTalker requires that the mobile device being placed in a stable environment. Wi-Wri [22] uses WiFi signals to recognize written letters. WiDraw [104] leverages WiFi signals from commodity mobile devices to enable hands-free drawing in the air. These two projects focus on the user's hand trajectory tracking, which is not WiTalk's research

target. The most related work to our work is WiHear [113]. Our work is inspired by WiHear, but we must point out that the system setting and techniques used are significantly different. WiHear uses specialized directional antennas to obtain usable CSI variations. It takes 5-7 seconds for stepper motors to adjust the emitted angle of the radio beam to locate the target's mouth, which is not acceptable for a real-time eavesdropping system in our setting. Furthermore, WiHear does not have enough noise filter mechanisms. It still needs the training process per location per user. On the other hand, WiTalk can be implemented on commercial WiFi devices and has the one-time training feature.

Lip reading. [34] present a combination of acoustic speech and mouth movement image to achieve higher accuracy of automatic speech recognition in noisy environment. [61] presents a vision-based lip reading system and compares viewing a person's facial motion from profile and front view. [32] shows the possibility of sound recovery from the silent video. SilentTalk [109] generates ultrasonic signals from mobile phone and analyzes the frequency-shift caused by mouth movements from the reflections. It can identify 12 basic mouth motion up to 95.4% accuracy. Chung et. [31] presents their recent results on lip reading which performs better than hum pros. The system was trained using 5000 hours of videos including 118,000 sentences.

5.3 CSI Preliminary and CSI-Speed Model

CSI-based motion sensing researches rely on the same principle that the change of CSI values has correlation with the motion to be detected. In this section, we briefly introduce the CSI related backgrounds, especially the CSI-speed model proposed in [117].

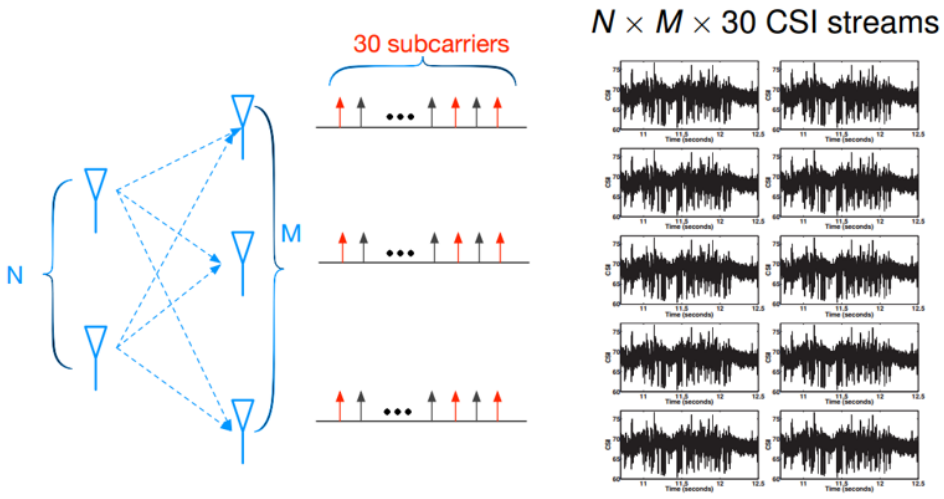

Figure 5.3: CSI streams. The time-series of the CSI matrix contains $30 \times N_{tx} \times N_{rx}$ CSI streams.

In WiFi protocols like IEEE 802.11a/n/ac, Orthogonal Frequency Division Multiplexing

(OFDM) is adopted as the modulation format. In OFDM, the channel frequency response (CFR) is measured on subcarrier level. Let $X(f,t)$ and $Y(f,t)$ be the transmitted and received signals in frequency domain respectively, then we have $Y(f,t) = H(f,t)X(f,t)$, where $H(f,t)$ is the CFR at frequency f and time t. As the FFT/IFFT operations are integrated in OFDM receivers, the receivers are ready to calculate CFRs. Taking advantage of the released tools [48, 124], CFR values are revealed from NIC firmware to drivers and then to upper layers in the format of CSI. In IEEE 802.11 standards, CFRs on 30 selected subcarriers are reported for every received 802.11 frame. If a WiFi link has N_{tx} and N_{rx} of emitting and receiving antennas respectively, then the reported CFRs form a *CSI matrix* in dimensions of $30 \times N_{tx} \times N_{rx}$. A CSI matrix is instantaneous. For a specific subcarrier on an antenna pair, we name the time-series of CFRs a CSI stream. Then the time-series of the CSI matrix contains $30 \times N_{tx} \times N_{rx}$ CSI streams. We can see that CSI characterizes the frequency response of the wireless channels. Please refer to Figure 5.3 for the definition of CSI streams.

In indoor environments, wireless signals arrive at a receiver antenna through multiple paths including the LOS path, paths reflected by static objects like walls and paths reflected by moving objects like human body. The signals transmitted through these paths have different amplitudes and phases. The CFR can be modeled as the sum of static and dynamic components [117]:

$$H(f,t) = e^{-j2\pi\Delta f t}(H_s(f) + H_d(f,t)) \tag{5.1}$$

where Δf is the carrier frequency difference between the sender and the receiver, $H_s(f)$ is the sum of static CFRs and $H_d(f,t)$ is the sum of dynamic CFRs:

$$H_d(f,t) = \sum_{k \in \mathscr{P}_d} a_k(f,t) e^{-j2\pi \frac{d_k(t)}{\lambda}} \tag{5.2}$$

where $\mathscr{P}_d$ is the set of dynamic paths, a_k is the attenuation and initial phase of k^{th} path and $d_k(t)$ is the length of path k at time t. If the static and dynamic components are in phase, the dynamic components are constructive factors, otherwise, they are desctructive factors.

The power of the CFR can be calculated to eliminate Δf:

$$|H(f,t)|^2 = \sum_{k\in\mathscr{P}_d} 2|H_s(f)a_k(f,t)|cos\Big(\frac{2\pi v_k t}{\lambda} + \phi_k(0)\Big)$$
$$+ \sum_{\substack{k,l\in\mathscr{P}_d \\ k\neq l}} 2|a_k(f,t)a_l(f,t)|cos\Big(\frac{2\pi(v_k - v_l)t)}{\lambda} + \phi_{k,l}(0)\Big)$$
$$+ \sum_{k\in\mathscr{P}_d} |a_k(f,t)|^2 + |H_s(f)|^2 \tag{5.3}$$

where $\phi_k(0)$ and $\phi_{k,l}(0)$ are initial phase and phase difference. The total CFR power is the sum of a constant offset and a set of sinusoids. The frequencies are functions of the speeds of path length changes, which is further correlated to human movement speed. This CSI-speed model is the technical principle of using CSI dynamics to detect human motion.

5.4 System Design

The design of WiTalk is illustrated in Figure 5.4. It consists of the following components: CSI data collection and preprocessing, interference elimination, segmentation, feature extraction, classification and error correction. In this chapter we mainly focus on three components: interference elimination, feature extraction and classification. We will briefly introduce CSI data collection and preprocessing, segmentation and error correction components because they are not the core contributions of this work.

5.4.1 Feasibility Analysis and Verification

We take lip reading as the example to analyze if it's feasible to do fine-grained motion sensing based on CSI dynamics. We make a reasonable assumption that when a person talks over the phone, he/she tends to hold the phone close to the mouth, specifically, with the top receiver covering the ear and the bottom microphone close to the mouth. We empirically assume that the mouth is less than 10 centimeters from the WiFi antenna of the phone. The analysis tool that is ready to use here is the Fresnel zone model [114].

When a signal is reflected, the phase of the signal reverses and its phase changes by $\pi/2$. The reflected path is longer than LOS path, so the signal phase is shifted further by the difference in path length. Fresnel zones refer to the concentric ellipses with foci in a pair of transceivers. As shown in Figure 5.5, T and R are the transmitter and receiver respectively. For every point Q on the blue lines, the distance of the multipath reflected at Q must be $n\lambda/2$ longer than the LOS path, that is:

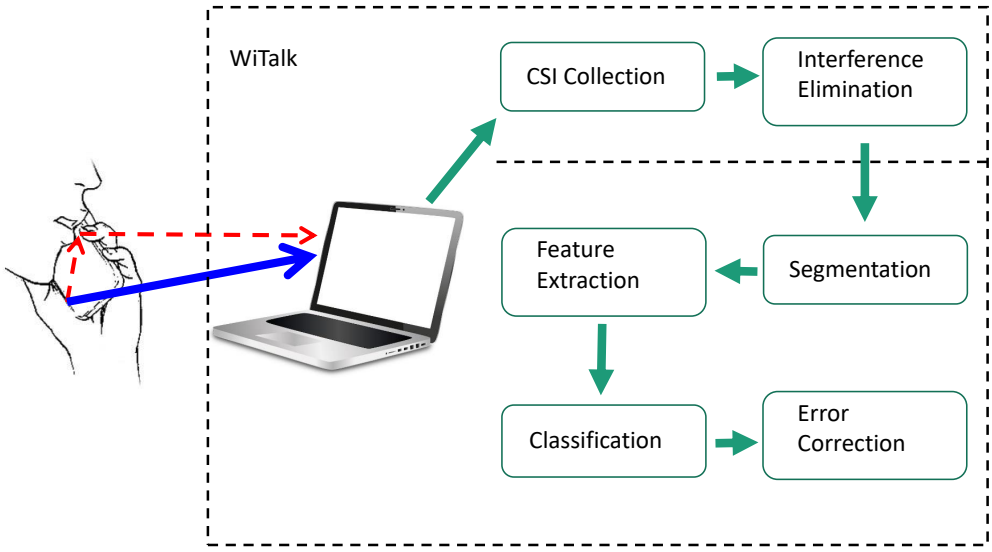

Figure 5.4: WiTalk System Design and Workflow. We take lip reading as an application example but it can be extended to any fine-grained motion detection.

$$|TQ| + |QR| - |TR| = n\lambda/2 \tag{5.4}$$

For the first Fresnel zone $F1$, the phase shift between the reflect and LOS path is path length difference π plus π at the reflection point, that is 2π. The two signals are in phase and the reflected signal is constructive. Similarly, other odd fresnel zones are also constructive and even fresnel zones are destructive.

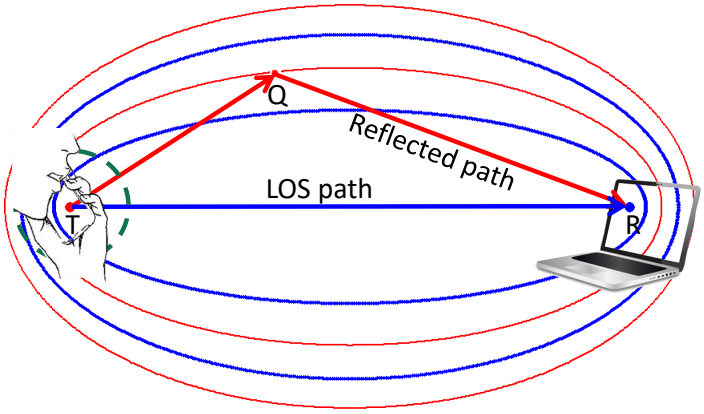

Figure 5.5: The first 4 Fresnel zones for $5.18GHz$ WiFi signals. Human mouth is in the first 4 fresnel zones when human talking over the phone.

Figure 5.5 shows the first 4 Fresnel zones for $5.18GHz$ WiFi signals where the wavelength is

about 5.8cm. According to the previous research, the significant zones for RF transmission are the first 8-12 zones, more than 70% of the energy is transferred via the first Fresnel zone [114]. The dotted green circle in Figure 5.5 has a radius of 10cm, which locates in the first 4 Fresnel zones. So it's reasonable for us to assume that the smartphone WiFi signals reflected from the mouth have some good level of energy.

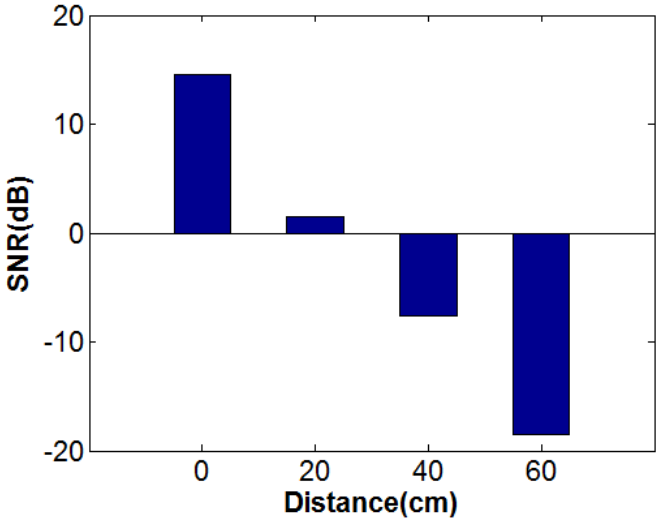

Figure 5.6: CSI SNR change with the distance of mouth and smartphone. When the distance is over 20cm, the SNR is near 0.

We verify whether the reflected energy is strong enough to be detected through experiment. We set the distance between the phone and the laptop to 1 meter at the same height in a normal lab environment. A speaker stays still and pronounces /æ/ for 5 times at an interval of 2s. The speaker then moves in the perpendicular direction of the LOS path for 20cm and repeats this process. The SNR results are shown in Figure 5.6. With the distance of human mouth to the phone antenna increases, the signal power decreases sharply. However, when the human mouth is close enough to the phone, the SNR is about 15dB, indicating it's feasible to do smartphone lip reading based on CSI dynamics.

5.4.2 CSI Data Collection and Preprocessing

WiTalk is implemented on the receiving end of a WiFi link and collects CSI measurements on each received packets. For each pair of sending and receiving antennas, 30 CSI streams are collected.

Different from the previous works which rely on two devices including both of the sender and the receiver to collect CSI data, we apply an approach that leverages Internet Control Message Protocol (ICMP) in hotspot to collect CSI data during the user accesses to the pre-installed access point. In particular, WindTalker periodically sends a ICMP Echo Request

to the victim smartphone, which will reply an Echo Reply for each request. To acquire enough CSI information of the victim, WindTalker needs to send ICMP Echo Request at a high frequency, which enforces the victim to replay at the same frequency. In practice, WindTalker can work well for several smartphones such as XiaoMi, Samsung and Nexus at the rate of 800 packets per second. It is important to point out that this approach does not require any permission of the target smartphone and is difficult to be detected by the victim. ICMP based CSI collection approach introduces a limited number of extra traffic. For a 98 bytes ICMP packet, when we are sending 800 ICMP packets per second to the victim, it needs only 78.4 kB/s for the attack where 802.11n can theoretically support the transmission speed up to 140 Mbits per second. It is clear that the proposed attack makes little interference to the WiFi experience of the victim.

CSI streams are firstly normalized to obtain its z score as $Z = (Y - m)/s$, where m and s are mean and standard deviation vector respectively. After normalization, Z has a mean of 0 and a standard deviation of 1. The reasons why we normalize CSI streams are two-folds. WiTalk uses CSI spectrograms in time-frequency domain, where the amplitude of CSI streams does not affect our analysis. Besides, CSI normalization helps in the PCA based filtering step because after normalization, all CSI streams contribute equally to PCA and none of them will dominate the PCA results.

5.4.3 Interference Elimination

CSI streams reported from WiFi NICs are very noisy. Figure 5.7a shows one original CSI stream collected at a sampling rate of $250Hz$. The noise sources include environmental noises and that are caused by WiFi NICs internal state transitions. These noises are in the high frequency zone on the spectrum. Besides the high frequency noises, some interferences also exit in CSI streams. Typical interferences include reflected signals from surrounding moving people and the movement of other body parts of the target like chest movements when breathing. In this section, we first use a Butterworth band pass filter to denoise the CSI streams and analyze its parameters. PCA based filter is then applied taking advantage of the correlation among CSI streams.

Band Pass Filtering

The key of designing a band pass filter is to determine its cut-off frequencies. Fine-grained human motion has low speed comparing to large-scale movements. For example, previous study on mechanical properties of lip movements [74,85] shows that average movement speed of human jaw and lips when speaking is between $3 - 6cm/s$, corresponding to $0.5 - 1.1Hz$ dynamics in CSI streams for $5.18GHz$ WiFi signals. Instantaneous speed is higher than the average speed, which means a higher CSI frequency. In WiHear [113] the authors use a frequency range of $2 - 5Hz$. In this work, We choose a wider frequency range of $1 - 10Hz$

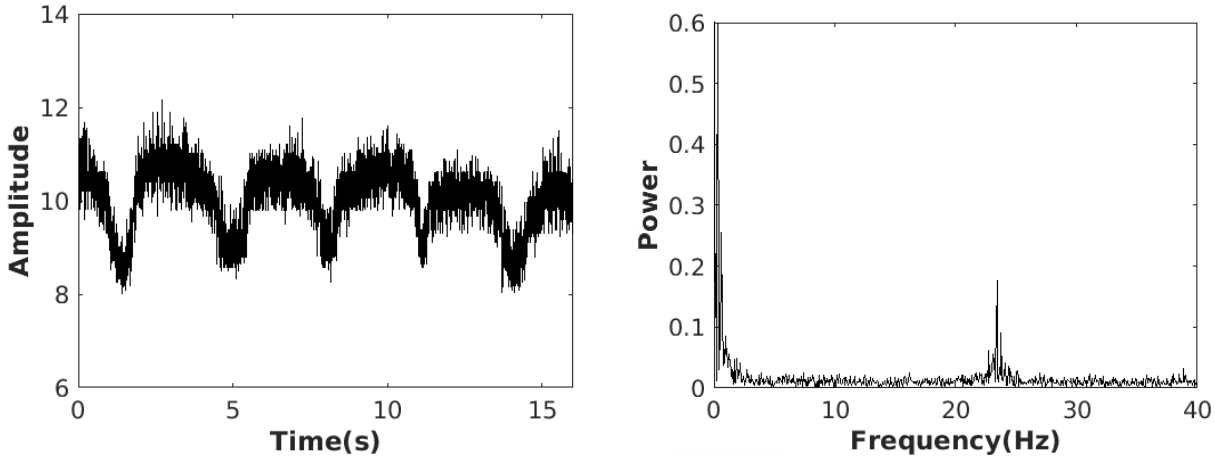

(a) Original CSI Stream (b) Spectrum

Figure 5.7: The original CSI stream contains breathing variations and noise, which can identified in the corresponding spectrum.

to keep more details. In application scenarios other than lip reading, the cut-off frequencies should be determined by the corresponding applications.

In a static environment, human respiration is the most significant interference existing in CSI streams. Figure 5.7a shows one original CSI stream in a static environment. The repeated pattern of breathing can be clearly observed in this figure. Typical respiratory rate for a healthy adult at rest is $12 - 20$ breaths per minute [19], corresponding to $0.2 - 0.33Hz$ dynamics in CSI streams. Figure 5.7b shows the spectrum of the CSI stream in Figure 5.7a.

To eliminate out-band interferences and noises, we use band-pass filter on CSI streams. According to what we discussed above, we set the cutoff frequency of the band-pass filter to be $1 - 10Hz$. We keep the frequency components up to $10Hz$ to get more details of the mouth movements. We choose 3-order Butterworth filter because it has a maximal flat amplitude response in the pass-band. Most of the high frequency burst noises and low frequency interference caused by respiration can be removed by the band-pass filter. Figure 5.8b shows the band-pass filter results of the original CSI stream in Figure 5.8a.

PCA Based Filtering

To further denoise the CSI streams and strengthen the effective CSI dynamics, we use principal components analysis(PCA) to track the correlation introduced in CSI streams by human motion. We get $30 \times 3 \times 1 = 90$ CSI streams in total when a WiTalk device has three antennas and the other end of the WiFi link has one antenna.

Among all the 90 CSI streams, we observe that not all of them show strong correlation. Specifically, the correlation is time varying and antenna related. Subcarriers from different

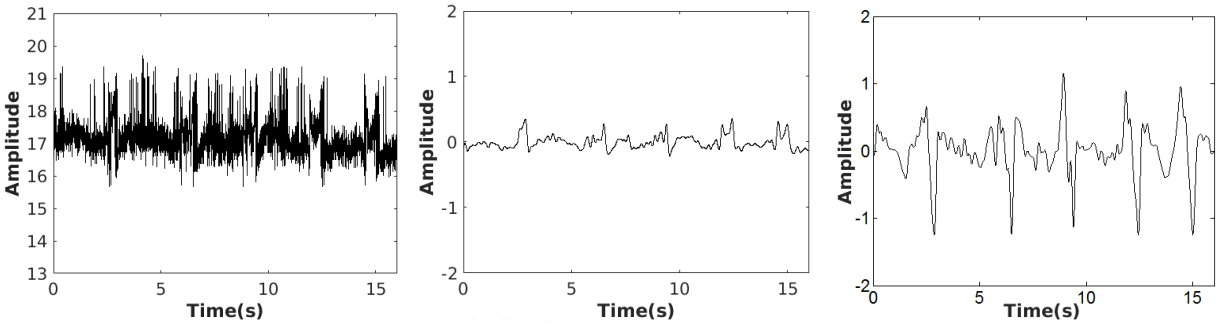

(a) Original CSI Stream (b) After Butterworth band-pass filter (c) After PCA based denoising

Figure 5.8: Denoising the CSI Streams. Bandpass filter keeps the signals between 1-10Hz. PCA filter utilizes the correlation between CSI streams to enhance filtering quality.

antennas tends to be uncorrelated. For example, Figure 5.9a shows three CSI streams that are collected from the three different antennas. Though the bottom two streams has some observable correlations, the top CSI stream from the third antenna does not seem to be correlated with them. CSI streams of the third antenna are more "noisy". If we use PCA on all 90 CSI streams from 3 antennas, noises from the third antenna will impinge the performance of PCA. Thus before PCA, we calculate the mean values of the correlation coefficients of the 30 CSI streams from an antenna, and setup a threshold to filter out the "noisy" antenna(s). We choose the threshold value 0.95. If none of the three antennas has a correlation coefficients higher than this threshold, we simply choose the antenna with the highest mean coefficient.

There are four main steps of applying PCA to CSI streams. The first step is data preprocessing. Data of CSI streams are segmented into small chunks to form a data matrix $\mathbf{H}$. Next, we calculate the correlation matrix of the data matrix as $\mathbf{H}^T \times \mathbf{H}$. The dimension of the correlation matrix is $N \times N$, where $N = 90$ is the number of CSI streams. The third step is to perform eigen-decomposition of the correlation matrix. In the last step, the principal components are reconstructed as $\mathbf{h}_i = \mathbf{H} \times \mathbf{q}_i$, where $\mathbf{q}_i$ is i^{th} eigenvector.

Only the first several principal components of PCA results with highest variance are valuable to our analysis. Due to correlated nature of CSI streams, all principal PCA components contain the same information. We discard the first principal component because noises caused by internal state changes are highly correlated and are captured in the first principal component [117]. We chose the second principal component as the input of the feature extraction step. Figure 5.8c shows the second principle component of the PCA results. Compared to the band-pass filtered result of the same CSI stream in Figure 5.8b, this PCA component contains more details of the CSI stream with higher strength.

5.4.4 Segmentation

Segmentation is an important preprocessing step to determine the start and end points of human motion. A good quality of segmentation will improve the performance of fine-grained motion sensing. WiTalk simply requires a short static interval between the movements to be detected. The static interval serves as the sentinel signal, helping WiTalk to segment the movements. We make this requirement because segmentation is not the research focus of this work. In lip reading application, more details about syllable and word segmentation can be found in [113].

5.4.5 Feature Extraction

The design of a context-free fine-grained motion sensing system requires us to find the intrinsic properties in CSI streams that are stable and correlated to human motion only.

Spectrogram Construction

Previous fine-grained motion sensing systems [13,67,110,113] use time domain CSI profiles to extract features for subsequent classification step. However, as time domain CSI waveforms change with different contexts, it is infeasible to use CSI waveforms as the discerning profiles in this work. We verify this claim by performing experiments on mouth movement sensing. Figure 5.9a shows the original CSI waveforms of /æ/ form three subcarriers on three different antennas. Figure 5.9b shows the corresponding band-pass filtered waveform. The top red line of Figure 5.9b is a CSI waveform of /æ/ collected at a different location. Please be noted that there are translations of the lines in Figure 5.9b to see them clearly. From Figure 5.9b we can see that the waveforms from different contexts are significantly different. This verify our claim that it's infeasible to use CSI waveforms as the profiles in context-free settings.

As discussed in Section 5.3, the CSi-Speed model proves that CSI spectrogram in time-frequency domain is a stable property of CSI streams that are highly correlated to human movement speeds. The movement speeds of different human body parts are correlated to a specific human activity like pronouncing a syllable. In the lip reading scenario, when pronouncing a specific syllable, there exists a specific movement pattern of all mouth parts [109]. A movement pattern includes the speed,direction and duration of the movements of every evolving mouth parts. WiTalk identifies CSI spectrogram in time-frequency domain as the stable property in CSI dynamics and extract features from these CSI spectrograms.

We take the second principle component of PCA based filtering process as the input to construct the spectrogram following these steps:

(1) Divide the input into equal-length segments. The segments must be short enough that the frequency content of the signal does not change appreciably within a segment. The

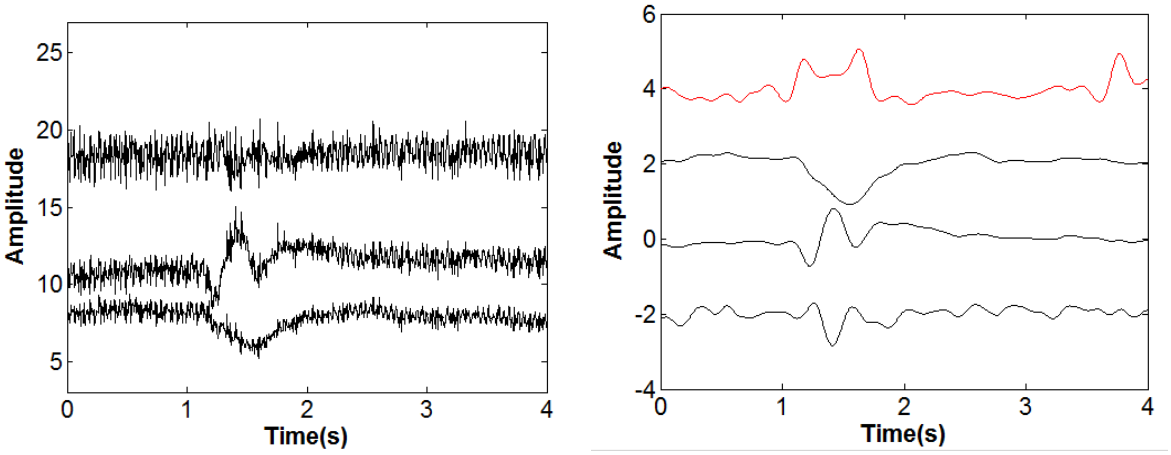

(a) Original CSI Stream (b) Filtered CSI Stream

Figure 5.9: Different CSI waveforms for the same syllable are quite different in time domain, indicating the difficulty of using time domain waveforms as the classification features.

segments may or may not overlap. We choose the segment size to be 128, corresponding to about 0.5 second of samples, so that the time is smaller than pronouncing a syllable and at the same time the number of samples is large enough to calculate the short-time Fourier transform. The overlap is set to be 126. Large overlap produces more spectrum lines and therefore a smoother spectrogram.

(2) Window each segment using a Hamming window and compute its spectrum using short-time Fourier transform.

(3) Display segment-by-segment the power of each spectrum in decibels and depict the magnitudes side-by-side as an image with magnitude-dependent colormap.

(4) Segment the CSI spectrogram using the static intervals to get the spectrograms for different syllables.

Figure 5.10 shows the spectrograms for three different syllables. The spectrograms show how the energy of each frequency component evolves with time, where high-energy components are colored in red. We can see that there exists distinguishable patterns in the spectrograms, though not very clearly. As an example, the energy of spectrogram of /æ/ concentrate in the center. It is because when pronouncing /æ/, the jaw moves at a relatively higher speed in a short time. On the contrary, the spectrogram of /s/ spreads wider than /æ/, because when we pronounce /s/, the lips move slower and last longer time.

Feature Extraction

Though the spectrogram patterns are human distinguishable, we need to further extract features from CSI spectrograms for classification of the fine-grained motion.

We find that discrete wavelet transform (DWT) on CSI spectrograms is not suitable for fine-grained motion sensing, which is used in coarse-grained solutions in quadrant II such as CARM [117]. Fine-grained motion like mouth movements have lower speed than large-scale human activities like walking or falling, which results in low frequency components in CSI spectrograms. Without enough frequency resolution, it is infeasible to extract frequencies at multiple resolutions on multiple time scales using DWT.

In WiTalk, we propose to first calculate the contours of the spectrogram images to extract features. The contours represent the edges of different energy levels of the spectrograms, and depicts the unique patterns of the spectrograms of fine-grained motion. Figure 5.10 shows three contour lines for the corresponding upper spectrograms. The top yellow contours mark the lines of signal energy and noise. The bottom blue contours enclose the major part the of signal energy.

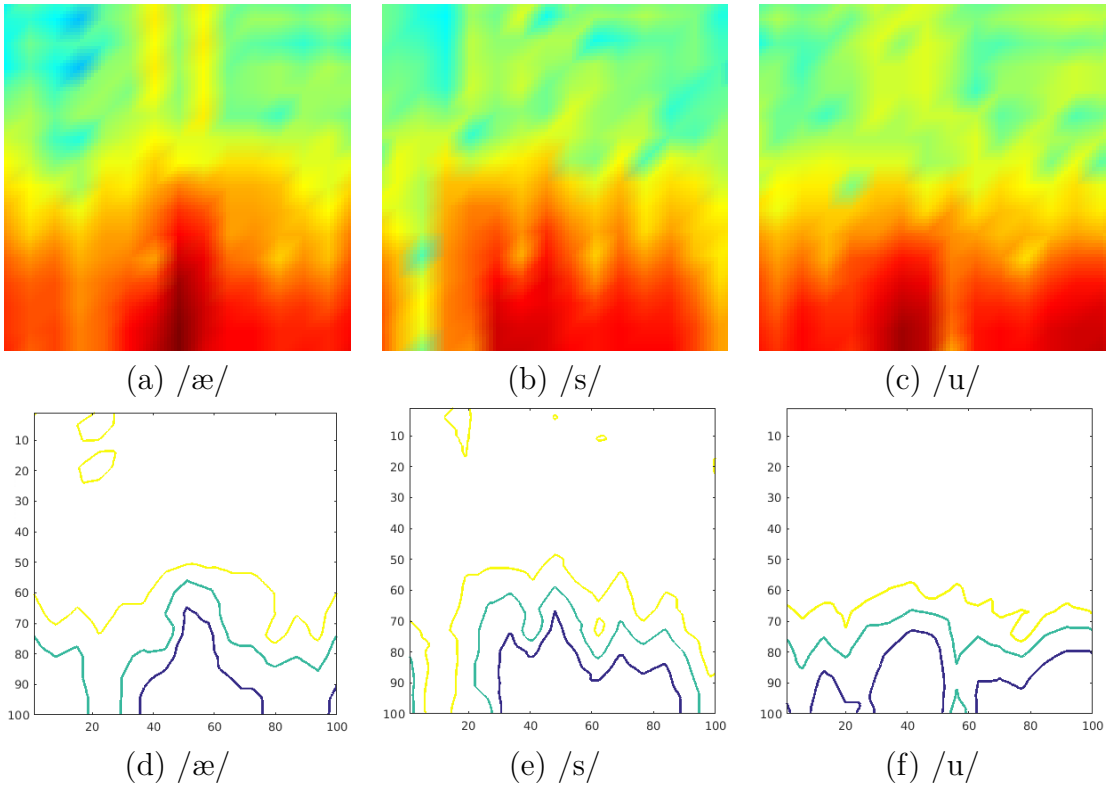

Figure 5.10: Spectrograms and contours of different syllables. The x axis and y axis are time and frequency respectively.

Directly using the contour lines as the classification features leads to high computational costs for classification. Therefore, we use the most relevant signal processing tool DWT on the contour lines to compress their length by extracting approximate sequences. In WiTalk we choose Daubechies wavelet filter of order 4 because it has the best classification performance.

5.4.6 Classification

People may perform the same micro motion at different speeds, and even for the same person, the motion speeds may vary from time to time. Dynamic time warping(DTW) can be used to measure similarity between two temporal sequences which may vary in speed. DTW calculates the optimal match between the two time sequences and warp the sequences to measure their similarity. The output of DTW is the distance between the two series. Low distance means high similarity between the two sequences. We build a classifier using the DWT compressed contours of the CSI spectrograms as features. The classifier calculate the DTW distances between the input and all the contours in the dataset. The one with the shortest distance is identified as the recognized motion.

5.4.7 Error Correction

The performance of fine-grained motion sensing can be further improved using application specific context information. For example, in the lip reading application, such information includes constraints that reject sentences that are not following these constraints. For example the sentence "The apple is red" will be accepted but "The apple is angry" will be rejected [8]. In WiTalk, we implement context-based error correction using a simple Bayesian method similar to [109].

5.5 Performance Evaluation

We implement WiTalk on a commercial laptop, and evaluate its performance in a typical lab environment. The system scenario of WiTalk is illustrated in Figure 5.11. WiTalk is implemented on the receiving end of a WiFi link. The transmitter continually sends packets to WiTalk at a speed of 250 packets/second. WiTalk collects CSI data and use the proposed algorithms to infer the fine-grained motion from the hidden patterns of CSI streams. We design experiments to detect a set of pronounced syllables, which is the bases for lip reading applications. We select lip reading as our example application scenario because it is the most fine-grained motion sensing in the literature that is previously reported using WiFi CSI dynamics [113].

5.5.1 System Setup

WiTalk is implemented on a commercial Thinkpad X301 laptop. The laptop is equipped with an Intel Core 2 U9600 processor, 4GB memory and an Intel 5300 NIC with 3 omni-directional antennas. The operating system running on the laptop is Ubuntu 14.04 LTS. We install and configure Linux 802.11n CSI Tool as described in [48]. The laptop works as

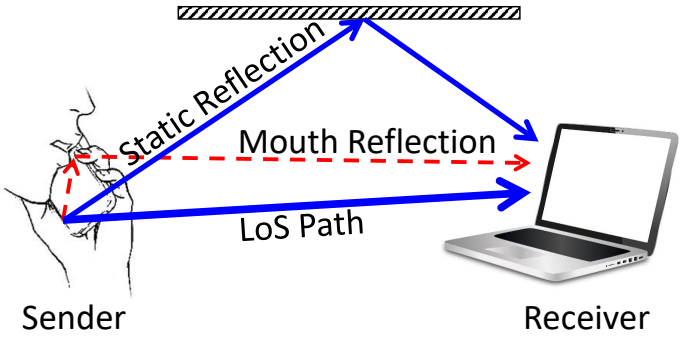

Figure 5.11: System application scenario of WiTalk. WiTalk is implemented on a commercial laptop.

the receiver and collects CSI streams using the CSI tool. Collected data are processed using Matlab scripts for signal processing and classification. Matlab version is R2016a. We do the experiments on channel 36 at $5.180GHz$.

We test WiTalk using two model of smartphones: a LG Nexus 5 with Android 6.0.1 and a Samsung Note 5 with Android 5.1.1. The smartphones work as the transmitters. The transmitter continually sends packets to WiTalk at a rate of 250 packets/second during the experiments. The CSI streams are collected and stored for later processing. WiTalk can also work in real time currently. By writing the CSI dynamics to a named pipe, Matlab script can read from the pipe and process the data simultaneously.

We test WiTalk in a normal lab environment depicted in Figure 5.12. The WiTalk device is tested at two positions marked as blue dots. We collect data with three volunteers(all males). The volunteers are asked to stand still at the positions marked as stars. They hold the phone steadily in normal phone call position the same way as depicted in Figure 5.11. Instead of making a real phone call, they are asked to read a set of syllables and a set of short sentences no more than six words. Static intervals are inserted intentionally between syllables and words to facilitate segmentation. The set of syllables includes 12 elements: /a/ /i/ /u/ /e/ /ɔ/ /b/ /f/ /d/ /g/ /j/ /ʃ/ /z/. Each volunteer reads the set of syllables 10 times at each test location, and the set of short sentences 5 times at each location.

5.5.2 Syllables Classification Accuracy

The recognition results for the syllables set is depicted in Figure 5.13 and Figure 5.14. We do the experiments in two steps to verify the syllable detection performance. We first train and test the classifier in the same context with the same volunteer at the same location. The confusion matrix is reported in Figure 5.13 with an average detection accuracy of 92.3%. Next we mix the data collected from different users, different transmitters at different locations

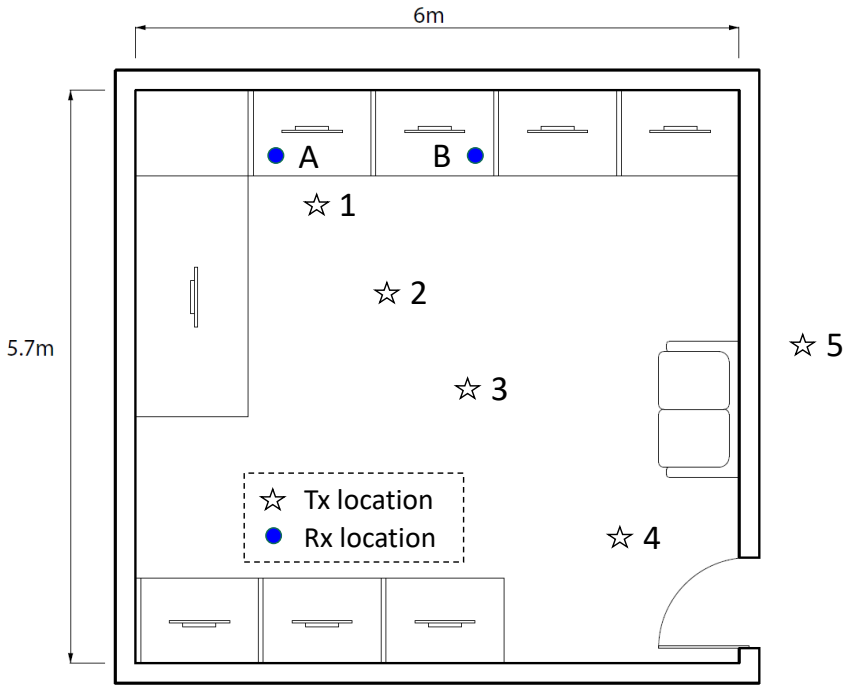

Figure 5.12: WiTalk test bed. The locations of WiTalk device are marked as the blue dots. The locations of the user are marked as stars.

for both training and testing. The confusion matrix is reported in Figure 5.14. In the mixed contexts situation, the average detection accuracy is 82.5%. The reasons for the lower accuracy in mix contexts situation are two-folds: 1) There are slight differences for different people to pronounce the same syllable. For example, in our experiments one of the volunteers tends to pronounce /u/ more lightly than others. His lips pucker very little when he makes this pronunciation, which impinges the detection accuracy of this syllable. 2) Signal reflection multipaths are significantly changed at different locations. This will introduce noises to CSI streams which cannot be removed completely. This impinges the classification performance compared to the same-context situation.

5.5.3 Sentence Recognition Accuracy

We evaluate the performance of sentence recognition with and without context-based error correction. The set of short sentences include sentences from 1 word to 6 words. As shown in Figure 5.15, with the increase of the number of words, the accuracy drops significantly. For 6 words situation, without context based correction, the recognition accuracy is only about 43%. With context based correction, the accuracy is improved by 16%. This is because the longer the sentences, the more they context information can be applied. The drop of the

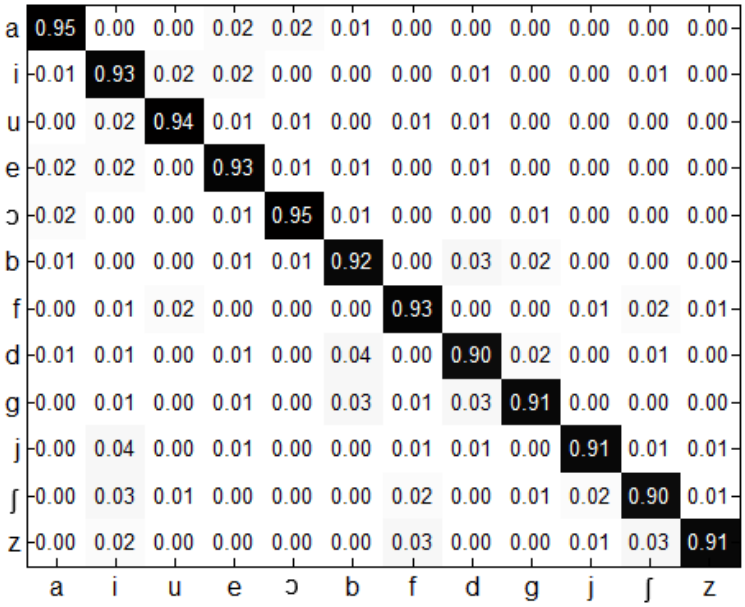

Figure 5.13: Confusion matrix of 12 syllables in the same context. The average detection accuracy is 92.3%.

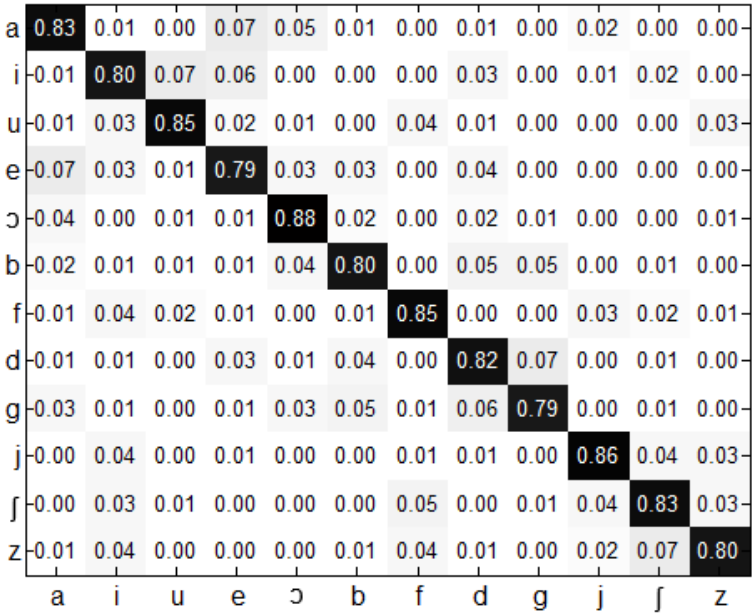

Figure 5.14: Confusion matrix of 12 syllables in the mixed contexts. The average detection accuracy is 82.5%.

performance is mainly because the difficulty of in-word syllables segmentation. To solve this problem, continuous lip reading model could be adopted as in [31].

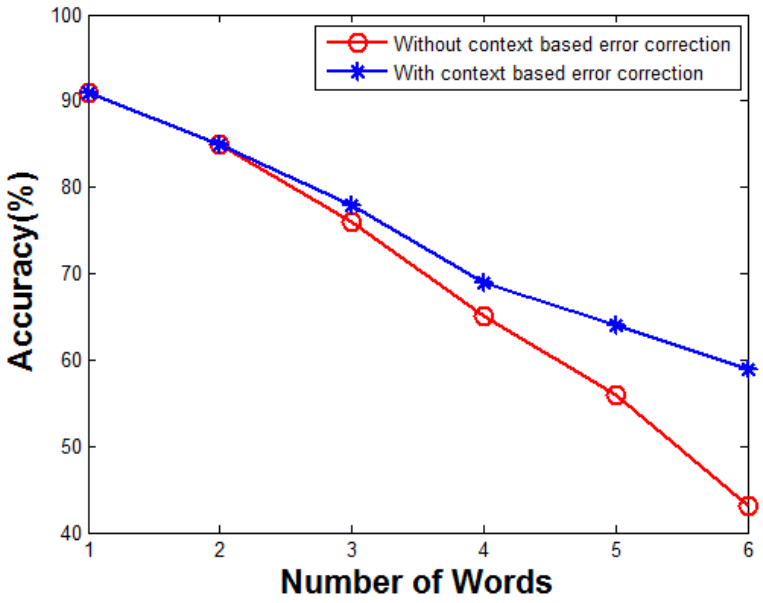

Figure 5.15: Sentence recognition accuracy drips significantly when the number of words increase because of the difficulty of in-word segmentation.

5.5.4 Performance with Distance

Figure 5.16 depicts the performance with increase of distance between the transceivers. For the receiver location marked as B, we only did the experiments at transmitter location 1, 2 and 5. The distance of $B1$,$B2$ and $B5$ are $1.5m$, $1.5m$ and $3m$ respectively. As we can see from Figure 5.16, the syllable discerning accuracy drops by 9% when the distance increase from $0.5m$ to $5m$ in the same room with LOS available. And the accuracy of sentence detection drops by 19%. However in through-the-wall scenario as in location 5, both syllable and sentence detection rate drop significantly by over 25% compared to location 4 at the same distance. To improve the performance and increase the working range of WiTalk, using a directional antenna will be a promising choice.

5.6 Summary of Contributions

WiTalk is the first fine-grained motion sensing system using CSI dynamics of WiFi. WiTalk can be implemented on a single WiFi device. We analyse and verify the feasibility of WiTalk in the application of CSI-based lip reading on smartphones. We propose to denoise CSI streams using band-pass filtering and PCA based filtering. We identify the spectrograms of CSI dynamics as the intrinsic features that correlate to human fine-grained motion only, and extract features from the contours of CSI spectrograms. WiTalk needs only one-time training and works for different environments. Experiment results show that WiTalk can

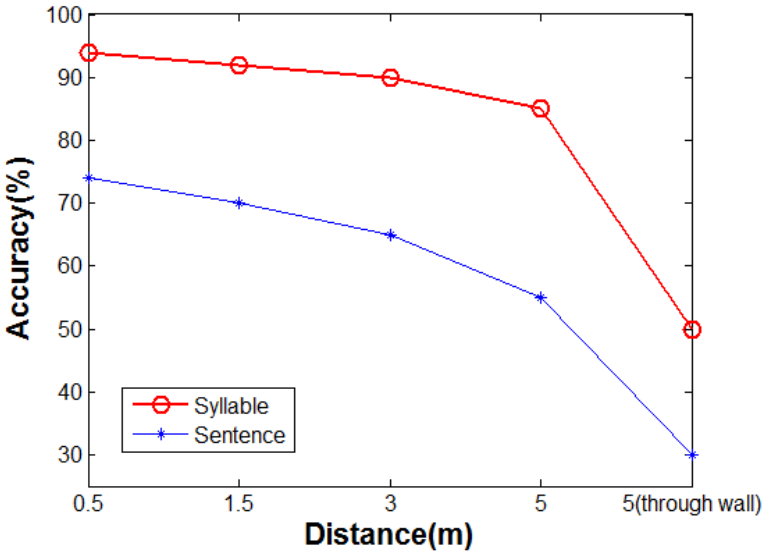

Figure 5.16: Identification performance drops with distance between WiTalk device and the user.

discern a set of 12 syllables with an accuracy of 92.3% and short sentences up to six words with an accuracy of 74.3%.

The current implementation of WiTalk has some limitations. First, the performance of WiTalk degrades with the increase of the distance between the two transceivers and the distance between the transceiver and moving human body parts. The main reason is that the reflected signal power from fine-grained motion is too small and is easily buried in noises and interferences. Using directional antennas is one possible solution, which we leave as future work.

Second, WiTalk requires the user staying relatively still for the fine-grained motion sensing. If the user talks over the phone while walking around, WiTalk will fail because the useful CSI dynamics will be buried in the CSI changes caused by the moving user body and legs. Even if the user stays still at one location, if he/she makes some hand or body gestures, the extraction of useful CSI dynamics will also become harder. How to eliminate these interferences will be our future research target.

Chapter 6

Conclusion

Withe the ubiquitous availability of wireless techniques, we need to pay attention to the sensing capabilities of wireless signals while we enjoy the convenience of wireless communications. Wireless sensing has endless possibility of helping us to know the physical world around us.

6.1 Research Summary

This dissertation focuses on the problem of exploring the sensing capability of wireless signals. The research approach is to first take measurements from physical layer of wireless connections, and then develop various techniques to extract or infer information about the environment use those measurements, like the locations of signal sources, the motion of human body, etc.

The research work in this dissertation has three contributions. My research starts from wireless signal attributes analysis. Specifically, the cyclostationarity properties of wireless signals are studied. Taking WiFi signals as an example, we propose signal cyclostationarity models induced by WiFi OFDM structure like pilots, cyclic prefix, and preambles. The induced cyclic frequencies is then applied to the Signal-Selective Direction Estimation problem. We are the first to provide complete model for OFDM features-induced cyclostationary properties. Tough we focus on WiFi signals, the analysis methods proposed can be generally applicable to other wireless signals. We verified the cyclic frequencies by simulation and compared the performance of the cyclic frequencies in direction estimation problem.

Second, based on the analysis of wireless signal attributes, we design and implement a prototype of a single device system, named MobTrack, which can locate indoor interfering radios. The goal of designing MobTrack is to provide a lightweight, handhold system that can locate interfering radios with sub-meter accuracy with as less antennas as possible. With a small

antenna array, the cost, complexity as well as size of this device are also reduced. MobTrack is the first single device indoor interference localization system without the requirement of multiple pre-deployed Access Points. To the best of our knowledge, MobTrack is the first single device indoor interference localization system without the requirement of multiple pre-deployed Access Points. We propose a novel algorithm to eliminate the multipath effect in the indoor environment. Our multipath suppression algorithm could robustly and efficiently isolate the LoS component from other reflected components. We propose a novel signal type identification algorithm for MobTrack to calculate the AoAs of only interfering radios, which significantly reduces the requirement to antenna numbers and device complexity.

Third, channel state information is studied in applications of human motion sensing. We design WiTalk, the first system which is able to do fine-grained human motion sensing like leap reading on smartphones using the CSI dynamics generated by human movements. WiTalk proposes a new fine-grained human motion sensing technique with the distinct context-free feature. To profile human motion using CSI, WiTalk generates CSI spectrograms using signal processing techniques and extracts features by calculating the contours of the CSI spectrograms. The proposed technique is verified in the application scenario of lip reading, where the fine-grained motion is the mouth movements. To the best of our knowledge, WiTalk is the first feasible system in the context-free fine-grained quadrant of motion sensing solution plane using WiFi CSI dynamics. We show the existence of this quadrant I solution by identifying the CSI spectrograms as the intrinsic stable properties that correlate to fine-grained human motion. We identify and extract effective features from CSI spectrograms by calculating the contours of CSI spectrograms. These new discerning features solve the problem of low time-frequency resolution using discrete wavelet transform(DWT). We verify the feasibility of WiTalk by applying it to the lip reading scenario. Experiment results show that WiTalk achieves comparable results to previous fine-grained context-related solutions.

6.2 Future Work

The current work in this dissertation is far from completion and perfection.

MobTrack is designed to be a single device system. However, the current prototype device is quite large, because of the size limitations of the antenna array. In the future, we need to find a better way of implementation. One possible method is to use a virtual antenna array, by moving a single antenna or a couple of antennas in a controlled direction. By measuring the moving direction and speed of the antenna(s), we can make some compensation using a software method to construct the virtual antenna array. Though it's ought to be many challenges, we believe this is a promising direction to further simplify the device.

The current implementation of WiTalk has some limitations. First, the performance of WiTalk degrades with the increase of the distance between the two transceivers and the distance between the transceiver and moving human body parts. The main reason is that

the reflected signal power from fine-grained motion is too small and is easily buried in noises and interferences. Using directional antennas is one possible solution, which we leave as future work.

Second, WiTalk requires the user staying relatively still for the fine-grained motion sensing. If the user talks over the phone while walking around, WiTalk will fail because the useful CSI dynamics will be buried in the CSI changes caused by the moving user body and legs. Even if the user stays still at one location, if he/she makes some hand or body gestures, the extraction of useful CSI dynamics will also become harder. How to eliminate these interferences will be our future research target.

Bibliography

[1] Gartner says 8.4 billion connected "things" will be in use in 2017, up 31 percent from 2016. https://www.gartner.com/newsroom/id/3598917. Accessed on 2018-04-01.

[2] Kinect. https://dev.windows.com/en-us/kinect. Accessed on 2018-04-01.

[3] Leap motion. https://www.leapmotion.com/. Accessed on 2018-04-01.

[4] Octoclock clock distribution module with gpsdo - ettus research. https://www.ettus.com/product/details/OctoClock-G. Accessed on 2018-04-01.

[5] Playstation camera. https://www.playstation.com/en-us/explore/accessories/vr-accessories/playstation-camera/. Accessed on 2018-04-01.

[6] Project soli. https://atap.google.com/soli/. Accessed on 2018-04-01.

[7] Sigfox world iot expo - watch the replay. https://www.sigfox.com/en/news/sigfox-world-iot-expo-watch-replay. Accessed on 2018-04-01.

[8] Speech recognition. https://en.wikipedia.org/wiki/Speech_recognition. Accessed on 2018-04-01.

[9] Synchronization and mimo capability with usrp devices. https://kb.ettus.com/index.php?title=Synchronization_and_MIMO_Capability_with_USRP_Devices&action=pdfbook&format=single. Accessed on 2018-04-01.

[10] That 'internet of things' thing. http://www.rfidjournal.com/articles/view?4986. Accessed on 2018-04-01.

[11] Fadel Adib, Zachary Kabelac, Dina Katabi, and Robert C Miller. 3d tracking via body radio reflections. In *NSDI*, volume 14, pages 317–329, 2014.

[12] Ian F Akyildiz, Weilian Su, Yogesh Sankarasubramaniam, and Erdal Cayirci. Wireless sensor networks: a survey. *Computer networks*, 38(4):393–422, 2002.

[13] Kamran Ali, Alex X Liu, Wei Wang, and Muhammad Shahzad. Keystroke recognition using wifi signals. In *Proceedings of the 21st Annual International Conference on Mobile Computing and Networking*, pages 90–102. ACM, 2015.

[14] Arjun Anand, Constantine Manikopoulos, Quentin Jones, and Cristian Borcea. A quantitative analysis of power consumption for location-aware applications on smart phones. In *Industrial Electronics, 2007. ISIE 2007. IEEE International Symposium on*, pages 1986–1991. IEEE, 2007.

[15] Shlomi Arnon. *Visible light communication*. Cambridge University Press, 2015.

[16] V.S. Bagad. *Radar System*. Technical Publications, 2009.

[17] Paramvir Bahl and Venkata N Padmanabhan. Radar: An in-building rf-based user location and tracking system. In *INFOCOM 2000. Nineteenth Annual Joint Conference of the IEEE Computer and Communications Societies. Proceedings. IEEE*, volume 2, pages 775–784. Ieee, 2000.

[18] Paolo Baronti, Prashant Pillai, Vince WC Chook, Stefano Chessa, Alberto Gotta, and Y Fun Hu. Wireless sensor networks: A survey on the state of the art and the 802.15. 4 and zigbee standards. *Computer communications*, 30(7):1655–1695, 2007.

[19] Kim E Barrett, Susan M Barman, Scott Boitano, and Heddwen Brooks. Ganong's review of medical physiology. 24. *NY: McGraw-Hill Medical*, 2012.

[20] David L Begley. Free-space laser communications: a historical perspective. In *Lasers and Electro-Optics Society, 2002. LEOS 2002. The 15th Annual Meeting of the IEEE*, volume 2, pages 391–392. IEEE, 2002.

[21] Chatschik Bisdikian. An overview of the bluetooth wireless technology. *IEEE Communications magazine*, 39(12):86–94, 2001.

[22] Xiaoxiao Cao, Bing Chen, and Yanchao Zhao. Wi-wri: Fine-grained writing recognition using wi-fi signals. In *Trustcom/BigDataSE/ISPA, 2016 IEEE*, pages 1366–1373. IEEE, 2016.

[23] Yuan Cao, Yu-Huai Li, Zhu Cao, Juan Yin, Yu-Ao Chen, Hua-Lei Yin, Teng-Yun Chen, Xiongfeng Ma, Cheng-Zhi Peng, and Jian-Wei Pan. Direct counterfactual communication via quantum zeno effect. *Proceedings of the National Academy of Sciences*, 114(19):4920–4924, 2017.

[24] Marcos E Castro. Cyclostationary detection for ofdm in cognitive radio systems. Master's thesis, Lincoln, Nebraska. University of Nebraska-Lincoln, 2011.

[25] Paul Castro, Patrick Chiu, Ted Kremenek, and Richard Muntz. A probabilistic room location service for wireless networked environments. In *International conference on ubiquitous computing*, pages 18–34. Springer, 2001.

[26] Pascal Charge, Yide Wang, and Joseph Saillard. An extended cyclic music algorithm. *IEEE Transactions on Signal Processing*, 51(7):1695–1701, 2003.

[27] Zhizhang Chen, Gopal Gokeda, and Yiqiang Yu. *Introduction to Direction-of-arrival Estimation*. Artech House, 2010.

[28] Eric Chin, David Chieng, Victor Teh, Marek Natkaniec, Krzysztof Loziak, and Janusz Gozdecki. Wireless link prediction and triggering using modified ornstein–uhlenbeck jump diffusion process. *Wireless Networks*, 20(3):379–396, 2014.

[29] Krishna Chintalapudi, Anand Padmanabha Iyer, and Venkata N Padmanabhan. Indoor localization without the pain. In *Proceedings of the sixteenth annual international conference on Mobile computing and networking*, pages 173–184. ACM, 2010.

[30] Mostafa Zaman Chowdhury, Md Tanvir Hossan, Amirul Islam, and Yeong Min Jang. A comparative survey of optical wireless technologies: architectures and applications. *IEEE Access*, 6:9819–9840, 2018.

[31] Joon Son Chung, Andrew Senior, Oriol Vinyals, and Andrew Zisserman. Lip reading sentences in the wild. In *Proceedings of the IEEE Conference on Computer Vision and Pattern Recognition*, pages 6447–6456, 2017.

[32] Abe Davis, Michael Rubinstein, Neal Wadhwa, Gautham J Mysore, Frédo Durand, and William T Freeman. The visual microphone: passive recovery of sound from video. *ACM Transactions on Graphics (TOG)*, 33(4):79, 2014.

[33] Svilen Dimitrov and Harald Haas. *Principles of LED light communications: towards networked Li-Fi*. Cambridge University Press, 2015.

[34] Paul Duchnowski, Martin Hunke, Dietrich Busching, Uwe Meier, and Alex Waibel. Toward movement-invariant automatic lip-reading and speech recognition. In *Acoustics, Speech, and Signal Processing, 1995. ICASSP-95., 1995 International Conference on*, volume 1, pages 109–112. IEEE, 1995.

[35] Hany Elgala, Raed Mesleh, and Harald Haas. Indoor optical wireless communication: potential and state-of-the-art. *IEEE Communications Magazine*, 49(9), 2011.

[36] Avshalom C Elitzur and Lev Vaidman. Quantum mechanical interaction-free measurements. *Foundations of Physics*, 23(7):987–997, 1993.

[37] Dave Evans. The internet of things: How the next evolution of the internet is changing everything. *CISCO*, 1:1–11, 04 2011.

[38] Ramsey Michael Faragher. *Effects of multipath interference on radio positioning systems*. PhD thesis, University of Cambridge, 2008.

[39] Klaus Finkenzeller. *RFID handbook: fundamentals and applications in contactless smart cards, radio frequency identification and near-field communication*. John Wiley & Sons, 2010.

[40] William A Gardner. Exploitation of spectral redundancy in cyclostationary signals. *IEEE Signal processing magazine*, 8(2):14–36, 1991.

[41] Jim Geier. *Designing and deploying 802.11 n wireless networks*. Pearson Education, 2010.

[42] Sinan Gezici, Zhi Tian, Georgios B Giannakis, Hisashi Kobayashi, Andreas F Molisch, H Vincent Poor, and Zafer Sahinoglu. Localization via ultra-wideband radios: a look at positioning aspects for future sensor networks. *IEEE signal processing magazine*, 22(4):70–84, 2005.

[43] Satashu Goel and Rohit Negi. Guaranteeing secrecy using artificial noise. *IEEE transactions on wireless communications*, 7(6), 2008.

[44] Yuki Goto, Isamu Takai, Takaya Yamazato, Hiraku Okada, Toshiaki Fujii, Shoji Kawahito, Shintaro Arai, Tomohiro Yendo, and Koji Kamakura. A new automotive vlc system using optical communication image sensor. *IEEE photonics journal*, 8(3):1–17, 2016.

[45] Sidhant Gupta, Daniel Morris, Shwetak Patel, and Desney Tan. Soundwave: using the doppler effect to sense gestures. In *Proceedings of the SIGCHI Conference on Human Factors in Computing Systems*, pages 1911–1914. ACM, 2012.

[46] Harald Haas, Liang Yin, Yunlu Wang, and Cheng Chen. What is lifi? *Journal of Lightwave Technology*, 34(6):1533–1544, 2016.

[47] Andreas Haeberlen, Eliot Flannery, Andrew M Ladd, Algis Rudys, Dan S Wallach, and Lydia E Kavraki. Practical robust localization over large-scale 802.11 wireless networks. In *Proceedings of the 10th annual international conference on Mobile computing and networking*, pages 70–84. ACM, 2004.

[48] Daniel Halperin, Wenjun Hu, Anmol Sheth, and David Wetherall. Tool release: Gathering 802.11 n traces with channel state information. *ACM SIGCOMM Computer Communication Review*, 41(1):53–53, 2011.

[49] Steven Siying Hong and Sachin Rajsekhar Katti. Dof: a local wireless information plane. In *ACM SIGCOMM Computer Communication Review*, volume 41, pages 230–241. ACM, 2011.

[50] IEEE. Ieee standard for information technology–telecommunications and information exchange between systems local and metropolitan area networks–specific requirements - part 11: Wireless lan medium access control (mac) and physical layer (phy) specifications. *IEEE Std 802.11-2016 (Revision of IEEE Std 802.11-2012)*, pages 1–3534, Dec 2016.

[51] Suman Jana, Sriram Nandha Premnath, Mike Clark, Sneha K Kasera, Neal Patwari, and Srikanth V Krishnamurthy. On the effectiveness of secret key extraction from wireless signal strength in real environments. In *Proceedings of the 15th annual international conference on Mobile computing and networking*, pages 321–332. ACM, 2009.

[52] Kiran Raj Joshi, Steven Siying Hong, and Sachin Katti. Pinpoint: Localizing interfering radios. In *NSDI*, pages 241–253, 2013.

[53] Shugo Kajita, Tatsuya Amano, Hirozumi Yamaguchi, Teruo Higashino, and Mineo Takai. Wi-fi channel selection based on urban interference measurement. In *Proceedings of the 13th International Conference on Mobile and Ubiquitous Systems: Computing, Networking and Services*, pages 143–150. ACM, 2016.

[54] Bryce Kellogg, Vamsi Talla, and Shyamnath Gollakota. Bringing gesture recognition to all devices. In *NSDI*, volume 14, pages 303–316, 2014.

[55] Mohammad Ali Khalighi and Murat Uysal. Survey on free space optical communication: A communication theory perspective. *IEEE Communications Surveys & Tutorials*, 16(4):2231–2258, 2014.

[56] Kyouwoong Kim, Ihsan A Akbar, Kyung K Bae, Jung-Sun Um, Chad M Spooner, and Jeffrey H Reed. Cyclostationary approaches to signal detection and classification in cognitive radio. In *New frontiers in dynamic spectrum access networks, 2007. DySPAN 2007. 2nd IEEE international symposium on*, pages 212–215. IEEE, 2007.

[57] Patrick Kinney et al. Zigbee technology: Wireless control that simply works. In *Communications design conference*, volume 2, pages 1–7, 2003.

[58] Lawrence E Kinsler, Austin R Frey, Alan B Coppens, and James V Sanders. Fundamentals of acoustics. *Fundamentals of Acoustics, 4th Edition, by Lawrence E. Kinsler, Austin R. Frey, Alan B. Coppens, James V. Sanders, pp. 560. ISBN 0-471-84789-5. Wiley-VCH, December 1999.*, page 560, 1999.

[59] Toshihiko Komine and Masao Nakagawa. Fundamental analysis for visible-light communication system using led lights. *IEEE transactions on Consumer Electronics*, 50(1):100–107, 2004.

[60] Parameshwaran Krishnan, AS Krishnakumar, Wen-Hua Ju, Colin Mallows, and SN Gamt. A system for lease: Location estimation assisted by stationary emitters for indoor rf wireless networks. In *INFOCOM 2004. Twenty-third AnnualJoint Conference of the IEEE Computer and Communications Societies*, volume 2, pages 1001–1011. IEEE, 2004.

[61] Kshitiz Kumar, Tsuhan Chen, and Richard M Stern. Profile view lip reading. In *Acoustics, Speech and Signal Processing, 2007. ICASSP 2007. IEEE International Conference on*, volume 4, pages IV–429. IEEE, 2007.

[62] Swarun Kumar, Stephanie Gil, Dina Katabi, and Daniela Rus. Accurate indoor localization with zero start-up cost. In *Proceedings of the 20th annual international conference on Mobile computing and networking*, pages 483–494. ACM, 2014.

[63] Andrew M Ladd, Kostas E Bekris, Algis Rudys, Lydia E Kavraki, and Dan S Wallach. Robotics-based location sensing using wireless ethernet. *Wireless Networks*, 11(1-2):189–204, 2005.

[64] Jeremy Landt. The history of rfid. *IEEE potentials*, 24(4):8–11, 2005.

[65] Jin-Shyan Lee, Yu-Wei Su, and Chung-Chou Shen. A comparative study of wireless protocols: Bluetooth, uwb, zigbee, and wi-fi. In *Industrial Electronics Society, 2007. IECON 2007. 33rd Annual Conference of the IEEE*, pages 46–51. Ieee, 2007.

[66] Chuan Li, David A Hutchins, and Roger J Green. Short-range ultrasonic digital communications in air. *IEEE transactions on ultrasonics, ferroelectrics, and frequency control*, 55(4):908–918, 2008.

[67] Mengyuan Li, Yan Meng, Junyi Liu, Haojin Zhu, Xiaohui Liang, Yao Liu, and Na Ruan. When csi meets public wifi: Inferring your mobile phone password via wifi signals. In *Proceedings of the 2016 ACM SIGSAC Conference on Computer and Communications Security*, pages 1068–1079. ACM, 2016.

[68] Hongbo Liu, Yu Gan, Jie Yang, Simon Sidhom, Yan Wang, Yingying Chen, and Fan Ye. Push the limit of wifi based localization for smartphones. In *Proceedings of the 18th annual international conference on Mobile computing and networking*, pages 305–316. ACM, 2012.

[69] Jian Liu, Yan Wang, Yingying Chen, Jie Yang, Xu Chen, and Jerry Cheng. Tracking vital signs during sleep leveraging off-the-shelf wifi. In *Proceedings of the 16th ACM International Symposium on Mobile Ad Hoc Networking and Computing*, pages 267–276. ACM, 2015.

[70] Kaikai Liu, Xinxin Liu, Lulu Xie, and Xiaolin Li. Towards accurate acoustic localization on a smartphone. In *INFOCOM, 2013 Proceedings IEEE*, pages 495–499. IEEE, 2013.

[71] Hai-Han Lu, Chung-Yi Li, Hwan-Wei Chen, Chun-Ming Ho, Ming-Te Cheng, Zih-Yi Yang, and Chang-Kai Lu. A 56 gb/s pam4 vcsel-based lifi transmission with two-stage injection-locked technique. *IEEE Photonics Journal*, 9(1):1–8, 2017.

[72] Ruifeng Ma, Linglong Dai, Zhaocheng Wang, and Jun Wang. Secure communication in tds-ofdm system using constellation rotation and noise insertion. *IEEE Transactions on Consumer Electronics*, 56(3), 2010.

[73] Koji Maeda, Anass Benjebbour, Takahiro Asai, Tatsuo Furuno, and Tomoyuki Ohya. Cyclostationarity-inducing transmission methods for recognition among ofdm-based systems. *EURASIP Journal on Wireless Communications and Networking*, 2008(1):586172, 2008.

[74] Shinji Maeda and Martine Toda. Mechanical properties of lip movements: How to characterize different speaking styles? In *Proc. 15th International Congress of Phonetic Sciences (ICPhS03)*, volume 1, pages 189–192, 2003.

[75] Aditi Malik and Preeti Singh. Free space optics: current applications and future challenges. *International Journal of Optics*, 2015, 2015.

[76] Alex T Mariakakis, Souvik Sen, Jeongkeun Lee, and Kyu-Han Kim. Sail: Single access point-based indoor localization. In *Proceedings of the 12th annual international conference on Mobile systems, applications, and services*, pages 315–328. ACM, 2014.

[77] Suhas Mathur, Wade Trappe, Narayan Mandayam, Chunxuan Ye, and Alex Reznik. Radio-telepathy: extracting a secret key from an unauthenticated wireless channel. In *Proceedings of the 14th ACM international conference on Mobile computing and networking*, pages 128–139. ACM, 2008.

[78] Patricia McDermott-Wells. What is bluetooth? *IEEE potentials*, 23(5):33–35, 2004.

[79] Brent A Miller and Chatschik Bisdikian. *Bluetooth revealed: the insider's guide to an open specification for global wireless communication*. Prentice Hall PTR, 2001.

[80] Amitav Mukherjee and A Lee Swindlehurst. Robust beamforming for security in mimo wiretap channels with imperfect csi. *IEEE Transactions on Signal Processing*, 59(1):351–361, 2011.

[81] Rajalakshmi Nandakumar, Krishna Kant Chintalapudi, and Venkata N Padmanabhan. Centaur: locating devices in an office environment. In *Proceedings of the 18th annual international conference on Mobile computing and networking*, pages 281–292. ACM, 2012.

[82] Rajalakshmi Nandakumar, Alex Takakuwa, Tadayoshi Kohno, and Shyamnath Gollakota. Covertband: Activity information leakage using music. *Proceedings of the ACM on Interactive, Mobile, Wearable and Ubiquitous Technologies*, 1(3):87, 2017.

[83] Shahriar Nirjon, Jeremy Gummeson, Dan Gelb, and Kyu-Han Kim. Typingring: A wearable ring platform for text input. In *Proceedings of the 13th Annual International Conference on Mobile Systems, Applications, and Services*, pages 227–239. ACM, 2015.

[84] Peter O'Shea. Phase measurement. *Electrical Measurement, Signal Processing and Displays*, pages 28–41, 1999.

[85] DJ Ostry and JR Flanagan. Human jaw movement in mastication and speech. *Archives of Oral Biology*, 34(9):685–693, 1989.

[86] Parth H Pathak, Xiaotao Feng, Pengfei Hu, and Prasant Mohapatra. Visible light communication, networking, and sensing: A survey, potential and challenges. *IEEE communications surveys & tutorials*, 17(4):2047–2077, 2015.

[87] Paolo Pignoli, Elena Tremoli, Andrea Poli, Pierluigi Oreste, and Rodolfo Paoletti. Intimal plus medial thickness of the arterial wall: a direct measurement with ultrasound imaging. *circulation*, 74(6):1399–1406, 1986.

[88] H. Vincent Poor and Rafael F. Schaefer. Wireless physical layer security. *Proceedings of the National Academy of Sciences*, 114:19–26, 2017.

[89] Qifan Pu, Sidhant Gupta, Shyamnath Gollakota, and Shwetak Patel. Whole-home gesture recognition using wireless signals. In *Proceedings of the 19th annual international conference on Mobile computing & networking*, pages 27–38. ACM, 2013.

[90] Lawrence R Rabiner and Ronald W Schafer. *Digital processing of speech signals*. Prentice Hall, 1978.

[91] Hanif Rahbari and Marwan Krunz. Secrecy beyond encryption: obfuscating transmission signatures in wireless communications. *IEEE Communications Magazine*, 53(12):54–60, 2015.

[92] Anshul Rai, Krishna Kant Chintalapudi, Venkata N Padmanabhan, and Rijurekha Sen. Zee: Zero-effort crowdsourcing for indoor localization. In *Proceedings of the 18th annual international conference on Mobile computing and networking*, pages 293–304. ACM, 2012.

[93] Sridhar Rajagopal, Richard D Roberts, and Sang-Kyu Lim. Ieee 802.15. 7 visible light communication: modulation schemes and dimming support. *IEEE Communications Magazine*, 50(3), 2012.

[94] Randy S Roberts, William A Brown, and Herschel H Loomis. Computationally efficient algorithms for cyclic spectral analysis. *IEEE Signal Processing Magazine*, 8(2):38–49, 1991.

[95] Richard Roy and Thomas Kailath. Esprit-estimation of signal parameters via rotational invariance techniques. *IEEE Transactions on acoustics, speech, and signal processing*, 37(7):984–995, 1989.

[96] Hatim Salih, Zheng-Hong Li, M Al-Amri, and M Suhail Zubairy. Protocol for direct counterfactual quantum communication. *Physical review letters*, 110(17):170502, 2013.

[97] Stephan V Schell, Robert A Calabretta, William A Gardner, and Brian G Agee. Cyclic music algorithms for signal-selective direction estimation. In *Acoustics, Speech, and Signal Processing, 1989. ICASSP-89., 1989 International Conference on*, pages 2278–2281. IEEE, 1989.

[98] Ralph Schmidt. Multiple emitter location and signal parameter estimation. *IEEE transactions on antennas and propagation*, 34(3):276–280, 1986.

[99] Steven R Schnur. *Identification and classification of OFDM based signals using preamble correlation and cyclostationary feature extraction*. PhD thesis, Monterey, California. Naval Postgraduate School, 2009.

[100] Souvik Sen, Romit Roy Choudhury, and Srihari Nelakuditi. Spinloc: Spin once to know your location. In *Proceedings of the Twelfth Workshop on Mobile Computing Systems & Applications*, page 12. ACM, 2012.

[101] Souvik Sen, Božidar Radunovic, Romit Roy Choudhury, and Tom Minka. You are facing the mona lisa: spot localization using phy layer information. In *Proceedings of the 10th international conference on Mobile systems, applications, and services*, pages 183–196. ACM, 2012.

[102] Tie-Jun Shan, Mati Wax, and Thomas Kailath. On spatial smoothing for direction-of-arrival estimation of coherent signals. *IEEE Transactions on Acoustics, Speech, and Signal Processing*, 33(4):806–811, 1985.

[103] François-Xavier Socheleau, Philippe Ciblat, and Sébastien Houcke. Ofdm system identification for cognitive radio based on pilot-induced cyclostationarity. In *Wireless Communications and Networking Conference, 2009. WCNC 2009. IEEE*, pages 1–6. IEEE, 2009.

[104] Li Sun, Souvik Sen, Dimitrios Koutsonikolas, and Kyu-Han Kim. Widraw: Enabling hands-free drawing in the air on commodity wifi devices. In *Proceedings of the 21st Annual International Conference on Mobile Computing and Networking*, pages 77–89. ACM, 2015.

[105] K.S. Suslick. *Ultrasound: Its Chemical, Physical, and Biological Effects*. VCH, 1988.

[106] Paul D Sutton, Keith E Nolan, and Linda E Doyle. Cyclostationary signatures in practical cognitive radio applications. *IEEE Journal on selected areas in Communications*, 26(1), 2008.

[107] Thomas L Szabo. *Diagnostic ultrasound imaging: inside out*. Academic Press, 2004.

[108] Tsutomu Takeuchi, Masahiro Sako, and Susumu Yoshida. Multipath delay estimation for indoor wireless communication. In *Vehicular Technology Conference, 1990 IEEE 40th*, pages 401–406. IEEE, 1990.

[109] Jiayao Tan, Cam-Tu Nguyen, and Xiaoliang Wang. Silenttalk: Lip reading through ultrasonic sensing on mobile phones. In *INFOCOM 2017-IEEE Conference on Computer Communications, IEEE*, pages 1–9. IEEE, 2017.

[110] Sheng Tan and Jie Yang. Wifinger: leveraging commodity wifi for fine-grained finger gesture recognition. In *Proceedings of the 17th ACM International Symposium on Mobile Ad Hoc Networking and Computing*, pages 201–210. ACM, 2016.

[111] Wade Trappe, Richard Howard, and Robert S Moore. Low-energy security: Limits and opportunities in the internet of things. *IEEE Security & Privacy*, 13(1):14–21, 2015.

[112] Deepak Vasisht, Swarun Kumar, and Dina Katabi. Decimeter-level localization with a single wifi access point. In *NSDI*, volume 16, pages 165–178, 2016.

[113] Guanhua Wang, Yongpan Zou, Zimu Zhou, Kaishun Wu, and Lionel M Ni. We can hear you with wi-fi! In *Proceedings of the 20th annual international conference on Mobile computing and networking*, pages 593–604. ACM, 2014.

[114] Hao Wang, Daqing Zhang, Junyi Ma, Yasha Wang, Yuxiang Wang, Dan Wu, Tao Gu, and Bing Xie. Human respiration detection with commodity wifi devices: do user location and body orientation matter? In *Proceedings of the 2016 ACM International Joint Conference on Pervasive and Ubiquitous Computing*, pages 25–36. ACM, 2016.

[115] Jue Wang, Deepak Vasisht, and Dina Katabi. Rf-idraw: virtual touch screen in the air using rf signals. In *ACM SIGCOMM Computer Communication Review*, volume 44, pages 235–246. ACM, 2014.

[116] Wei Wang, Alex X Liu, and Muhammad Shahzad. Gait recognition using wifi signals. In *Proceedings of the 2016 ACM International Joint Conference on Pervasive and Ubiquitous Computing*, pages 363–373. ACM, 2016.

[117] Wei Wang, Alex X Liu, Muhammad Shahzad, Kang Ling, and Sanglu Lu. Understanding and modeling of wifi signal based human activity recognition. In *Proceedings of the 21st Annual International Conference on Mobile Computing and Networking*, pages 65–76. ACM, 2015.

[118] Xuyu Wang, Lingjun Gao, Shiwen Mao, and Santosh Pandey. Csi-based fingerprinting for indoor localization: A deep learning approach. *IEEE Transactions on Vehicular Technology*, 66(1):763–776, 2017.

[119] Yan Wang, Jian Liu, Yingying Chen, Marco Gruteser, Jie Yang, and Hongbo Liu. E-eyes: device-free location-oriented activity identification using fine-grained wifi signatures. In *Proceedings of the 20th annual international conference on Mobile computing and networking*, pages 617–628. ACM, 2014.

[120] Roy Want. An introduction to rfid technology. *IEEE pervasive computing*, 5(1):25–33, 2006.

[121] Kristen Woyach, Daniele Puccinelli, and Martin Haenggi. Sensorless sensing in wireless networks: Implementation and measurements. In *Modeling and Optimization in Mobile, Ad Hoc and Wireless Networks, 2006 4th International Symposium on*, pages 1–8. IEEE, 2006.

[122] Kaishun Wu, Jiang Xiao, Youwen Yi, Dihu Chen, Xiaonan Luo, and Lionel M Ni. Csi-based indoor localization. *IEEE Transactions on Parallel and Distributed Systems*, 24(7):1300–1309, 2013.

[123] Kaishun Wu, Jiang Xiao, Youwen Yi, Min Gao, and Lionel M Ni. Fila: Fine-grained indoor localization. In *INFOCOM, 2012 Proceedings IEEE*, pages 2210–2218. IEEE, 2012.

[124] Yaxiong Xie, Zhenjiang Li, and Mo Li. Precise power delay profiling with commodity wifi. In *Proceedings of the 21st Annual International Conference on Mobile Computing and Networking*, pages 53–64. ACM, 2015.

[125] Jie Xiong and Kyle Jamieson. Arraytrack: a fine-grained indoor location system. In *Proceedings of the 10th USENIX conference on Networked Systems Design and Implementation*, pages 71–84. USENIX Association, 2013.

[126] Chao Xu, Parth H Pathak, and Prasant Mohapatra. Finger-writing with smartwatch: A case for finger and hand gesture recognition using smartwatch. In *Proceedings of the 16th International Workshop on Mobile Computing Systems and Applications*, pages 9–14. ACM, 2015.

[127] Takaya Yamazato, Isamu Takai, Hiraku Okada, Toshiaki Fujii, Tomohiro Yendo, Shintaro Arai, Michinori Andoh, Tomohisa Harada, Keita Yasutomi, Keiichiro Kagawa, et al. Image-sensor-based visible light communication for automotive applications. *IEEE Communications Magazine*, 52(7):88–97, 2014.

[128] Jie Yang, Simon Sidhom, Gayathri Chandrasekaran, Tam Vu, Hongbo Liu, Nicolae Cecan, Yingying Chen, Marco Gruteser, and Richard P Martin. Detecting driver phone use leveraging car speakers. In *Proceedings of the 17th annual international conference on Mobile computing and networking*, pages 97–108. ACM, 2011.

[129] Zheng Yang, Zimu Zhou, and Yunhao Liu. From rssi to csi: Indoor localization via channel response. *ACM Computing Surveys (CSUR)*, 46(2):25, 2013.

[130] Moustafa Youssef and Ashok Agrawala. The horus wlan location determination system. In *Proceedings of the 3rd international conference on Mobile systems, applications, and services*, pages 205–218. ACM, 2005.

[131] Faheem Zafari, Athanasios Gkelias, and Kin Leung. A survey of indoor localization systems and technologies. *arXiv preprint arXiv:1709.01015*, 2017.

[132] Wen-Jun Zeng, Xi-Lin Li, Xian-Da Zhang, and Xue Jiang. An improved signal-selective direction finding algorithm using second-order cyclic statistics. In *Acoustics, Speech and Signal Processing, 2009. ICASSP 2009. IEEE International Conference on*, pages 2141–2144. IEEE, 2009.

[133] Yunze Zeng, Parth H Pathak, and Prasant Mohapatra. Wiwho: wifi-based person identification in smart spaces. In *Proceedings of the 15th International Conference on Information Processing in Sensor Networks*, page 4. IEEE Press, 2016.

[134] Dian Zhang, Yunhuai Liu, Xiaonan Guo, Min Gao, and Lionel M Ni. On distinguishing the multiple radio paths in rss-based ranging. In *INFOCOM, 2012 Proceedings IEEE*, pages 2201–2209. IEEE, 2012.

[135] Junqing Zhang, Trung Q Duong, Alan Marshall, and Roger Woods. Key generation from wireless channels: A review. *IEEE Access*, 4:614–626, 2016.

[136] Junqing Zhang, Trung Q Duong, Roger Woods, and Alan Marshall. Securing wireless communications of the internet of things from the physical layer, an overview. *Entropy*, 19(8):420, 2017.

[137] Junqing Zhang, Biao He, Trung Q Duong, and Roger Woods. On the key generation from correlated wireless channels. *IEEE Communications Letters*, 21(4):961–964, 2017.

[138] Junqing Zhang, Alan Marshall, Roger Woods, and Trung Q Duong. Efficient key generation by exploiting randomness from channel responses of individual ofdm subcarriers. *IEEE Transactions on Communications*, 64(6):2578–2588, 2016.

[139] Junqing Zhang, Roger Woods, Trung Q Duong, Alan Marshall, Yuan Ding, Yi Huang, and Qian Xu. Experimental study on key generation for physical layer security in wireless communications. *IEEE Access*, 4:4464–4477, 2016.

[140] Keqi Zhang, Shu-Ching Chen, Dean Whitman, Mei-Ling Shyu, Jianhua Yan, and Chengcui Zhang. A progressive morphological filter for removing nonground measurements from airborne lidar data. *IEEE transactions on geoscience and remote sensing*, 41(4):872–882, 2003.

[141] Linghan Zhang, Sheng Tan, and Jie Yang. Hearing your voice is not enough: An articulatory gesture based liveness detection for voice authentication. In *Proceedings of the 2017 ACM SIGSAC Conference on Computer and Communications Security*, pages 57–71. ACM, 2017.

[142] Ouyang Zhang and Kannan Srinivasan. Mudra: User-friendly fine-grained gesture recognition using wifi signals. In *Proceedings of the 12th International on Conference on emerging Networking EXperiments and Technologies*, pages 83–96. ACM, 2016.

[143] Zengbin Zhang, David Chu, Xiaomeng Chen, and Thomas Moscibroda. Swordfight: Enabling a new class of phone-to-phone action games on commodity phones. In *Proceedings of the 10th international conference on Mobile systems, applications, and services*, pages 1–14. ACM, 2012.

[144] Zhong Zheng, Lu Liu, and Weiwei Hu. Accuracy of ranging based on dmt visible light communication for indoor positioning. *IEEE Photonics Technology Letters*, 29(8):679–682, 2017.

[145] Zimu Zhou, Chenshu Wu, Zheng Yang, and Yunhao Liu. Sensorless sensing with wifi. *Tsinghua Science and Technology*, 20(1):1–6, 2015.

[146] Yulong Zou, Jia Zhu, Xianbin Wang, and Lajos Hanzo. A survey on wireless security: Technical challenges, recent advances, and future trends. *Proceedings of the IEEE*, 104(9):1727–1765, 2016.